



# LUND UNIVERSITY

## Protein Dimensions and Interactions at Immune-Cell Contacts

Junghans, Victoria

2019

*Document Version:*

Publisher's PDF, also known as Version of record

[Link to publication](#)

*Citation for published version (APA):*

Junghans, V. (2019). *Protein Dimensions and Interactions at Immune-Cell Contacts*. [Doctoral Thesis (compilation), Faculty of Science]. Lund University, Faculty of Science.

*Total number of authors:*

1

### General rights

Unless other specific re-use rights are stated the following general rights apply:

Copyright and moral rights for the publications made accessible in the public portal are retained by the authors and/or other copyright owners and it is a condition of accessing publications that users recognise and abide by the legal requirements associated with these rights.

- Users may download and print one copy of any publication from the public portal for the purpose of private study or research.
- You may not further distribute the material or use it for any profit-making activity or commercial gain
- You may freely distribute the URL identifying the publication in the public portal

Read more about Creative commons licenses: <https://creativecommons.org/licenses/>

### Take down policy

If you believe that this document breaches copyright please contact us providing details, and we will remove access to the work immediately and investigate your claim.

LUND UNIVERSITY

PO Box 117  
221 00 Lund  
+46 46-222 00 00



# Protein Dimensions and Interactions at Immune-Cell Contacts

VICTORIA JUNGHANS | PHYSICAL CHEMISTRY | LUND UNIVERSITY





# Protein Dimensions and Interactions at Immune-Cell Contacts

by

Victoria Junghans



**LUND**  
UNIVERSITY

DOCTORAL DISSERTATION

by due permission of the Faculty of Science, Lund University, Sweden.  
To be defended on the 13<sup>th</sup> of December, in lecture hall B at the Centre for  
Chemistry and Chemical Engineering at Lund University.

*Faculty opponent*

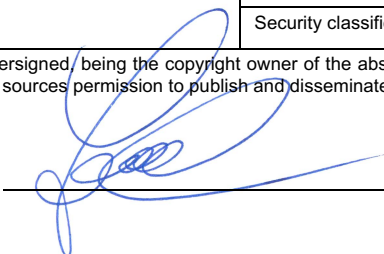
Prof. Michael L. Dustin

University of Oxford

<b>Organisation</b> <b>LUND UNIVERSITY</b> Department of Chemistry Box 124 SE-221 00 LUND Sweden		<b>Document name</b> <b>DOCTORAL DISSERTATION</b>	
		<b>Date of disputation</b> 2019-12-13	
<b>Author(s)</b> Victoria Junghans		Sponsoring organisation	
<b>Title and subtitle</b> Protein Dimensions and Interactions at Immune-Cell Contacts			
<b>Abstract</b> Immune cells, such as B and T cells, fight pathogens infecting the human body. To fulfil this function the immune cells need to form a contact during which different membrane proteins play an important role. A key event in this contact is the interaction between the T-cell receptor (TCR) and an antigenic peptide-presenting major histocompatibility complex (MHC) protein. If this interaction is sufficiently strong then the T cell gets activated leading to an immune response. The TCR-MHC together with other partaking proteins are highly organised within the cell-cell contact in respect to their size and function. However, information about their lateral interactions, height-dependent orientation and the consequences of this for binding are largely missing, but important in order to understand how an immune response is initiated on a molecular scale. The aim of this thesis was to shed light on this. For investigating protein size and lateral interactions an important negative regulator of TCR signalling, the phosphatase CD45, was studied. It was postulated by the kinetic segregation model that the tall glycoprotein CD45 is excluded from the contact area. The segregation from the TCR in the contact results in a net positive signalling event and thus in T-cell activation. The size of CD45 is a key factor but complete structural information at the cell surface is lacking. By using a technique called hydrodynamic trapping I determined the dimensions of CD45 and quantified its lateral interactions with other CD45 molecules in a cell membrane model. This was done by trapping CD45 anchored to a supported lipid bilayer (SLB) causing high local protein densities below a micropipette through which a negative pressure was applied. Using this method, it was found that CD45 has a lower apparent height than estimated previously which is accounted for by a high flexibility of the protein on the model membrane.  When investigating protein binding in this thesis the focus was on the binding strength (affinity) of TCR-MHC interactions. Each TCR has a specific affinity for their cognate peptide MHC, which varies from very weak to strong depending on the presented peptide. Agonist (pathogenic) peptides typically generate strong binding and an activation of the immune response. Measuring affinities in a cellular system is however complicated due to various protein interactions taking place at the same time. By using a model system in which cells bind to an SLB, the two-dimensional affinity of a TCR binding to an agonist MHC on the opposing cell was measured herein. It was found that high ligand densities affected the cells' cytoskeletal reorganisation, observed as strong lamellipodia formation, which caused a significant increase in the amount of bound ligands. Additionally, it was observed that the binding strength of the TCR-MHC interaction was influenced by the presence of the auxiliary protein CD2 and decreased with increasing amounts of CD2 in the contact. Using the methods described in this thesis allows to measure and interpret weak interactions such as to 'self' (body's own) peptide MHCs. In addition, my hydrodynamic trapping studies of proteins on functionalised SLBs could give new information about membrane protein behaviour, for example how protein flexibility can decrease the effective protein height and thus influence molecular exclusion at cell-cell contacts, and how glycosylation can increase the repulsion, which might prevent protein aggregation.			
<b>Key words</b> T cells, TCR, MHC, CD2, CD4, CD45, Antigen, Affinity, Two-Dimensional Affinity, TIRF Microscopy, SLBs			
Classification system and/or index terms (if any)			
Supplementary bibliographical information		<b>Language</b> English	
ISSN and key title		<b>ISBN (Print)</b> 978-91-7422-712-3	
Recipient's notes	Number of pages 208	Price	
	Security classification		

I, the undersigned, being the copyright owner of the abstract of the above-mentioned dissertation, hereby grant to all reference sources permission to publish and disseminate the abstract of the above-mentioned dissertation.

Signature



Date: 2019-11-05

# Protein Dimensions and Interactions at Immune-Cell Contacts

by

Victoria Junghans



**LUND**  
UNIVERSITY

Faculty of Science

Department of Chemistry

Division of Physical Chemistry

A doctoral thesis at a university in Sweden takes either the form of a single, cohesive research study (monograph) or a summary of research papers (compilation thesis), which the doctoral student has written alone or together with one or several other author(s).

In the latter case the thesis consists of two parts. An introductory text puts the research work into context and summarises the main points of the papers. Then, the research publications themselves are reproduced, together with a description of the individual contributions of the authors. The research papers may either have been already published or are manuscripts at various stages (in press, submitted, or in draft).

Coverphoto by Tithi Luadthong (*via* Shutterstock ID: 224881369)

Copyright Victoria Junghans

Paper I © Scientific Reports

Paper II © Frontiers in Immunology

Paper III © by the authors (manuscript unpublished)

Funding information: This work was supported by grants from the Swedish Research Council (number: 621-2014-2907), the Royal Physiographic Society in Lund, the Crafoord Foundation, the Royal Swedish Academy of Sciences and the European Research Council (ERC) under the European Union's Horizon 2020 research and innovation program (Grant agreement No. 757797).

Faculty of Science at Lund University, Department of Chemistry

ISBN (Print): 978-91-7422-712-3

ISBN (PDF): 978-91-7422-713-0

Printed in Sweden by Media-Tryck, Lund University, Lund 2019



Media-Tryck is an environmentally certified and ISO 14001:2015 certified provider of printed material. Read more about our environmental work at [www.mediatryck.lu.se](http://www.mediatryck.lu.se)

**MADE IN SWEDEN** 

*Only the one who knows his goal will find the path.*

-Laotse-





# Table of Contents

List of Publications .....	IV
Authors Contribution.....	V
Abbreviations.....	VI
Popular Science Summary .....	VII
Populärwissenschaftliche Zusammenfassung.....	X
<b>An Introduction to the Human Immune System .....</b>	<b>3</b>
Contents.....	3
The Immune System .....	4
MHC Classes and Co-Receptors .....	6
T-Cell Activation.....	6
Organisation of Immune-Cell Proteins in Cell-Cell Contacts.....	9
The Role of Adhesion Molecules .....	11
The Role of Glycoproteins.....	11
Aims of the Thesis .....	12
Thesis Outline.....	13
<b>1 Supported Lipid Bilayers and Fluorescence Microscopy .....</b>	<b>19</b>
Contents.....	19
1.1 Cell Membranes .....	20
1.2 Supported Lipid Bilayers .....	21
1.2.1 Formation of Supported Lipid Bilayers.....	21
1.2.2 Transmembrane Proteins in SLBs.....	22
1.2.3 Non-Covalently Linked Proteins in SLBs .....	23
1.2.4 Bilayer Formation and Protein Production .....	26
1.3 Microscopy Techniques to Quantify Functionalised SLBs.....	28
1.3.1 Epifluorescence Microscopy.....	29
1.3.2 Total Internal Reflection Fluorescence Microscopy .....	31
1.3.3 Confocal Microscopy.....	34

1.3.4 Spinning Disk Confocal Microscopy .....	37
1.3.5 Fluorescence Recovery After Photobleaching .....	38
1.3.6 Transmission Light Microscopy.....	39
1.3.7 Summary of the Applied Methods .....	40
<b>2 Dimensions and Orientations of Glycoproteins on Model Membranes.....</b>	<b>45</b>
Contents.....	45
2.1 T-Cell Receptor Triggering .....	46
2.1.1 Conformational Change and Force.....	47
2.1.2 Kinetic Segregation.....	49
2.2 Large Glycoproteins.....	51
2.2.1 CD45 and its Isoforms .....	51
2.2.2 CD43 .....	52
2.2.3 Structural Studies Using Microscopy .....	53
2.3 Trapping of CD2, CD4 and CD45RABC.....	57
2.3.1 Principle of Hydrodynamic Trapping.....	57
2.3.2 Considerations of the Method .....	59
2.3.3 The Measured Proteins.....	60
2.3.4 Dimensions and Orientations of CD2, CD4 and CD45RABC.....	61
2.3.5 Conclusion .....	66
2.4 Dimensional Studies of CD45 and CD43 .....	67
2.4.1 Trapping of CD45D1-D4, CD45R0 and CD43.....	68
2.4.2 Dimensions in Solution .....	70
2.4.3 Summary .....	74
2.4.4 Outlook.....	74
<b>3 Affinity Measurements of Immune-Cell Proteins.....</b>	<b>77</b>
Contents.....	77
3.1 Introduction .....	78
3.2 Dissociation Constants and Affinity .....	79
3.2.1 Three-Dimensional Affinities .....	80
3.2.2 Two-Dimensional Affinities .....	82
3.3 The Zhu-Golan Method.....	87
3.4 The Study of an Agonistic TCR-MHC Affinity .....	90
3.4.1 Receptor Pairs.....	90
3.4.2 Changes to the Zhu-Golan Method.....	91
3.4.3 Single Ligand Affinities.....	93

3.4.4 Multiple Ligand Affinities .....	94
3.4.5 Contact Size and High Ligand Densities .....	96
3.4.6 High-Binding Interaction .....	97
3.4.7 Conclusion .....	99
3.5 TCR Binding to Self-Peptide MHC – a Measurable Affinity? .....	99
3.5.1 HLA-DQ8 and L3-12 TCR .....	100
3.5.2 HLA-A02 and 1G4 TCR .....	101
3.5.3 Summary .....	103
3.5.4 Outlook.....	104
<b>Conclusion.....</b>	<b>109</b>
<b>References.....</b>	<b>113</b>
<b>Acknowledgements .....</b>	<b>127</b>
<b>Scientific Publications.....</b>	<b>131</b>

## List of Publications

This thesis is based on the following publications, referred to by their roman numerals:

**I Hydrodynamic Trapping Measures the Interaction Between Membrane-Associated Molecules.**

Victoria Junghans, Jana Hladilkova, A. Mafalda Santos, Mikael Lund, Simon J. Davis and Peter Jönsson

*Scientific Reports* **8**, 12479 (2018).

**II Dimensions and Interactions of Large T-Cell Surface Proteins.**

Victoria Junghans, Ana Mafalda Santos, Yuan Lui, Simon J. Davis, and Peter Jönsson

*Frontiers in Immunology* **9**, 2215 (2018).

**III Two-Dimensional Dissociation Constant of L3-12 T-Cell Receptor Binding Human Leukocyte Antigen-DQ8 and the Influence of Cellular Context**

Victoria Junghans, A. Mafalda Santos, Lena M. Svensson, Simon J. Davis and Peter Jönsson

*Manuscript*

The publications are appended at the end of the thesis.

## Authors Contribution

### **I Hydrodynamic Trapping Measures the Interaction Between Membrane-Associated Molecules.**

VJ did the experiments. PJ designed the study and analysed the data. JH and ML did the MC simulations. AMS and SJD made the immune-cell proteins. PJ and VJ wrote the paper.

### **II Dimensions and Interactions of Large T-Cell Surface Proteins.**

VJ, SJD and PJ planned and wrote the paper with input from AMS and YL. PJ did the MC simulations.

### **III Two-Dimensional Dissociation Constant of L3-12 T-Cell Receptor Binding Human Leukocyte Antigen-DQ8 and the Influence of Cellular Context**

VJ designed the study, did the experiments and analysed the data. VJ and PJ wrote the paper with input from SJD and AMS.

## Abbreviations

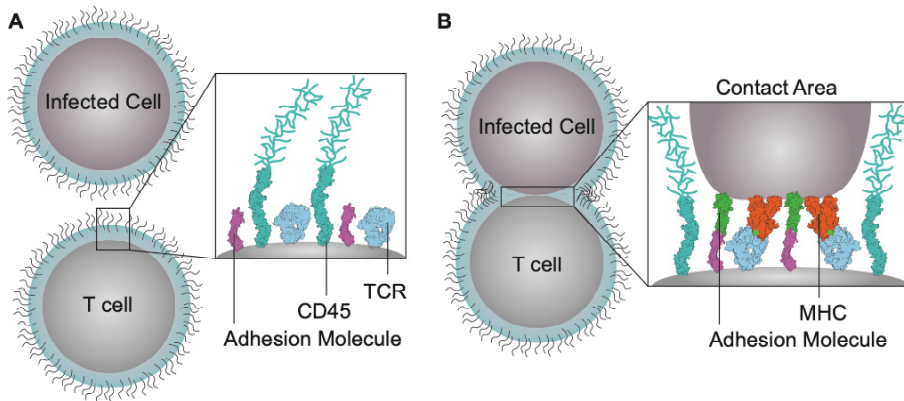
2D	Two Dimensional	KS	Kinetic Segregation
3D	Three Dimensional	LAT	Linker for Activated T cells
APC	Antigen Presenting Cell	Lck	Lymphocyte-Specific Protein Tyrosine Kinase
ATP	Adenosine Triphosphate	LFA-1	Lymphocyte Function-Associated Antigen 1
BFP	Biomembrane Force Probe	LSCM	Laser Scanning Confocal Microscopy
BSA	Bovine Serum Albumin	MHC	Major Histocompatibility Complex
CD	Cluster of Differentiation	NA	Numerical Aperture
D	Diffusion Constant	NTA	Nitrilotriacetic Acid
DC	Dendritic Cell	PDB	Protein Data Bank
DLS	Dynamic Light Scattering	PE	Phycoerythrin
EDTA	Ethylene Diamine Tetra Acetic Acid	PEI	Polyethyleneimine
EM	Electron Microscopy	RICM	Reflection Interference Contrast Microscopy
FLIC	Fluorescence Interference Contrast Microscopy	RBC	Red Blood Cell
FRAP	Fluorescence Recovery After Photobleaching	RU	Response Unit
FRET	Förster Resonance Energy Transfer	rCD2	rat CD2
GPI	Glycosylphosphatidylinositol	SAIM	Scanning Angle Interference Microscopy
GUV	Giant Unilamellar Vesicle	SAXS	Small Angle Light Scattering
HBS	Hepes Buffer Saline	SEC	Size Exclusion Chromatography
His-tag	Histidine Tag	SLB	Supported Lipid Bilayer
HLA	Human Leukocyte Antigen	SMAC	Supramolecular Activation Cluster
ICAM-1	Intercellular Adhesion Molecule 1	SPR	Surface Plasmon Resonance
IDA	Iminodiacetic Acid	SUV	Small Unilamellar Vesicles
Ig	Immunoglobulin	TCR	T-cell Receptor
IL2	Interleukin-2	TIRF	Total Internal Reflection Fluorescence
IMAC	Immobilised Metal Affinity Chromatography	VA-TIRF	Variable Angle TIRF
ITAM	Immunoreceptor Tyrosine-Based Activation Motif	ZAP-70	Zeta-Chain Associated Protein 70
K <sub>d</sub>	Dissociation Constant		

## Popular Science Summary

The human body is exposed to pathogens such as bacteria or viruses on a daily basis. Most of these pathogens are neutralised immediately. However, in rare cases the pathogens are infectious and cause diseases such as the common cold (flu). Typically, we feel sick only for a couple of days after which we can go back to our daily routine. This is possible due to the body's defence mechanism, the immune system. The immune system is composed of specialised cells that circulate through blood and tissue constantly searching for unwanted invaders. These cells are called immune cells and have the ability to distinguish between healthy and infected cells. When the immune cells find the pathogens, they eliminate them without damaging the body's healthy cells. A specific type of immune cells are called T cells. They possess very important receptors, which are small molecules that can bind to other molecules, on their surface. These T-cell receptors can recognise specific molecules from pathogens that are presented by a second type of receptors, called MHC proteins (short for major histocompatibility complex), on other cells in the body and bind to it. This interaction is similar to a 'key-in-lock' principle and only one specific T-cell receptor (key) can recognise one specific pathogenic molecule on the MHC (lock). As soon as they find the right 'lock' the T cells become activated. Activated T cells cross-talk with several different cells that are part of the immune system to eliminate the pathogen. T cells that bind to healthy cells with MHC proteins presenting body own sequences typically do not get activated and continue the scanning process for pathogenic molecules.

The work in this thesis focussed mainly on the 'key-lock' interaction between a healthy and an infected cell to better understand how the T cell gets activated. Even though it seems there are only two molecules involved in this process it actually requires many different molecules or proteins similar to the T-cell receptor. Among these, adhesion proteins play an important role in the formation of a cell-cell contact essential for the T-cell receptor (TCR) to bind to its MHC (see **Schematic Figure**). Other proteins inhibit T-cell activation and are important to be excluded from the contact to decrease their effect. CD45, a tall protein, is such an inhibitory protein and is believed to be excluded from the contact due to its large size guaranteeing T-





**Schematic figure of two approaching cells and cells in contact.**

(A) Represents two cells, the T cell and the infected cell that both have the glycocalyx layer around them. Zooming in on the layer (see square) some of the proteins on the cell surface are shown. The adhesion molecule (*pink*), the T-cell receptor (TCR-*blue*) and the tall glycoprotein, CD45 (*in cyan*). (B) The two cells in contact showing CD45 exclusion from the contact zone (see square). Shown are also the proteins on the infected cell with the MHC (*in red*) and the other adhesion molecule (*in green*).

cell activation. It is known that CD45 is a complex built protein containing a folded region which is connected to a long-unfolded chain governed by a lot of negatively charged sugars, however, important structural data of CD45 at the cell surface are missing (see **Schematic Figure**). The focus of the first subproject was therefore to study the structural properties such as how repulsive (due to the sugars) and tall CD45 is on a model membrane since taller, more upright standing proteins are more likely to be excluded from the contact area. I found that CD45 is highly repulsive and exists in its extended structure (it looks like a rod rather than a ball). However, CD45 seemed to be more flexible around its anchoring point to the membrane causing it to have a lower height compared to if it would stand upright like a rigid pole. The cell surface is a very crowded place with various amounts of different proteins. Especially large proteins such as CD45 are covering more than 10% of the cell surface forming a cushion hair-like layer, the glycocalyx, around the cell (see **Schematic Figure**). This high amount of proteins is most likely decreasing the flexibility of CD45 forcing it into a more upright, constrained, position causing its exclusion.

The second project focussed on trying to understand how T-cell receptors distinguish between infected and healthy cells. It is hypothesised that binding to infected cells will be stronger than to healthy cells. This binding strength dictates if the T cell is activated or not. Weak binding interactions such as the T-cell receptor binding to healthy cells are hard to study and depend on the addition of adhesion molecules to ensure contact formation. However, the effect of this addition on binding strength is unknown. Furthermore, the effect of protein crowding has also not been looked at in these systems when measuring binding strength. To understand this better I investigated a system in which a T-cell receptor binds to a pathogenic molecule presented by MHC at (i) low and high protein densities as well as (ii) in the presence of an adhesion molecule. I show an increased amount of binding at high protein densities and that the binding strength was reduced when high densities of adhesion molecules were added to the system. This finding has important implications for future studies of protein binding interactions, especially of weak ones such as the T-cell receptor binding to MHCs on healthy cells.

Taken together, I have found further structural support for CD45 exclusion from contact areas that is considered to be crucial for T-cell activation and how to measure the binding strength between a T-cell receptor and MHC in a cell-cell contact model I have investigated how this is influenced by protein density and protein composition with the latter providing insights into how different factors can affect cell-cell binding. It underlines how binding in cell-cell contacts are influenced by more parameters than just the receptor-ligand interaction.

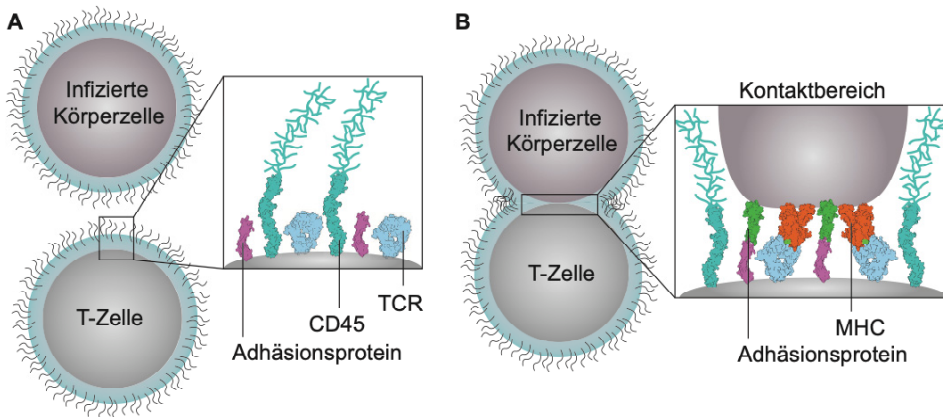
## Populärwissenschaftliche Zusammenfassung

Der menschliche Körper ist täglich einer Vielzahl von Krankheitserregern wie Bakterien oder Viren ausgesetzt. Während die meisten dieser sogenannten Pathogene sofort neutralisiert werden und somit keinen Schaden anrichten können, sind manche infektiös und damit Krankheitsverursachend. In der Regel fühlt man sich aber nur für einige Tage schlecht, nach denen man schnell wieder in den normalen Alltag zurückkehren kann. Das ist nur möglich durch unseren körpereigenen Abwehrmechanismus, das Immunsystem. Unser Immunsystem besteht aus speziellen Zellen, die kontinuierlich durch Blut und Gewebe zirkulieren und dabei nach unerwünschten Eindringlingen suchen. Diese sogenannten Immunzellen können leicht zwischen gesunden und infizierten Körperzellen unterscheiden und die "kranken" Zellen gezielt eliminieren. Besonders wichtig dafür sind die T-Zellen. Sie besitzen spezielle T-Zell-Rezeptoren (TCR) auf ihrer Oberfläche, die es ihnen ermöglichen, Sequenzen von Krankheitserregern zu erkennen und von körpereigenen Proteinsequenzen zu unterscheiden. Diese Sequenzen werden von einem zweiten Rezeptortyp, dem MHC Protein (kurz für den englischen Begriff *major histocompatibility complex*), der auf vielen Körperzellen sitzt, präsentiert. Die Interaktion zwischen dem T-Zell Rezeptor und dem MHC ähnelt dem „Schlüssel-Schloss“-Prinzip, bei dem nur ein bestimmter T-Zell Rezeptor (Schlüssel) eine bestimmte pathogene Sequenz auf dem MHC (Schloss) erkennen kann. Sobald ein Eindringling gefunden ist, werden die T-Zellen aktiviert, die sich im Anschluss mit anderen Immunzellen austauschen, um den Krankheitserreger zu eliminieren. Wenn jedoch T-Zell Rezeptoren an MHC Proteine binden, die körpereigene Sequenzen präsentieren, wird die T-Zelle nicht aktiviert womit garantiert wird, dass unsere T-Zellen nicht unsere gesunden Körperzellen angreifen.

Das Ziel meiner Arbeit bestand hauptsächlich darin, die "Schlüssel-Schloss"-Verbindung zwischen einer gesunden Immunzelle und einer infizierten Körperzelle zu untersuchen und zu verstehen, wie T-Zellen aktiviert werden. Obwohl zunächst nur zwei Proteine an diesem Prozess beteiligt zu sein scheinen, werden tatsächlich

viele weitere benötigt, die dem T-Zell Rezeptor strukturell ähnlich sind. Ein Beispiel hierfür sind Adhäsionsproteine, die für die Kontaktbildung zwischen Immun- und Körperzelle essentiell sind und somit eine Voraussetzung für die Wechselwirkung zwischen dem T-Zell Rezeptor und MHC darstellen (siehe **Schematische Abbildung**). Im Gegensatz dazu gibt es jedoch auch Proteine, welche die T-Zell-Aktivierung hemmen und daher von dem Zell-Zell-Kontakt ausgeschlossen werden sollten. Ein Beispiel für ein solch hemmendes Protein ist CD45. Trotz dessen, dass CD45 eine so wichtige „negative“ Rolle einnimmt ist aufgrund seiner komplexen Struktur nicht bekannt wie sich dieses Protein auf der Zelloberfläche verhält. CD45 ist zum Teil mit einer großen Anzahl negativ geladener Zuckermoleküle versehen, die keine wirkliche Struktur einnehmen und daher mit aktuellen analytischen Methoden nicht genau bestimmt werden kann wie groß dieses Protein ist. Deswegen lag der Fokus meines ersten Teilprojekts dieser Arbeit auf der Untersuchung von CD45 hinsichtlich seiner Größe und darauf, wie stark sich CD45-Proteine gegenseitig abstoßen, wenn sie sich in unmittelbarer Umgebung befinden. Diese Abstoßung wird durch die Zuckermoleküle verursacht. Im Rahmen meiner Arbeit habe ich herausgefunden, dass CD45 eine längliche Struktur einnimmt und sehr abstoßend ist. CD45 scheint sich jedoch nicht wie ein starrer Pfahl auf der Membran zu verhalten, sondern ist flexibel und kann sich rotierend bewegen was im Umkehrschluss dazu führte das CD45 in meinen Messungen kleiner erschien als von der theoretischen Struktur angenommen. Da die Zellmembran mit sehr vielen Proteinen ausgestattet ist, wird die Flexibilität von CD45 verringert, wodurch es in eine aufrechte Position gebracht und somit vom Kontakt zwischen T-Zelle und Körperzelle ausgeschlossen wird (siehe **Schematische Abbildung**).

In einem zweiten Teilprojekt habe ich untersucht, wie T-Zell Rezeptoren zwischen infizierten und gesunden Zellen unterscheiden können. Es wird angenommen, dass T-Zell Rezeptoren stärker an infizierte Zellen als an gesunde Zellen binden. Diese Bindungsstärke bestimmt dann wiederum, ob die T-Zelle aktiviert wird. Schwache Bindungen sind schwer zu untersuchen und können nur in Gegenwart von Adhäsionsproteinen gemessen werden. Ob diese Adhäsionsproteine allerdings die Bindungsstärke der untersuchten Proteinbindung beeinflussen, ist derzeit nicht bekannt. Es ist auch nicht klar, ob die von Natur aus hohe Proteindichte auf der



**Schematische Abbildung der Interaktion zwischen einer T-Zelle und einer infizierten Körperzelle.**

(A) Dargestellt sind eine T-Zelle und eine infizierte Körperzelle. Die Vergrößerung zeigt relevante Proteine auf der Oberfläche der T-Zelle; die Adhäsionsproteine in pink, der T-Zell-Rezeptor (TCR) in hellblau und CD45 in cyanblau. (B) Ein Zell-Zell-Kontakt bei dem CD45 aus der Kontaktzone ausgeschlossen ist. Das MHC-Protein ist in orange dargestellt, die Adhäsionsproteine in grün und pink, TCR in hellblau und CD45 in cyanblau.

Zellmembran einen Einfluss auf die Bindung zwischen dem T-Zell Rezeptor und MHC hat. Um diesen Aspekt besser zu verstehen, habe ich die Bindungsstärke von einem T-Zell Rezeptor das an ein Pathogen-präsentierendes MHC bindet gemessen, und dabei den Effekt (i) von niedriger und hoher Proteindichte sowie (ii) vom Vorhandensein eines Adhäsionsprotein untersucht. Ich habe herausgefunden, dass eine hohe Proteindichte für eine erhöhte Rezeptorbindung sorgt und dass die Bindungsstärke zwischen dem T-Zell Rezeptor und MHC abnimmt, wenn dem System hohe Mengen von Adhäsionsproteinen zugesetzt werden. Diese Ergebnisse sind wichtig für zukünftige Studien zu Proteinbindungswechselwirkungen, vor allem von schwachen wie der von T-Zell Rezeptoren die an körpereigene-Sequenz-präsentierende MHCs binden, da diese nur in Abhängigkeit von Adhäsionsproteinen stattfinden können.

Zusammenfassend habe ich einen weiteren strukturellen Beweis für den Ausschluss von CD45 aus Zell-Zell-Kontakten geliefert, der wiederum ein entscheidendes Kriterium für die T-Zell-Aktivierung darstellt. Zudem habe ich gezeigt, wie die Bindungsstärke zwischen dem T-Zell Rezeptor und MHC in einem Zell-Zell-Kontakt gemessen werden kann und wie diese durch die Proteindichte und die

Proteinzusammensetzung beeinflusst wird. Letzteres gibt Aufschluss darüber, wie unterschiedliche Faktoren die Zell-Zell-Bindung beeinflussen können und unterstreicht, dass die Proteinbindung in Zell-Zell-Kontakten von mehreren Parametern als nur der Rezeptor-Rezeptor-Wechselwirkung bestimmt wird.



# Background

*Come to me Eragon, for I have answers to all you ask.*

-Christopher Paolini, *Eragon*, 2002-





# An Introduction to the Human Immune System

## Contents

---

The Immune System.....	4
MHC Classes and Co-Receptors.....	6
T-Cell Activation.....	6
Organisation of Immune-Cell Proteins in Cell-Cell Contacts.....	9
The Role of Adhesion Molecules.....	11
The Role of Glycoproteins.....	11
Aims of the Thesis.....	12
Thesis Outline.....	13

---

The body's immune system protects us from harmful infections every minute of the day and is orchestrated by many cells and proteins. The most important interaction is between two cells bearing the two key receptors, TCR and MHC, through which an infected state of the body is translated into a defensive immune response. This interaction is governed by many different proteins and the main subject in this thesis was to investigate the dimensions, lateral interactions and binding strength of some of the most important ones in the cell-cell contact. To help understand the TCR-MHC interaction and all the terminology used the important processes and proteins involved in initiating an immune response are set out in this introductory chapter. The aims and the outline of the thesis are summarised in more detail at the end of the chapter.

## The Immune System

The body is continually exposed to a large variety of microorganisms many of which cause diseases such as malaria, influenza and chicken pox. In most cases these pathogens are eliminated by the body's defence mechanism, the immune system. White blood cells also known as lymphocytes are one of the most important effector cells within this system. They recognise and target the pathogenic microorganism for elimination or destruction. Lymphocytes are part of the adaptive immune system which develops during an individual's lifetime. The adaptive immune response typically takes days to develop and is dependent on a more rapidly acting primary defence mechanism, the innate immune response, which evaluates the severity and kind of threat. The link between the innate and the adaptive immune system is made by dendritic cells (DC). Dendritic cells migrate through the bloodstream and tissues and take up matter by phagocytosis. Through this process pathogens are ingested and destroyed intracellularly. Engulfed pathogenic proteins are degraded into peptides, which are small amino acid hetero oligomers, and displayed on the cell surface of DCs to activate the adaptive arm of the immune system. Immune cells capable of performing this function, such as DCs, are known as antigen presenting cells (APC). The peptides are presented on special receptors called major histocompatibility complex (MHC) proteins. MHC molecules are transmembrane glycoproteins of which many different variants exist within the population, *i.e.*, they are highly polymorphic molecules. This guarantees a wide range of bound and presented peptides. MHC molecules present mainly naturally occurring peptides from the body's own peptide pool and carry only a few pathogenic ones upon infection. T-cell receptors (TCR) expressed by a special type of lymphocyte called T cells recognise these peptide MHC molecules specifically. Each T cell bears about 30 000 identical TCRs that differ on each of the billions of T cells circulating in the body creating a huge variety of possible interactions<sup>1</sup>. The TCR consists of two different polypeptide chains, with each chain composed of two immunoglobulin (Ig) domains characterised by an amino acid sequence that is folded in an antiparallel  $\beta$ -sheet structure (**Figure 1**). The two chains are typically expressed in complex with the signalling protein cluster of differentiation 3 (CD3). Structurally the TCR molecule is very similar to the antigen binding fragment of an antibody and possesses

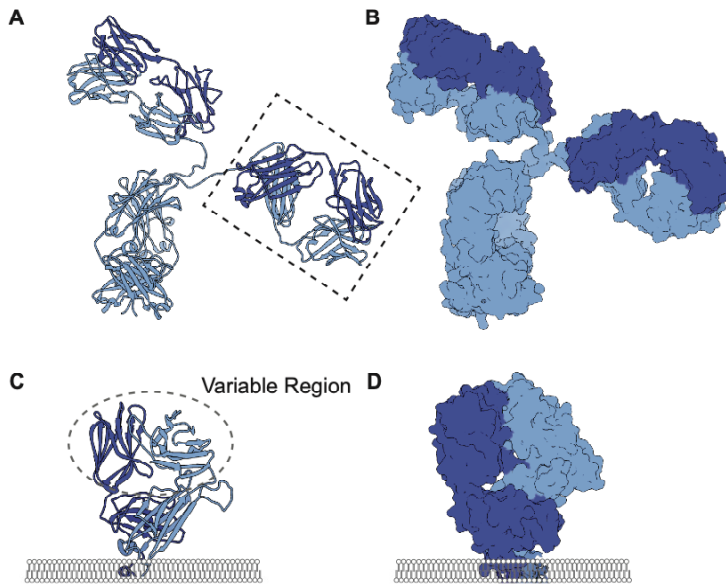


**Figure 1. Structure of an antibody and a T-cell receptor.**

(A, B) Crystal structure of an antibody (PDB: 1IGY)<sup>2</sup> in (A) the ribbon format showing the  $\beta$ -sheet structure common to Ig domains and (B) the projected surface area. Light chains are shown in dark blue, heavy chains in light blue. (C, D) Crystal structure of the extracellular domain of a TCR (from the protein data bank (PDB), code 6JXR)<sup>3</sup> bound to a membrane in (C) ribbon and (D) surface structure. The two chains ( $\alpha$ - and  $\beta$ -chain) are represented in light and dark blue. The variable domains are shown in the dashed grey circle. The dashed square in A represents the part of the antibody that is similar in structure to the extracellular domains of the TCR shown in C.

highly variable membrane distal Ig domains (Figure 1). A high variability of the antigen binding domain results in an immense TCR repertoire with one TCR being specific to at least one individual peptide presented by a particular MHC molecule. This specificity enables the recognition of a pathogenic peptide among a sea of self peptides causing T-cell activation, initiation of an adaptive immune response and destruction of the pathogen.

## MHC Classes and Co-Receptors

T cells respond to a wide range of pathogens that can infect the cell either intracellularly or extracellularly and must exert different effector functions accordingly. There are several types of T cells characterised by the kind of TCR they express and by certain T cell markers like co-receptors. Most T cells express either CD8 or CD4 as co-receptors which define the two main functional classes of T cells, cytotoxic and helper T cells. Cytotoxic T cells express CD8 and act against virus infected cells by directly killing the cell and preventing further viral replication. CD4 expressing T cells typically recognise antigens that were taken up by phagocytosis from the extracellular milieu. They act indirectly by producing cytokines which activate other effector mechanisms such as antibody production by B lymphocytes (B cells) to protect against the pathogen. The co-receptors are argued to stabilise the TCR-MHC interaction and are known to be crucial in the signalling process by associating with an activating kinase and carrying it to the TCR-MHC complex<sup>4-7</sup>. Moreover, CD8 and CD4 recognise different subclasses of MHC molecules, *i.e.*, MHC class I and MHC class II, respectively. MHC class I molecules present viral peptides and are expressed on most cells providing an important defence mechanism against intracellular viral infections. MHC class II molecules, in contrast to MHC class I, are primarily expressed by professional APCs such as DCs or B cells and present extracellularly derived peptides from bacteria or fungi.

## T-Cell Activation

T-cell activation follows the interaction of a TCR with a peptide MHC. However, the binding of the TCR to its MHC faces several obstacles. One of the major problems is the affinity of agonistic TCR-MHC interactions which have been shown to be relatively low in solution, more than two magnitudes lower, than what has been found for structurally similar antibodies binding their antigen<sup>8</sup>. This difference may be facilitated by the fact that B cells, the producers of antibodies, commonly undergo an affinity maturation process to produce antibodies of high affinity for their antigen. In contrast, T cells with a high affinity TCR for self-peptide MHCs

get eliminated during their development and also do not undergo an additional affinity maturation process, both preventing self-reactivity. The selection of low affinity TCRs has also been speculated to be important for a rapid scanning of the MHC molecules<sup>9-11</sup>. It is unclear how this rather lower affinity receptor can activate the signalling machinery so effectively. Intriguingly, it has been shown that the TCR-MHC affinity is similar to that of a strong adhesive binding-pair interaction when measured in a cell-cell contact suggesting that the lateral confinement through the membrane increases specificity<sup>12</sup>. However, measuring the affinity in a cellular context is difficult and the existing data are limited. The second problem, as pointed out above, is the low amount of specific peptides presented by an APC. An APC presents many different peptides of both 'self' and pathogenic (agonist) origin and the number of agonist MHC molecules among these is likely to be very low. To respond effectively T cells must be able to recognise these few complexes. Estimates suggests that T cells can become activated by fewer than 10 agonistic peptide MHC molecules representing this sensitivity<sup>13-15</sup>.

How exactly the extracellular interaction between the TCR and peptide MHC is transmitted across the membrane to activate the T cell is not clear and an area of active research. Several models exist explaining this phenomenon and will be discussed in more detail below (Chapter 2). However, more is known about the intracellular signals generated after the T cell has bound an APC. The first signal is phosphorylation of the TCR in complex with the CD3 molecule by the lymphocyte-specific protein tyrosine kinase (Lck) (**Figure 2**). The phosphorylated TCR-CD3 complex is a binding site for the tyrosine kinase ZAP-70 (zeta-chain associated protein kinase 70), a signalling protein. ZAP-70 recruitment to the cell membrane gives rise to an amplified signal (the second signal) and allows the activation of the scaffold protein LAT (linker for activated T cells) and other adaptor proteins which together form a signalling complex<sup>16</sup> (**Figure 2**). This signalling complex activates additional enzymes affecting (i) transcription of genes such as the cytokine interleukin-2 (IL-2) which is crucial for sustained clonal expansion of the interacting T cells, and (ii) cell metabolism by promoting cell survival and increasing the utilisation of glucose. The third intracellular signal enhances the stability of the TCR-MHC interaction by localising the TCR-MHC complex into an

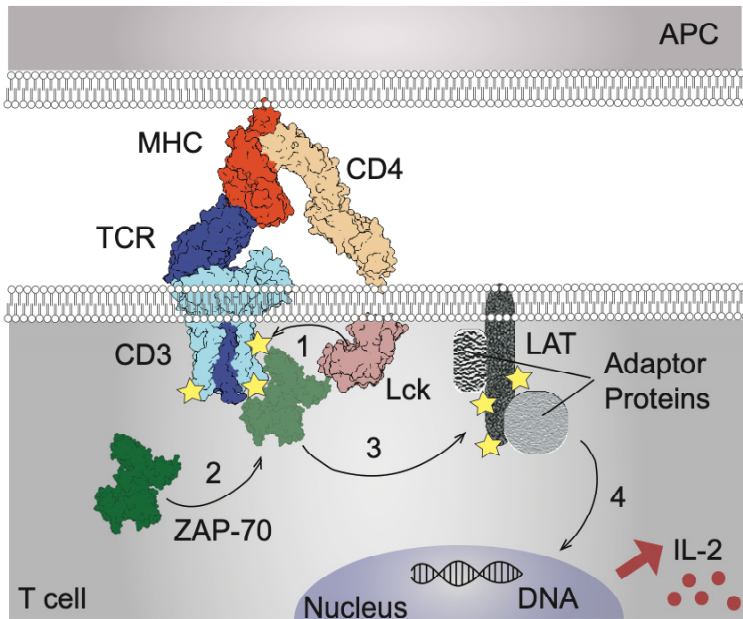


**Figure 2. Signalling process in a T cell.**

Two opposing cells bind to each other. The MHC class II molecule (*red*) on the APC is bound by the TCR on the T cell. CD4 co-localises by binding to the membrane proximal domain of the MHC II molecule. Lck, which can non-covalently attach to CD4, is brought into close proximity to the TCR-CD3 complex (*blue* and *light blue*). (1) Lck phosphorylates the tyrosine of the TCR complex (*yellow stars*) upon which (2) ZAP-70 is recruited and binds to the newly phosphorylated sites. (3) ZAP-70 activates LAT to which adaptor proteins bind (*grey*) causing downstream processes (4) that can lead to the transcription of genes such as the cytokine IL-2. There are many more molecules involved which have been excluded for simplicity. The crystal structures were obtained from the PDB: for TCR/CD3 complex (6JXR)<sup>3</sup>, MHC II and CD4 binding (3T0E)<sup>20</sup>, Lck (3LCK)<sup>3</sup> and for ZAP-70 (4K2R)<sup>21</sup>.

immunological synapse (described in the next section)<sup>17–19</sup>. The immune synapse forms within minutes upon TCR-MHC interaction, promoting sustained TCR engagement and signalling<sup>17,19</sup>. It is characterised by a specific organisation of receptors and integrin family adhesion molecules, with the latter forming a ring-like structure surrounding the TCR-MHC complexes. Together with the formation of an immune synapse a reorganisation of the actin cytoskeleton is stimulated and is for example required to ensure cytokine secretion from the T cell to the target cell.

## Organisation of Immune-Cell Proteins in Cell-Cell Contacts

A further obstacle for T-cell activation is that TCR as well as MHC are small molecules, approximately 7 nm in size, compared to the glycoproteins forming the negatively charged barrier of the cell, the glycocalyx, which can extend up to 40 nm from the cell surface. Additionally, the tall glycoproteins bury and shield the TCR and MHC molecules from each other and hamper their engagement. However, cell-cell contacts do form and hence the adhering cells must overcome this repulsive layer. Most of the attractive force to do so is suggested to come from adhesion molecules such as the lymphocyte-function associated antigen-1 (LFA-1)<sup>8,17,22</sup>. LFA-1 is relatively tall, 16 nm, and extends well into the glycocalyx. It is expressed on the surface of T cells and binds, on non-activated T cells, weakly to its counter receptor ICAM-1 (intracellular-adhesion molecule-1) which is expressed on a wide variety of cells. This interaction supports the initial contact formation between a T cell and an APC. Importantly, LFA-1 can undergo a conformational change upon T-cell activation causing the interaction with ICAM-1 to be of high affinity which stabilises the cell-cell contact. Another adhesion molecule is CD2, a small molecule that is similar in size to the TCR and buried within the glycocalyx. It binds to its counter-receptor CD58 and does not undergo any conformational changes. It has been suggested that CD2 mediates adhesion sufficiently enough to bring the two membranes in close proximity (approximately 15 nm) helping the TCR-MHC to make contact<sup>22,23</sup>. Based on this small gap size molecules like LFA-1 or larger glycoproteins are unlikely to 'fit' in and have been shown to be excluded from the contact area<sup>19,24</sup>. This principle is an important characteristic of synapse formation which occurs in the following steps (**Figure 3**). Initially, the migrating T cell binds *via* weak LFA-1-ICAM-1 interactions to the APC overcoming the barrier of repulsion. This step causes the generation of close contact areas where smaller molecules such as the TCR and CD2 can bind their respective counter-receptor. The second step involves the active transport of TCR-MHC complexes distributed in small contact areas from the periphery to the center of the contact. The TCR-MHC complexes thereby exchange their position with the tall LFA-1 molecules causing the exclusion of LFA-1 to the outer area of the cell-cell contact. Rearranging the proteins leads to the formation of a central supramolecular activation cluster (c-SMAC)



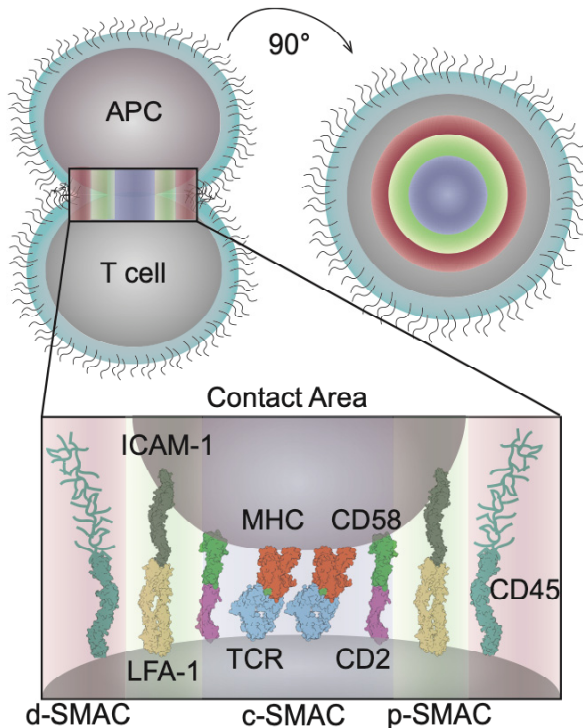


**Figure 3. Schematic composition of the immunological synapse.**

Shown is an APC in contact with a T cell in side view (*left*) and top view (*right*). The coloured areas resemble the c-SMAC (*blue*), the p-SMAC (*green*) and the d-SMAC (*red*). The protein organisation within the SMACs is shown in the insert. Smaller molecules such as the TCR-MHC and CD2-CD58 accumulate in the c-SMAC, LFA-1 and ICAM-1 in the p-SMAC and taller molecules like CD45 in the d-SMAC. The crystal structures were obtained from the PDB: for TCR/CD3 complex (6JXR)<sup>3</sup>, MHC II (3T0E)<sup>20</sup>, CD45 (5FMV)<sup>24</sup>, CD2 (1HNG)<sup>25</sup> and for CD58 (1CCZ)<sup>26</sup>. The crystal structures for ICAM-1 and LFA-1 are arbitrary.

containing TCR-MHC complexes as well as other similarly-sized receptors such as CD2, and a peripheral SMAC (p-SMAC) containing LFA-1-ICAM-1 complexes (Figure 3). Additionally, tall glycoproteins orientate themselves in a distal SMAC around the p-SMAC (Figure 3). The rearrangement occurs after the TCR has been activated or ‘triggered’ and includes the reorganisation of the cytoskeleton, aligning different cellular components for example the secretory Golgi-apparatus to the immune synapse<sup>18</sup>. Immune synapse formation results in the stabilisation of the T cell-APC interaction and without this process T-cell activation terminates.

## The Role of Adhesion Molecules

LFA-1, CD2 and TCR all play a role during T-cell activation and immune synapse formation. Both LFA-1 and CD2 are believed to aid in contact formation of apposing APC and TCR membranes to facilitate TCR-peptide-MHC interactions<sup>8</sup>, thus effectively increasing the sensitivity of the TCR for its agonist-peptide MHC<sup>8,17,22</sup>. However, it has also been demonstrated that TCR and peptide MHC can interact without these supporting molecules<sup>27</sup>. The order of LFA-1, CD2 and TCR binding events therefore remains unclear as all three could enhance the ability of the others to bind. For example, TCR activation alters LFA-1's conformation into a higher affinity state<sup>17</sup>. However, prior to this LFA-1 can exist in a lower affinity state which could facilitate TCR-MHC interaction, TCR triggering and its own conformational change. Ultimately, it is likely that all three proteins act synergistically.

## The Role of Glycoproteins

The glycocalyx is an outer layer around the cell formed by glycolipids and glycoproteins extending from the cell membrane and has crucial roles in cell-cell recognition, adhesion and communication. It further protects the cell membrane from physical stress maintaining its integrity. Transmembrane glycoproteins that possess an elongated, flexible and highly glycosylated extracellular region are important components of the glycocalyx. These structures are commonly called mucins and are very similar to a polymer brush structure describing long, flexible extended or loop-containing polymer chains grafted onto a surface<sup>28</sup>. Two of the most abundantly expressed glycoproteins are CD43, resembling an extended polymer brush, and CD45 that has a more complex structure comprised of a mucin-like region attached to a rigid domain (**Figure 3**). Interestingly, the expression levels of CD43 and CD45 vary with the developmental stages of lymphocytes and the size and charge density of the protein can change accordingly<sup>29,30</sup>. Of these, CD45 is a particularly interesting molecule as it contains an intrinsic phosphatase domain able to dephosphorylate tyrosine. As noted above, tyrosine phosphorylation is crucial for

T-cell activation through the TCR-CD3 complex. Dephosphorylation of the TCR complex, facilitated by CD45, inhibits T-cell activation and the subsequent immune response. However, due to its extended structure the glycoprotein CD45 gets excluded from the contact area similar to LFA-1. This causes the spatial segregation of the phosphatase and the phosphorylated TCR-CD3 complex, which in the immunological synapse organise into the distal SMAC and the central SMAC, respectively. The phosphatase exclusion from the contact area has also been suggested to cause the initial step in TCR triggering and is described by the kinetic segregation (KS) model offering one explanation for how the TCR and MHC interaction can be translated into a cellular signal.

## Aims of the Thesis

The lion's share of the above presented knowledge is based on *in vitro* studies and may not precisely reflect what happens *in vivo*, however, the findings provide a great insight into the role of TCR-MHC interactions. The main mechanism of how the TCR is triggered, despite many proposed models, is unresolved. One popular attempt to explain the initial TCR phosphorylation is given by the KS model suggesting an important role of CD45 in the process. Nevertheless, crucial evidence for the model as well as certainty of the structure of CD45 on the cell surface are missing. The first main aim of this thesis was to understand the complex structure of CD45 better and to resolve the question of whether it extends upright from the membrane. For this a model system has been used in which the extracellular region of the protein has been attached to a model membrane. CD45 was studied together with the smaller proteins CD2 and CD4 to investigate the impact of glycosylation and flexibility on the organisation and orientation of various-sized proteins.

It has been suggested that the binding strength of the TCR-MHC interaction regulates the activation of the T cell. Strong binding to agonist peptides mounts an immune response and weak binding to self-peptides does not. However, to measure affinities particularly in a cellular environment has been challenging. Relatively few data exist on the binding strength of the TCR to foreign peptides and information about binding to self-peptide MHC is lacking. To measure weak interactions like

‘self’ the presence of adhesion proteins such as CD2 to support contact formation and possible binding is necessary. It is unknown whether auxiliary proteins or high protein densities commonly occurring in the contact area effect the binding strength. This inspired the second main aim of this thesis: to investigate the affinity of a TCR binding an agonist MHC in a model cell-cell contact, and to determine whether the binding is affected by high ligand densities and the presence of auxiliary binding molecules. The results were finally put in context to set up a working model for measuring ‘self’ interactions.

## Thesis Outline

A graphical outline of the thesis is shown in **Figure 4** and summarises the three main subjects included.

### Chapter 1

One of the most common ways to study complex cell-cell interactions is by using reconstituted membranes either in the form of lipid vesicles or model membranes supported by a solid material known as a supported lipid bilayer (SLB). Various microscopy techniques allow for the visualisation of these interactions and with that a greater understanding of protein organisation such as that in the immunological synapse. I have used SLBs mimicking the cell membrane of a T cell and fluorescence microscopy to image the studied processes. An introduction to the reconstitution of cell membrane models and the microscopy techniques used in this work is given in Chapter 1.

### Chapter 2

After clarifying what systems I have been using and why, I will move on to Chapter 2, which summarises the main findings of **Paper I** and **Paper II**. The focus in Chapter 2 is on structural studies of the tall glycoprotein CD45 including two major isoforms of CD45 called CD45RABC and CD45R0 and the rigid domain region

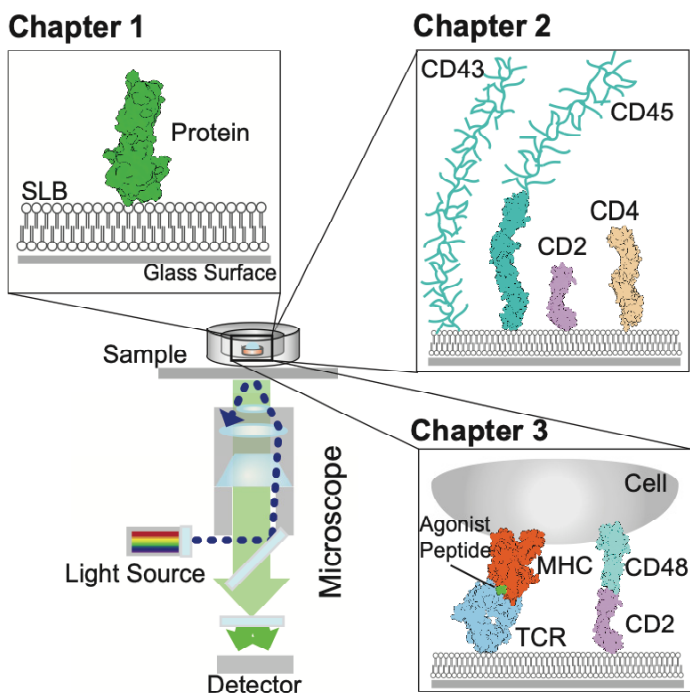


**Figure 4. Illustrative summary of the different chapter contents.**

Chapter 1 covers the formation of SLBs, and various microscopy techniques used in this thesis. Chapter 2 focuses on height and interaction measurements of CD43, CD45, CD2 and CD4. Chapter 3 is dedicated to two-dimensional affinity measurements of TCR to MHC and how this depends on different conditions such as having CD2 binding CD48.

CD45D1-D4, of CD43 as well as of CD2 and CD4. I introduce a more detailed concept of TCR triggering with a focus on the KS model and then summarise the main structural features of CD45 and CD43. This lays the foundation for a better understanding of the results in **Paper I**, which will be presented next. Finally, the findings of **Paper I** and **II** are complemented with more recently obtained data and Chapter 2 ends with an outlook towards future experiments.

### Chapter 3

In Chapter 3, I will explain the concept of affinity and why it is important followed by an introduction into the common techniques used to measure either three-dimensional (solution) affinities or two-dimensional (cell-membrane confined)

affinities. The focus will then move on to the fluorescence-based method used to measure the two-dimensional affinities in this work. I will give a summary of the results in **Paper III** where I have studied how TCR binding to an agonist MHC is affected by ligand density and the inclusion of an auxiliary binding molecule, and elaborate on preliminary results regarding affinity measurements of TCR binding to self-peptide presenting MHCs. The Chapter ends with a short outlook.



# Chapter 1

*You jump - I jump, Jack.*

-Amy Sherman-Palladino-





# 1

## Supported Lipid Bilayers and Fluorescence Microscopy

### Contents

---

1.1 Cell Membranes.....	20
1.2 Supported Lipid Bilayers.....	21
1.2.1 Formation of Supported Lipid Bilayers.....	21
1.2.2 Transmembrane Proteins in SLBs.....	22
1.2.3 Non-Covalently Linked Proteins in SLBs.....	23
1.2.4 Bilayer Formation and Protein Production.....	26
1.3 Microscopy Techniques to Quantify Functionalised SLBs.....	28
1.3.1 Epifluorescence Microscopy.....	29
1.3.2 Total Internal Reflection Microscopy.....	31
1.3.3 Confocal Microscopy.....	34
1.3.4 Spinning Disk Confocal Microscopy.....	37
1.3.5 Fluorescence Recovery After Photobleaching.....	38
1.3.6 Transmission Light Microscopy.....	39
1.3.7 Summary of the Applied Methods.....	40

---

Chapter 1 will give an introduction of the theoretical background to the techniques used in the following chapters. The focus is herein on supported lipid bilayers used as model membranes for all conducted studies, and on the applied microscopy techniques for image acquisition. The main reasons why these techniques were chosen are summarised at the end of subchapter 1.2 and 1.3. Chapter specific techniques and methods are explained within their respective chapter.

## 1.1 Cell Membranes

Cell membranes are 5-10 nm thin semi-permeable biological membranes that separate the cell interior from the outside environment protecting the integrity of cellular components. Cell membranes are involved in many cellular processes such as protein transport, cell growth and cell signaling<sup>31</sup>. Typically, they are negatively charged and composed of proteins, lipids and sterols such as cholesterol (**Figure 1.1.1**). Of those, proteins can constitute up to 50% of the cell membrane. Most of them are embedded into the membrane either partly (integral membrane proteins) or fully spanning through it (transmembrane proteins) (**Figure 1.1.1**). The membrane itself is formed by lipids which arrange into a thin sheet of two opposing lipid molecules, *i.e.*, a lipid bilayer (**Figure 1.1.1**)<sup>32</sup>. The most prominent membrane lipids are phospholipids, which are amphiphilic molecules that contain a water-attracted, hydrophilic, part (head group) and a water-repelled, hydrophobic, part (tail). In an aqueous solution, the hydrophilic head group of the phospholipid will orient itself towards the water and the hydrophobic tails will orient towards each other excluding water by forming a double layer or bilayer. Due to this amphiphilic characteristic of the lipid bilayer incorporated proteins can freely diffuse laterally through the membrane which is crucial for many cellular processes and protein functions. Mixing of proteins into the lipids gives the membrane a mosaic-like structure and is, together with its high fluidity, commonly described with the fluid mosaic model of the cell membrane<sup>33</sup>.

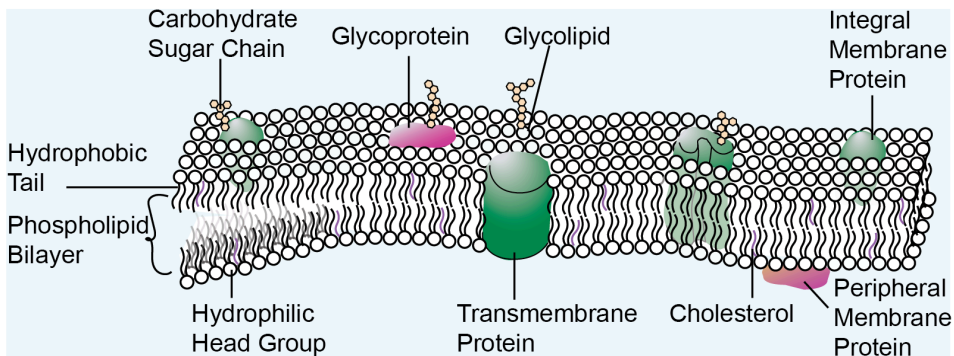


**Figure 1.1.1. Schematic representation of a cell membrane.**

## 1.2 Supported Lipid Bilayers

Over the last decades cell membranes and especially the function of many transmembrane proteins involved in cell signalling have been intensely studied<sup>34</sup>. However, the sheer amount of membrane proteins made it challenging to study the function of single membrane proteins that play important roles in cell-cell contacts and signalling. The very first approach to circumvent this problem was the use of cell membrane models, so called black lipid membranes<sup>35</sup>. This system is based on the painting of phospholipid molecules across a less than one-millimeter hole between two opposing walls that separate two chambers. One major advantage of this method is the absence of an underlying substrate<sup>35,36</sup>, which allows for the inclusion of transmembrane proteins and access of the planar bilayer from both sides. However, the stability of the formed membrane is low and possible detection methods limited<sup>36</sup>. A major breakthrough was achieved by McConnell *et al.* in the early 1980s by introducing glass-supported lipid bilayers<sup>37</sup>. These act as model membranes in cellular assays wherein one contacting cell is exchanged with the phospholipid bilayer formed on a solid surface. Supported lipid bilayers (SLBs) have since then become a very popular tool both because of their high stability and accessibility of detection methods as well as the freedom of controlling and manipulating them for every user's need.

### 1.2.1 Formation of Supported Lipid Bilayers

There are various methods of forming SLBs<sup>38</sup>. The three main methods are (i) the deposition of a monolayer from an air-water interface and the formation of a bilayer following the transfer of a second monolayer onto the first one (**Figure 1.2.1A**)<sup>37,39</sup>, (ii) the spreading of lipids from a lipid reservoir onto the solid substrate and the formation of a bilayer upon hydration (**Figure 1.2.1B**)<sup>40</sup>, and (iii) lipid vesicle fusion (**Figure 1.2.1C**)<sup>41,42</sup>. All methods result in the formation of a 5 nm thick continuous lipid bilayer on a solid surface but vesicle fusion, originally introduced in 1984, is to date the most commonly used method of forming SLBs<sup>43</sup>. Lipid vesicles form immediately after the hydration and mixing of dry lipids. These vesicles can be unilamellar or multilamellar and of various sizes ranging from nm to  $\mu\text{m}$ . However,

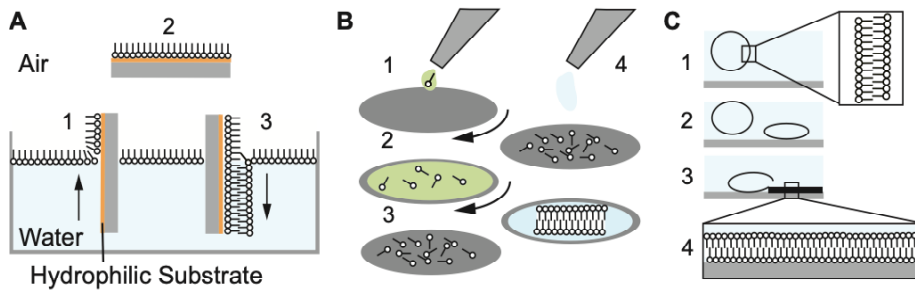


**Figure 1.2.1. Various methods to prepare supported lipid bilayers.**

**(A)** The deposition of a lipid monolayer from a water-air interface (1) onto a substrate with a hydrophilic layer (orange) (2) and the subsequent deposition of a second monolayer onto the first one resulting in a lipid bilayer (3). **(B)** The addition of lipids in an organic solvent (green) onto a spinning supporting material (1). Due to the spinning the lipids spread (2) and the organic solvent evaporates leaving dry lipids on the support (3). The addition of an aqueous solution (4) leads to the instant formation of an SLB. **(C)** SUVs in an aqueous solution are added to the supporting material (1). The vesicles deform (2) and rupture (3) resulting in the formation of an SLB (4).

to enable the formation of SLBs through vesicle fusion the vesicles have to be small and unilamellar, commonly known as small unilamellar vesicles (SUVs). They typically have a radius of 15-30 nm and are less stable (more prone to fuse) than larger sized vesicles. The most efficient method to produce SUVs is using sonication, in which sound energy or sonic waves are applied to the vesicle solution agitating the vesicles. This leads to a continuous rupture and reformation of vesicles until SUVs are formed. SUVs added to a solid surface adsorb to it, rupture and subsequently fuse together forming a continuous and fluidic phospholipid bilayer. The fluidity or free lateral diffusion of the lipids is preserved by a thin water layer ( $\sim 1-2$  nm) between the supporting material and the bilayer. The glass surface can either be planar or in the shape of microbeads (1-10  $\mu\text{m}$  diameter) allowing for various applications such as the investigation of proteins in cell-SLB contacts<sup>19,39,44</sup>.

## 1.2.2 Transmembrane Proteins in SLBs

Most proteins in the cell membrane that are important in cell-cell contacts are transmembrane proteins. However, using supported model membranes to study transmembrane proteins has been problematic especially because the proteins are immobile in SLBs<sup>39,41</sup>. This immobilisation is based on direct interactions of the

proteins with the solid support<sup>45</sup>. The surrounding lipids are not affected by the insertion of transmembrane proteins and maintain their lateral diffusivity. However, many interactions such as the formation of the immunological synapse are dependent on both the diffusivity of lipids and of proteins. Thus, lateral mobility of the studied proteins in supported bilayers is important and can be achieved by forming SLBs on a polymer cushion, which prevents non-specific binding of the protein to the support by separating the lipid bilayer sufficiently far from the solid surface. Extracting and purifying transmembrane proteins from the cell is a difficult process and demands less complex methods to tether proteins to SLBs. It is well known that many cell membrane proteins do not necessarily have a transmembrane domain but are modified with a glycosylphosphatidylinositol (GPI) linker. GPI is a glycolipid that is post-translationally attached to the C-terminus of proteins and results in the incorporation of these GPI-anchored proteins into the membrane (**Figure 1.2.2**)<sup>46</sup>. In addition to naturally occurring GPI-anchored proteins, many proteins can be genetically engineered and linked to GPI<sup>46-48</sup> simplifying their extraction and the subsequent formation of protein tethered SLBs (**Figure 1.2.2**). The GPI-anchored proteins are laterally mobile and have been widely used for membrane protein studies using SLBs<sup>47,48</sup>. Even though extracting these proteins and incorporating them into SLBs is easier than for transmembrane proteins it is still a complex and time-consuming procedure and has been in many cases exchanged with a simpler method linking proteins non-covalently to the model membranes.

### 1.2.3 Non-Covalently Linked Proteins in SLBs

#### Streptavidin-Biotin SLBs

Besides anchoring GPI-linked proteins into SLBs there are several techniques involving non-covalent attachment of proteins to supported model membranes. The very first approach was using phospholipids with modified head groups that can be recognised by antibodies specific for these altered lipids<sup>49,50</sup>. About twenty years later, a second, more widely applicable method evolved using biotinylated lipids and avidin as a linker<sup>51</sup>. Biotin is a B-vitamin and plays a key role in many carboxylation reactions especially in the citric acid cycle that produces energy in the form of adenosine triphosphate (ATP). It is predominantly found in food but is also

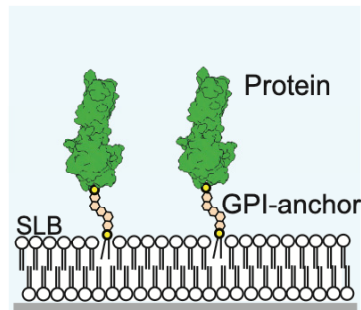


**Figure 1.2.2. Sketch of GPI-anchored proteins to an SLB.**

synthesised by intestinal bacteria. This small molecule can be strongly bound by avidin, a protein that has been found in egg whites of birds, reptiles and amphibians and that is thought to act as an antibiotic protecting the embryo from bacterial growth. Avidin is a highly glycosylated protein and has a tetrameric structure with which it can bind up to four biotin molecules. Another, structurally very similar, protein, streptavidin has a comparable affinity for biotin but lacks glycosylation making it more specific. The binding strength of avidin or streptavidin to biotin is the strongest known non-covalent interaction between two proteins which has been made use of in many biological applications<sup>52,53</sup>. Both, avidin and streptavidin, bind to biotinylated lipids and the unoccupied binding sites can be engaged by genetically modified proteins that have, instead of a GPI-anchor, a biotin molecule attached to the C-terminus enabling the anchoring of biotinylated proteins to SLBs (Figure 1.2.3A).

### Nickel-Chelating SLBs

A third similar, yet more simple, approach makes use of nickel-chelating lipids. Chelators are molecules that strongly bind to metal ions which become chemically inert upon binding. The first theory of metal-ligand binding was proposed by Alfred Werner in 1893 and the most common chelator ethylene diamine tetra acetic acid (EDTA) has been known since the 1920s were it was used in the textile industry to remove calcium during the processing of fabric<sup>54</sup>. Today it is a widely used chemical in medicine and science. Besides EDTA other chelating molecules such as iminodiacetic acid (IDA) or nitrilotriacetic acid (NTA) have been developed. Both

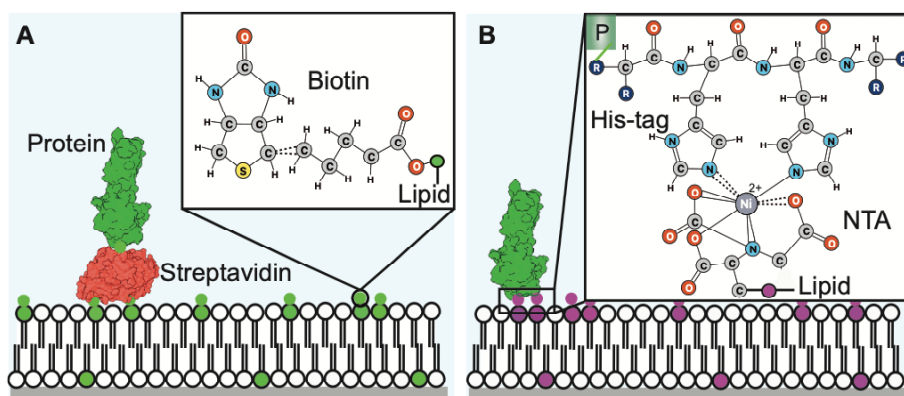


**Figure 1.2.3. Schematic representation of non-covalent protein anchoring to SLBs.**

(A) A biotinylated protein attached to streptavidin that is non-covalently bound to biotinylated lipids (*green lipids*) within an SLB. (B) A protein modified to express six consecutive histidines (His-tag) at its C-terminus binding to NTA-chelated lipids (*purple lipids*) via an ionic interaction to the chelated  $\text{Ni}^{2+}$  ion. *P* is the protein.

are commonly used as a resin in immobilised metal affinity chromatography (IMAC) a method in which proteins are purified from cell lysates. IMAC was first introduced by Porath *et al.* in 1975 when they made use of the strong binding characteristic of histidine to zinc or copper ions<sup>55</sup>. Fixing the ions in an IDA including resin and passing through human serum led to the prominent binding of histidine containing proteins to the resin<sup>55</sup>. Nowadays this process is more specific. Proteins of interest are genetically modified with six or more consecutive histidine molecules at the C-terminus (His-tag), which enables their efficient binding during IMAC and a subsequently better purification from other, non-binding, proteins in the solution. The principle of IMAC has been applied to SLBs by synthesizing lipids with chelating head groups able to bind His-tagged proteins (**Figure 1.2.3B**)<sup>56–58</sup>. The most common chelating agent linked to phospholipids is  $\text{Ni}^{2+}$ -NTA.

Both proteins that are linked to lipids *via* streptavidin-biotin or  $\text{Ni}^{2+}$ -NTA possess, like GPI-anchored proteins, lateral mobility at the SLB and are a perfect tool when studying inter- or intra-protein interactions. However, these two methods work mainly for genetically engineered, so called recombinant, soluble proteins and not for naturally occurring ones such as transmembrane or GPI-linked proteins.



## 1.2.4 Bilayer Formation and Protein Production

### Lipid Bilayer Formation

For the work following in the next chapters SLBs were prepared using vesicle fusion and subsequent protein attachment *via* NTA-His-tag interactions. Consequently, 95% of phospholipids were mixed with 5% NTA-chelating lipids. To ensure a successful formation of SLBs the vesicle solution was sonicated yielding SUVs and the glass support was thoroughly cleaned with piranha solution, a mixture of sulfuric acid and hydrogen peroxide. The cleaning step was necessary to remove any traces of organic residues on the support as well as to render the support hydrophilic. The vesicles were added to the support and incubated for one hour. Unruptured vesicles were washed off before the His-tagged proteins were added and attached to the SLB. The main advantage of using vesicles was the formation of continuous and robust unilamellar bilayers through a very simple approach (**Figure 1.2.4A-C**). Spin coating is also a simple way of distributing lipids onto a support but gives inconsistent unilamellar or multilamellar bilayers after hydration (**Figure 1.2.4D-F**). Moreover, the lipids are distributed over the whole area of the supporting material resulting in an excess use of lipids and proteins. Working with vesicle-solutions allowed for a high freedom over the total area of the formed SLBs since the solutions can be added to either the whole support or a confined area on it reducing the amount of added lipids and proteins (**Figure 1.2.4A, D**). Distributing a bilayer from the water-air interface is particularly useful in preparing asymmetrical bilayers, but the method due to its complexity and specific usage is not further considered.

### Producing and Tethering Proteins

All of the studied proteins in this work (besides Streptavidin) were attached to the SLBs *via* His-tags. The recombinant proteins were modified with a single (6x His) or double (12x His) His-tag in place of the transmembrane and cytoplasmic domains, and were produced *via* transient transfections in human cell lines<sup>59</sup>. Transient transfection is the process of incorporating genetic material (*e.g.*, DNA) into cells temporarily, *i.e.*, the DNA does not incorporate into the cell's genome<sup>59</sup>. The gene of interest was carried on a plasmid (circular DNA) into the cells *via* a

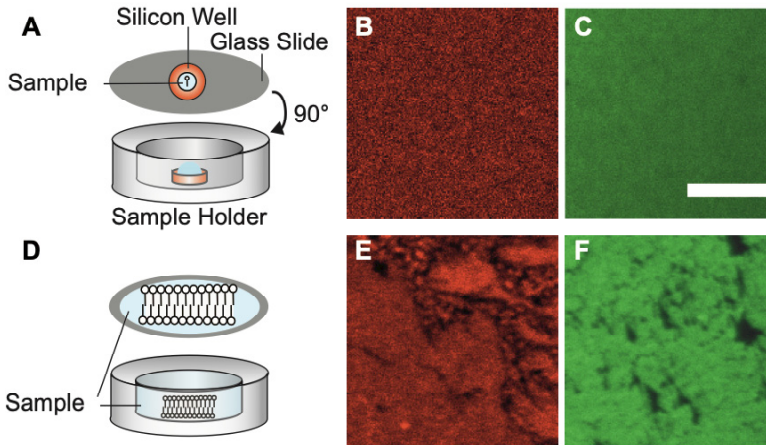


**Figure 1.2.4. Comparison between vesicle fusion and spin coating.**

(A) Schematic representation of the sample for vesicle fusion. Using a silicon well on the glass slide reduces the area of the formed bilayer and the amount of added proteins. (B, C) Confocal images of continuous fluid SLBs formed *via* vesicle fusion. Scale bar 5  $\mu\text{m}$ . (D) Schematic representation of the spin coated sample on the glass slide and in the sample holder. The whole glass slide is covered. (E, F) Confocal images of SLBs formed *via* spin coating. The SLBs are patchy due to unevenly formed SLBs. Red and green areas represent fluid fluorescent bilayers. Areas in black show no SLBs formation.

cationic polymer (polyethyleneimine (PEI) or gene juice<sup>®</sup>) to allow the entrance of the negatively charged nucleic acid into the cell. Once the DNA is in the cell it is delivered to the nucleus ready to be transcribed and translated into the respective proteins. The introduced DNA contains a specific signal sequence that directs the cells to transport the newly synthesised proteins to the cell membrane. Since the proteins no longer express a transmembrane and cytoplasmic domain this transport leads to the secretion of the His-tagged proteins into the cell media, *i.e.*, supernatant. The protein containing supernatant was collected over 5-7 days. To separate the His-tagged proteins from other proteins (especially bovine serum albumin (BSA)) and chemicals in the supernatant  $\text{Ni}^{2+}$ -NTA-beads were used to bind the His-tagged proteins according to the IMAC principle. To further remove trace contaminants and protein aggregates size exclusion chromatography (SEC) was used. IMAC and SEC in combination allowed for purification of pure, concentrated protein. The proteins were then labelled with fluorophores called Alexa Fluor<sup>®</sup> 647, a red

fluorescent dye, or Alexa Fluor® 488, a green fluorescent dye, and stored at  $-80^{\circ}\text{C}$  in HBS-buffer (HEPES buffered saline) until further.

The use of non-covalently linked proteins was preferred over the use of GPI-linked proteins due to the simplicity in producing, purifying and attaching them to the SLBs. Moreover, the aim of the thesis work was to investigate protein interactions and binding affinities. As outlined above there are two established methods to non-covalently link proteins to SLBs either *via* NTA-chelating lipids or biotin-streptavidin interactions. Of these NTA-chelating lipids were preferred here as (i) NTA-chelating lipids introduce only a minor extension of the protein to SLB distance and (ii) interaction studies are not affected by the bulk of a second protein. This was especially critical for the work in Chapter 2, where the height of proteins and interprotein interactions were studied as well as for Chapter 3 investigating the binding behaviour of two receptor/ligand systems spanning an important membrane to membrane distance of  $\sim 15$  nm. Using streptavidin-biotin linked proteins would have extended the protein-SLB distance by at least 5 nm, the height of streptavidin, and would have had hard to distinguish effects on the effective height and intermolecular interactions of the studied proteins as well as their binding behaviour in cell-SLB contacts. A minor drawback of attaching proteins *via* the ionic  $\text{Ni}^{2+}$ -NTA-Histidine interaction is that the proteins detach from the SLBs over time<sup>60</sup>. This is particularly problematic when working with more than one protein species at the bilayer since they compete for the same binding positions. However, this can be compensated for by adjusting the protein concentrations and/or limiting the time of the measurements.

### 1.3 Microscopy Techniques to Quantify Functionalised SLBs

Microscopy has evolved as the main method to visualise and quantify SLBs and proteins or cells bound to it. This is facilitated by the planar geometry of the support and various possible material choices ranging from glass over silicon to mica. A non-invasive and widely used microscopy technique to examine functionalised SLBs on glass is fluorescence microscopy. It is an optical imaging technique used in light microscopes which allows for the excitation of fluorophores. Fluorophores are

chemical compounds that can absorb and re-emit light. The absorption of a photon (a light particle) leads to a brief excitation of an electron in a fluorophore that subsequently enters the ground state again by emitting the energy as a photon of a longer wavelength (lower energy) in comparison to the shorter wavelength (higher energy) of the absorbed photon. The emitted photons are detectable by a camera or photomultiplier tube creating an intensity dependent grey scale image. Fluorescence microscopy is a highly sensitive and reliable method used to study the localisation of molecules as well as to visualise dynamic processes in cells, cell membranes or at SLBs. Different microscopy techniques based on fluorescence exist allowing for a wide range of image resolution and extracted information. Whereas conventional fluorescence microscopy techniques, such as confocal microscopy or epifluorescence techniques can resolve structures to a maximum of 200 nm, super-resolution techniques can distinguish structures down to a level of 20 nm. These are however not yet applicable to a high variety of studied systems due to major potential drawbacks such as the requirement for special fluorophores, slow image acquisition and the occurrence of high phototoxicity (for further information see references<sup>61,62</sup>). The applied microscopy methods in this work are explained in the following subsections.

### 1.3.1 Epifluorescence Microscopy

Fluorescence microscopy is a powerful tool that became particularly popular in the 1960s after J.S. Phloem refined the use of epi-fluorescence microscopy<sup>63–65</sup>. “Epi” originates from the Greek, meaning “same” and describes the illumination of a sample with an incident light ray coming from the same side at which the emitted light is collected (**Figure 1.3.1**). To allow for epifluorescence or epi-illumination a dichroic mirror is used separating the excitation light from the emission light (**Figure 1.3.1**). It does this by reflecting shorter wavelengths coming from the light source and transmitting longer wavelengths of the emitted fluorescence from the sample. Additionally, excitation filters as well as emission filters are commonly used together with the dichroic mirror. The excitation filter preselects the excitation wavelength and the emission filter allows specific longer wavelength to pass through to the detector (**Figure 1.3.1**). Hence, in epifluorescence microscopy the excitation light

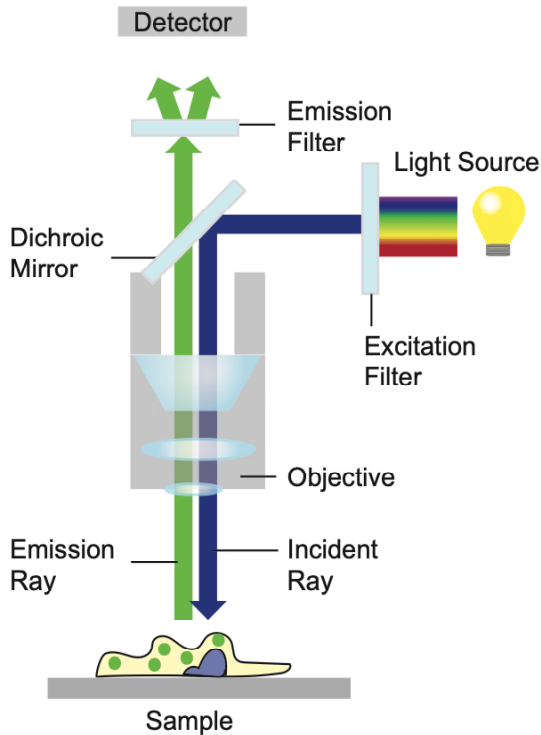


**Figure 1.3.1. Schematic illustration of an epifluorescence microscope setup.**

The excitation light passes through an excitation filter specific for one wavelength (*blue line*), continues via the dichroic mirror through the objective onto the sample and excites the fluorophores. The emitted fluorescent signal by the fluorophores is collected by the objective and reaches the detector upon passing the dichroic mirror and the emission filter.

interferes less with the fluorescent signal from the sample than in transmission light microscopy (see Section 1.3.5), generating more reliable data. Epifluorescence microscopy has been widely used for co-localisation studies of different fluorescently-labelled molecules as well as for structural studies in cell biology. However, objects that are less than 200 nm apart cannot be resolved using conventional epifluorescence microscopy. Moreover, in-focus as well as out-of-focus light will be collected by the detector causing low resolution in three dimensions. The need for techniques avoiding out-of-focus light and with the development of more powerful light sources (lasers) than arc lamps (mercury or xenon), two, more technically advanced, methods evolved from epifluorescence microscopy: Total Internal Reflection Fluorescence Microscopy (TIRF) and Laser Scanning Confocal Microscopy (LSCM).

### 1.3.2 Total Internal Reflection Fluorescence Microscopy

Fluorescence microscopy techniques are the natural choice to observe single events and molecules at high resolution. Most of the common techniques such as epifluorescence and confocal microscopes, however, are not optimal for imaging near the plasma membrane or SLBs. In epifluorescence, as mentioned above, strong background fluorescence appears from fluorescent proteins in the bulk or from the autofluorescence of other cellular structures in the cytosol. Hence, small structures and single molecules near the membrane cannot be distinguished from the 'background-noise'. A development that overcame this problem was evanescent field fluorescence microscopy. TIRF microscopy is one of the most common techniques using the advantage of an evanescent field or wave<sup>66-68</sup> and allows for the selective excitation of fluorophores near the sample surface while minimising background fluorescence from the bulk.

#### Principle of TIRF

There are two main optical arrangements for TIRF, one that uses a prism and another one that uses a high numerical aperture (NA) microscope objective to direct the light towards the total internal reflection interface. The latter one is also called the "through-the-objective" TIRF and is today the most commonly used TIRF technique. This section focusses therefore on through-the-objective TIRF microscopy. Total internal reflection is the basis of TIRF microscopy and occurs when light passes from a high refractive index ( $n_1$ ) medium into a medium with a low refractive index ( $n_2$ ) (**Figure 1.3.2**). The refractive index ( $n$ ) describes how fast light travels through a specific medium in respect to how fast it travels in vacuum. A high refractive index means that the light travels slower through the medium. At the interface of two media that differ in their refractive indices, the light beam experiences a change in speed and direction of propagation due to refraction which can cause total internal reflection. Total internal reflection is dependent on two angles, the incident ( $\theta_1$ ) and the critical angle ( $\theta_{\text{critical}}$ ). The incident angle is usually smaller than the critical angle and the light that hits the sample (medium with the low refractive index) passes through it (**Ray A, Figure 1.3.2**). If the incident angle

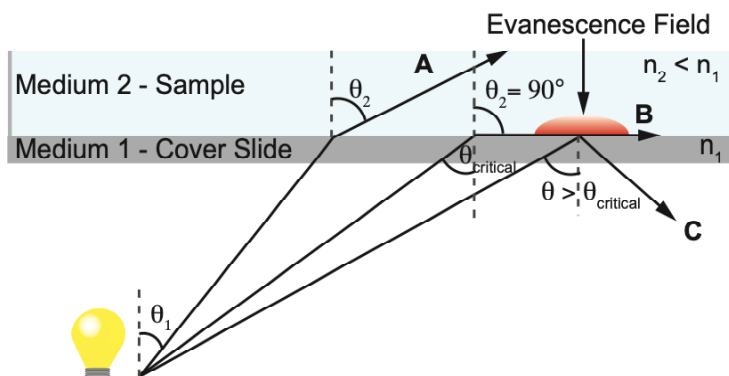


**Figure 1.3.2. Schematic drawing of the cross over from refraction to reflection.**

**(Ray A)** Incident light hits an interface between two media at an angle ( $\theta_1$ ) that is smaller than the critical angle ( $\theta_{\text{critical}}$ ). The light passes through the sample. **(Ray B)** The angle of the incident light equals the critical angle and the refractive angle ( $\theta_2$ ) is  $90^\circ$ . The light travels along the interface. **(Ray C)** Increasing the incident angle even further leads to total internal reflection at the interface creating an evanescence field indicated in red.  $n_1$  and  $n_2$  denote the refractive indices of the two media which are a cover slide and an aqueous sample, respectively.

increases and reaches the value of the critical angle, the light does not pass through the sample but travels along the interface (**Ray B, Figure 1.3.2**). An even further increase of the incident angle leads to a total internal reflection at the interface between the sample and the cover slip (**Ray C, Figure 1.3.2**). In that case, no incident light is passing through the sample but some of the incident energy penetrates across the interface and creates an energy wave called the evanescence wave or evanescence field. This thin electromagnetic field has the same frequency as the incident light and has enough energy to excite fluorophores near the surface. The electromagnetic field decays exponentially in intensity with distance from the surface avoiding any excitation of fluorophores farther into the sample. A minimal exposure to light leads to a very low background and almost no out-of-focus fluorescence. Hence, captured images are of high contrast with a maximum penetration depth of about 100 nm which gives a better resolution along the  $z$ -axis than what can be obtained using epifluorescence microscopy.

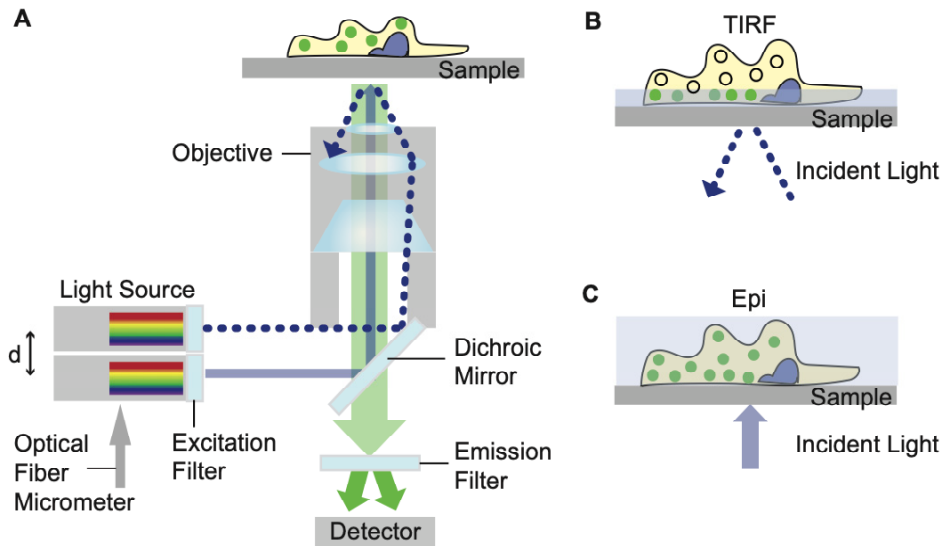


**Figure 1.3.3. Concept of TIRF and epi-illumination.**

(A) Schematic representation of the optical path for epifluorescence (solid blue line) and TIRF (dashed blue line) in an inverted microscope illuminating a sample placed on a cover slide. An optical fiber micrometer allows for a controlled movement of the optical fiber, where  $d$  represents the change in distance that is necessary to reach TIRF mode from epifluorescence mode. (B) In TIRF mode only the fluorophores in the area of the evanescent field are excited and visualised. (C) In epifluorescence mode, the whole sample is illuminated which excites all fluorophores.

### Advantages

Through-the-objective TIRF has advantages that were particularly useful for the two projects in this thesis. First, TIRF is compatible with other microscopy techniques as the angle of incident light can be adjusted and turn the TIRF mode into epifluorescence mode and *vice versa* (Figure 1.3.3A). The optical fiber micrometer (or mirrors) plays a key role in adjusting this angle. Moving the micrometer (or mirrors) leads to a change of the optical fiber position with respect to the optical axis and increases or decreases the axial radial distance. TIRF occurs at an increased axial radial distance at which the critical angle is exceeded (Figure 1.3.3B). Decreasing the axial radial distance positions the laser beam into epifluorescence mode (Figure 1.3.3C). As mentioned before, another advantage is that by using TIRF only a very thin section at the lower part of the sample is excited and thus illuminated, whereas the rest of the sample is not exposed to excitation light. This results in less out-of-focus fluorescence as well as a low amount of phototoxicity throughout the cell.



Dependent on the sensitivity of the camera and the depth of the evanescent field TIRF microscopy allows for imaging of single molecules and their motion across the sample view. These motions can be used to calculate the diffusion coefficient of the molecule. At higher molecule or protein densities the diffusion coefficient is obtained by bleaching an area of fluorescently-labelled proteins and following the intensity recovery of the fluorescent signal due to the exchange or motion of other proteins into the bleached region. This process is called fluorescence recovery after photobleaching (FRAP) and is commonly used together with TIRF (see Section 1.3.4). One major drawback of TIRF is that despite TIRF allowing for a higher  $z$ -resolution ( $<100$  nm) than confocal microscopy, with a resolution limit of around 300 nm, it is limited by the evanescent wave to areas near the objective (close to the surface). Thus, TIRF does not allow for imaging of thicker samples such as a complete cell for which confocal microscopy was the method of choice.

### 1.3.3 Confocal Microscopy

Confocal microscopy, similar to TIRF microscopy, has the advantage of a decreased out-of-focus glare over epifluorescence microscopy and is furthermore able to collect serial optical sections throughout the sample offering an important advantage over TIRF microscopy too. It was originally introduced by Marvin Minsky in 1957 and has since become one of the standard techniques used in biomedical science<sup>69</sup>. The most important feature of a confocal microscope is the placing of a pinhole in front of the detector rejecting most of the out-of-focus information, which increases the  $z$ -resolution but at the cost of signal intensity. A specific technique of confocal microscopy is LSCM where the illumination of the sample is achieved by scanning the sample with a focussed beam of light usually generated by a laser. This focussed laser beam is considered to be a point light source that illuminates the sample consecutively and builds up the image point by point, in contrast to conventional widefield microscopy in which the entire sample is illuminated at once.

## Principle of Laser Scanning Confocal Microscopy

LSCM is based on the principles of epifluorescence microscopy (see Section 1.3.1) with just minor differences in the setup of the microscope. Light emitted by the laser system, the excitation source, passes through a pinhole aperture placed in front of the light source resulting in a point-like laser beam (**Figure 1.3.4**). The laser beam then hits a dichroic mirror and is reflected through an objective onto the sample in defined focal planes scanning various sections of the sample. The emitted light from the sample passes back through the objective as well as the dichroic mirror towards a second pinhole that is placed in front of the detector (**Figure 1.3.4**). The pinhole is placed in a *conjugated* plane to the *focus* point on the sample describing the main feature of *confocal* microscopy in which the emitted light is focussed as a confocal point on the detector's pinhole aperture. As for epifluorescence the dichroic mirror is accompanied by an excitation and emission filter. Any fluorescent signal that occurs below or above the original focal plane is predominantly not confocal with the detector's pinhole aperture and thus not collected by the detector, typically a photomultiplier tube (**Figure 1.3.4**). The focus on the sample ( $z$ -axis) can be changed by the user. This shifts the excitation and emission points to a new ( $x$ - $y$ ) plane along the  $z$ -axis that is automatically confocal with the pinhole apertures in the system. By laterally scanning the point-like laser beam over the specific  $x$ - $y$  plane that was placed in focus (at a particular  $z$ -axis depth) the sample's fluorescence intensity in that plane is reconstructed pixel-by-pixel in an  $x$ - $y$  image. Scanning through various  $z$ -depths and recording an  $x$ - $y$  image on each allows for a three-dimensional (3D) reconstruction of the sample (**Figure 1.3.5**). The resolution in the  $z$ -axis is not the same as in  $x$  and  $y$ , and mainly controlled by the pinhole size and the amount of rejected light. Thus, the smaller the pinhole the better the  $z$ -axis resolution. However, the collected light minimises with decreasing pinhole sizes limiting the minimum useful size of a pinhole, which is typically of one Airy unit (the diffraction limit of light) (see below).

## Resolution in the Horizontal and Vertical Plane

Resolution describes the distance at which two objects remain distinguishable from each other. Lateral resolution depends on the wavelength of light ( $\lambda$ ) and the

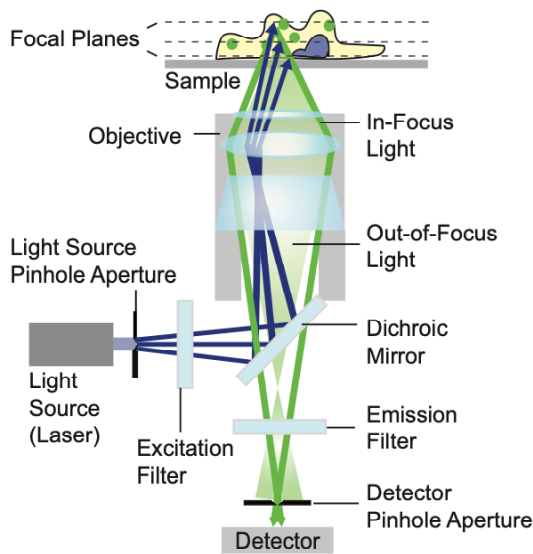


**Figure 1.3.4. Concept of LSCM<sup>70</sup>.**

The laser beam (*blue*) passes through a pinhole and an excitation filter onto a dichroic mirror. The dichroic mirror reflects the laser beam towards the objective which focusses it onto the sample. The emitted light (*green*) from the sample passes back through the objective, the dichroic mirror and an emission filter to the pinhole in front of the detector. Out-of-focus light will mostly be rejected, and in-focus light passes through to the detector. The light can be focussed at different focal planes allowing to scan the sample in *x-y-z*.

numerical aperture (NA), which is a dimensionless value that represents the range of angles over which light can be collected by the optical system, and is given by:

$$r = \frac{0.61 \lambda}{NA} \quad \text{Eq. 1.1}$$

where  $r$  is the minimum resolved distance between two points. This relation is commonly known as the Rayleigh criterion and is based on the model of Airy disks. An Airy disk describes a point-focussed spot of light limited only by diffraction and is basically the image of a single point object in a microscope image. It appears as a bright circular region surrounded by less intense concentric rings and is dependent on the wavelength of light and the NA (see Eq. 1.1). Thus, in the Rayleigh criterion,  $r$  is the radius of the Airy disk describing the distance between the maximum intensity in the center and the first minimum of the Airy disk. The radius of the maximum intensity within the Airy disk, *i.e.*, one Airy unit, defines the minimum pinhole radius used in confocal microscopy and thus the minimum distance at which two points can be individually distinguished. Light intensities along the vertical axis vary in a different manner compared to the horizontal plane. Thus, the Rayleigh criterion cannot easily be transferred to explain vertical or axial resolution (*z*-axis) since the axial resolution is mainly dependent on the amount of light that is excluded by the pinhole and the relation between the area of the out-of-focus light and the

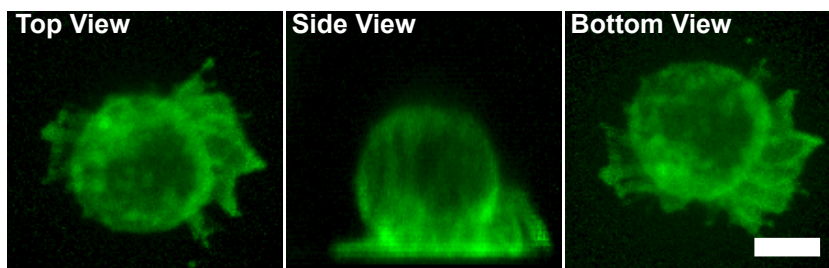


**Figure 1.3.5. Single cell visualised in a 3D-stack.**

Confocal images of a cell bound to a glass surface. The membrane was labelled with a green fluorescent dye and images were taken at various focal planes throughout the cell. The resolution in the  $z$ -axis (*side view*) is blurrier compared to the ones of each focal plane or the composite of all in  $x$ - $y$  (*top and bottom view*). Scale bar 5  $\mu\text{m}$ .

pinhole size. The amount out-of-focus light spreads is dependent on the NA and a higher NA increases the axial resolution. However, whereas the horizontal resolution depends linearly on the NA, the axial resolution changes with  $\text{NA}^2$ <sup>71</sup>. Hence, the resolution in the vertical plane is constantly worse compared to the horizontal plane (**Figure 1.3.5**).

### 1.3.4 Spinning Disk Confocal Microscopy

LSCM is generally appreciated for its high-image quality however, there is a trade-off between image resolution and speed. Capturing the full image by scanning the sample pixel by pixel is accompanied by a system dependent time delay for images covering larger areas<sup>72</sup>, introducing a substantial error in time dependent image acquisition. For fixed samples this might not be a limiting factor, however when analysing mobile proteins or cell signalling events this time effect might be significant. Spinning disk confocal microscopy overcomes this limitation by using an expanded collimated beam illuminating a collection of micro-lenses prearranged on a (collector) disk (**Figure 1.3.6**)<sup>73,74</sup>. To each micro-lens there is a pinhole aperture laterally co-aligned. All pinholes are arranged on a second disk which is axially positioned at the focal plane of the micro-lenses (**Figure 1.3.6**). An electric motor drives the disc to rotate at high speed leading to an array of focussed laser beams that scan the sample at various positions simultaneously. This approach decreases the time it takes to scan the entire image considerably and was here used for measuring

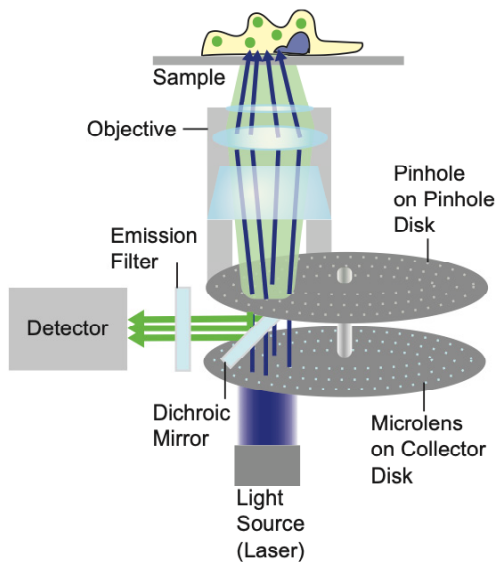


**Figure 1.3.6. Schematic illustration of a spinning disk confocal microscope.**

A collimated laser beam (*blue*) is focussed by micro-lenses arranged on a collector disk and pinholes arranged on a pinhole disk through the objective and onto the sample allowing the scanning of different areas of the sample at the same time. The emitted light (*green*) travels back through the objective and the pinholes on the pinhole disk and lastly gets reflected by the dichroic mirror towards the detector.

the diffusion coefficient of cell membrane proteins (see Section 1.3.5).

### 1.3.5 Fluorescence Recovery After Photobleaching

Bleaching is an unwanted side-effect of fluorophores and describes the permanent loss of fluorescent signal emitted from the fluorophore. Theoretically the excited electrons can cycle between ground state and excitation state infinitely, but this is not the case in reality and exposure to high energy light can lead to photochemical alteration and hence, bleaching of the fluorophore. This phenomenon was used in the 1970s by Axelrod *et al.* to measure the two-dimensional (2D) lateral mobility or diffusion of fluorescently-labelled molecules in a single region of a cell membrane<sup>75</sup>. To that end a small area of the fluorescent sample is exposed to a focussed laser beam of high intensity resulting in the bleaching of the fluorescent signal in this area (Figure 1.3.7). The recovery of the fluorescence can subsequently be visualised by the same but attenuated laser beam (Figure 1.3.7). Hence, the method is called fluorescence recovery after photobleaching, in short FRAP. Since bleaching is a permanent reaction the recovery of the fluorescence is observed due to new fluorescent molecules mixing with the bleached ones by moving in and out of the bleached region, respectively (Figure 1.3.7). Following fluorescence recovery gives

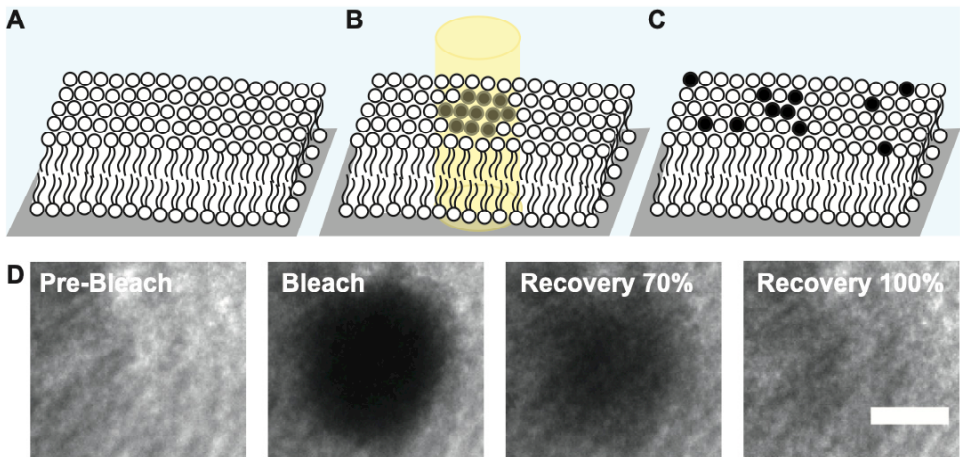


**Figure 1.3.7. Mechanism of FRAP.**

(A-C) Schematic representation of FRAP on a fluorescently-labelled SLB. (A) A fluid SLB with fluorescently-labelled lipids. (B) Bleaching of some of the fluorophores with a high intensity laser beam in a confined area. (C) The exchange of fluorescently-labelled and bleached lipids due to diffusion. (D) Images of a fluorescently-labelled SLB taken with a TIRF microscope before bleaching and immediately after bleaching at  $t=0$  seconds when all the fluorescence in the bleached area is destroyed (appears in *black*). The two images to the right show the recovery of the fluorescence intensity due to lipid diffusion as represented in (C). Scale bar is 10  $\mu\text{m}$ .

information about the mobility of the molecules within the surface they are moving in, and about the fractions of mobile and immobile proteins. FRAP measurements are an important tool for estimating the diffusion coefficient of the fluorescently-labelled molecules and were done on a routine basis in this work to estimate the fluidity of the proteins on the SLBs. It was mainly a measure of successful bilayer formation since fluorescently-labelled proteins on glass or on a disrupted bilayer are immobile and thus, no fluorescence recovery occurs. Moreover, FRAP was used in Chapter 3 to estimate both the mobility of the studied cell membrane receptors as well as the diffusivity of proteins within a cell-SLB contact (Paper III).

### 1.3.6 Transmission Light Microscopy

Transmission light microscopy is a light microscopy technique that does not require a fluorescent sample. It is based on a white light ray passing through the sample towards the objective of the microscope. Before the light reaches the sample, it is

directed through a condenser that controls the angle at which the concentrated light ray hits the sample allowing for the right contrast and resolution. Both, the condenser and the light-collecting objective are oriented on two separate axes that need to be aligned to permit a sharp image. Transmission light microscopy is a very useful technique to observe whole living organisms or thicker tissue structures. One technique based on transmission light microscopy is bright field microscopy. In this technique transmitted light is attenuated by thicker parts of the sample leading to darker, sample defined, areas on a light background. Using bright field in this study permitted distinction of dead and live cells bound to protein functionalised SLBs.

### 1.3.7 Summary of the Applied Methods

Most of the work in this thesis involved protein-functionalised SLBs, and TIRF was chosen as the main microscopy method to visualise these. TIRF was preferred over epifluorescence due to a diminished effect of background fluorescence from the bulk improving the image quality. Additionally, TIRF has a faster throughput and higher laser intensity than LSCM. This combined with a sensitive camera allows for the distinction of fine structures in the membranes or fine intensity changes such as the process of bilayer formation from vesicle fusion (**Figure 1.3.8**). For complete cell imaging confocal microscopy was favoured over TIRF owing to its better resolution in the  $z$ -axis. The mobility of proteins within cell membranes and cell-SLB contacts was measured using a spinning disk confocal microscope allowing for a higher sensitivity and faster image acquisition.

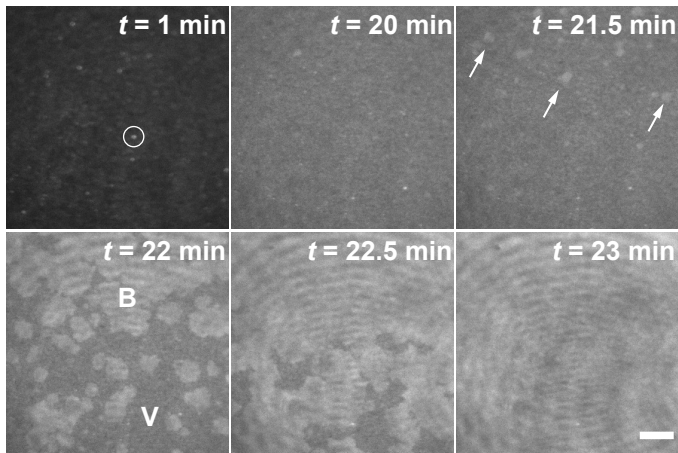


**Figure 1.3.8. SLB formation after vesicle fusion.**

Shown are TIRF images of landing vesicles (see *white circle*) on to the cleaned glass support. The intensity increases over 20 minutes since more vesicles land. At roughly 21.5 minutes nucleation points of bilayer formation (indicated by arrows) appear. 30 seconds later the nucleation spreads from top to bottom forming bilayer patches (B) and unruptured vesicle patches (V). After 23 minutes all vesicles have ruptured and the SLB has formed. Scale bar is 10  $\mu\text{m}$ .





## Chapter 2

*Sie hat alles, was sie braucht, alles außer den Eiern. Eier...  
sind schwer aufzutreiben.*

-David Benioff, *Stadt der Diebe*, 2008-



# 2 Dimensions and Orientations of Glycoproteins on Model Membranes

## Contents

---

2.1 T-Cell Receptor Triggering.....	46
2.1.1 Conformational Change and Force.....	47
2.1.2 Kinetic Segregation.....	49
2.2 Large Glycoproteins.....	51
2.2.1 CD45 and its Isoforms.....	51
2.2.2 CD43.....	52
2.2.3 Structural Studies Using Microscopy.....	53
2.3 Trapping of CD2, CD4 and CD45RABC.....	57
2.3.1 Principle of Hydrodynamic Trapping.....	57
2.3.2 Considerations of the Method.....	59
2.3.3 The Measured Proteins.....	60
2.3.4 Dimensions and Orientations of CD2, CD4 and CD45RABC.....	61
2.3.5 Conclusion.....	66
2.4 Dimensional Studies of CD45 and CD43.....	67
2.4.1 Trapping of CD45D1-D4, CD45R0 and CD43.....	68
2.4.2 Dimensions in Solution.....	70
2.4.3 Summary.....	74
2.4.4 Outlook.....	74

---

In Chapter 2 I will introduce the concept of T-cell receptor triggering and briefly review current models explaining the translational-step between cell contact formation and signalling. The focus will then move on to explain the kinetic segregation model and the role of tall glycoproteins in more detail. How the structures of these proteins have been studied so far will be laid out next. The recent findings of **Paper I** and **II** in which the new method, hydrodynamic trapping, has been used to obtain information about the dimensions and orientations of transmembrane proteins including glycoproteins will be summarised and further extended by the latest observations.

## 2.1 T-Cell Receptor Triggering

Central to the body's immune system are TCRs that recognise pathogenic peptides presented on MHCs. This process must be highly specific since the expressed MHCs on an infected cell display abundant numbers of self (body's own) peptides and only a few pathogenic peptides. A common belief is that the affinity with which the TCR binds to foreign or self-peptide MHCs varies and that high affinity complexes and/or complexes of a long lifetime induce signalling. This supports the kinetic proofreading model proposed by McKeithan in 1995<sup>76</sup>. The model suggests that the TCR-MHC interaction does not cause an immediate signal for T-cell activation but that instead several intermediate events occur and accumulate to a final (critical) event necessary for signalling<sup>76</sup>. All of those steps take time separating the initial binding event from the signalling outcome. Thus, only 'long-lived' and/or higher affinity TCR-MHC interactions induced by pathogenic peptides lead to activation of the TCR. Short lived interactions between TCRs binding to self-peptide MHCs dissociate before the final signalling event(s) can occur maintaining the cell in a non-activated state. It has been argued that a high affinity characterised by a fast on-rate (how fast the TCR binds to the MHC) and a slow off-rate (how slowly they dissociate) determines the lifetime of the TCR-MHC complex<sup>8</sup>. However, in other studies it has been shown that a fast on-rate alone is sufficient for T-cell activation<sup>12,77</sup>. A fast on-rate lowers the number of TCRs that need to be engaged for successful peptide MHC binding increasing the overall fraction of bound TCRs to agonist MHCs. It is yet to be determined whether affinity, lifetime, or both determine the levels of T-cell activation.

The activation of a T cell is, as noted in the Introductory Chapter, a multistep process and starts with the phosphorylation of the TCR. The TCR itself has no signalling components but associates naturally with the CD3 co-receptor and  $\zeta$ -chains forming the TCR-CD3 complex. The cytoplasmic domains of CD3 and the  $\zeta$ -chains contain the immunoreceptor tyrosine-based activation motifs (ITAM) that are the sites for phosphorylation by Lck<sup>78</sup>. Lck is either freely diffusing or associated with the cytoplasmic tail of the CD4 or CD8 co-receptor that colocalise with the TCR-MHC complex bringing Lck in close proximity to the TCR-CD3 complex<sup>78</sup>.

Once the ITAMs are phosphorylated they create binding sites for ZAP-70 which causes subsequent T-cell activation<sup>79</sup>. Whereas all the following downstream signals are well known (reviewed for example here<sup>80,81</sup>) the mechanism of how the TCR complex is triggered has, despite extensive studies, not been resolved. Several models have been proposed to explain what causes the initial phosphorylation by Lck upon MHC binding and these include conformational changes in the TCR, mechanotransduction and kinetic segregation of TCR and CD45 molecules<sup>16,82,83</sup>. CD45 is a key molecule in the latter model due to its structure<sup>82</sup> but structural information about this complex molecule on the cell membrane is lacking. Hence, there is a need for new techniques to obtain structural data about CD45 as well as other large glycoproteins such as CD43 to fully understand their role in the cellular context including the KS model. Before the KS model will be described in detail a brief introduction into other competing ideas will be given.

### 2.1.1 Conformational Change and Force

The kinetic proofreading model led to several possibilities on what defines the first step in T-cell activation. One model type suggests that the TCR-MHC interaction causes a conformational change in the TCR resulting in dimerisation or aggregation. However, comparing the structures of TCRs that are bound to MHC or not, revealed structural changes mainly in the hypervariable loops which are part of the variable Ig domains responsible for binding to the peptide and the MHC cleft holding it but not distal to this binding site<sup>16,84</sup>. Other studies suggest a conformational change by a reorientation of the TCR versus its associated CD3 and  $\zeta$ -chains<sup>85,86</sup>. These conformational changes could be of various types including, *e.g.*, that the ITAMs of CD3 and the  $\zeta$ -chains associate with acidic phospholipids in the membrane burying the tyrosine residues (**Figure 2.1.1A**). Binding to MHC would release these ITAMs, which become immediately accessible for phosphorylation (**Figure 2.1.1A**). Another conformational change model involves the two  $\zeta$ -chains that are spread apart when the TCR complex is in an unbound state but reorient after TCR-MHC binding leading to signalling (**Figure 2.1.1B**)<sup>87</sup>. What exactly causes these conformational changes is not obvious but recent experimental evidence suggests that the TCR complex responds to mechanical forces<sup>16,87–89</sup>. This force can

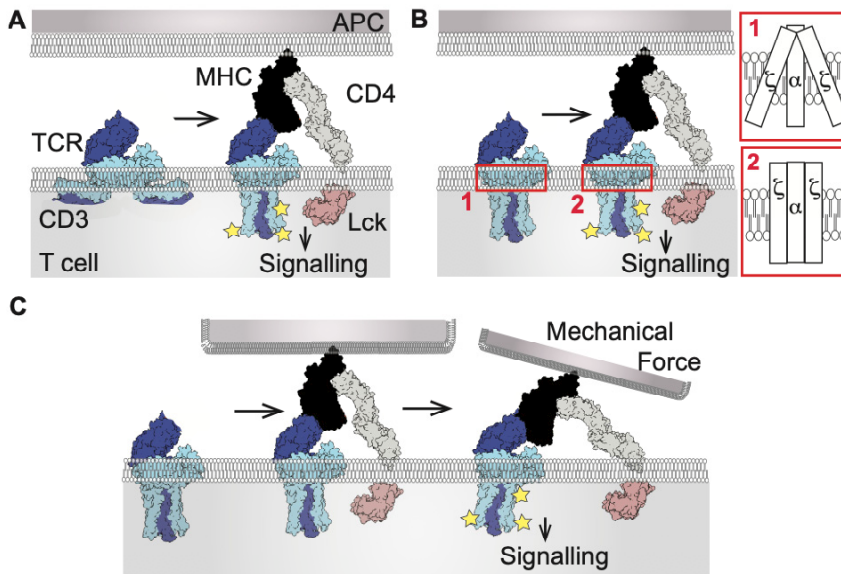


**Figure 2.1.1. TCR triggering by conformational change and mechanotransduction.**

(A) CD3 ITAMs are buried in the membrane. Upon binding of MHC they change conformation and can be phosphorylated. (B) A conformational change in the  $\zeta$ -chains of the TCR-CD3 complex upon MHC binding. (C) Conformational changes such as shown in A and B can be induced by a force exerted through the crawling of a T cell over an APC.

be exerted by a cytoskeletal mechanism acting internally on the receptors or by the T cell crawling over the APC while binding to the MHC. In the latter case TCR-MHC binding exerts a bending force on the TCR, because of the T cell movement, inducing conformational changes (Figure 2.1.1C). Direct evidence for TCRs acting as mechanosensors was shown experimentally using optically trapped beads and exerting shear forces onto the TCR-MHC complex or by using a biomembrane force probe (see Chapter 3), revealing that force can, dependent on its magnitude, induce signalling events<sup>90,91</sup>. Despite some compelling studies the exact mechanism by which the structural changes occur is not known and thus, more research is required to understand and clarify the role of force and TCR conformational changes in initiating TCR phosphorylation.

### 2.1.2 Kinetic Segregation

The KS model is based on the dynamic phosphorylation of the TCR by kinases and phosphatases<sup>82</sup>. This occurs as T cell membrane proteins freely diffuse laterally in the membrane exposing the ITAMs of the TCR-CD3 complex to kinases like Lck and phosphatases such as CD45 (**Figure 2.1.2A**). The continuous phosphorylation (activation) and dephosphorylation (deactivation) does, however, not lead to T-cell activation since the phosphorylated TCR-CD3 complex is only short lived as the phosphatases are in large excess. When a T cell encounters an APC CD2 or other small sized cell-cell recognition proteins initiate close contact formation by spanning a ~15 nm distance between the two opposing membranes<sup>82</sup>. The close contacts facilitate the surface scanning of APCs by TCRs and subsequent binding of the TCR to agonist-peptide MHCs, as well as the passive exclusion of tall glycoproteins such as the phosphatase CD45 (**Figure 2.1.2B and C**)<sup>8,82</sup>. This shifts the kinase phosphatase balance within the contact, resulting in net phosphorylation of the TCRs distributed in the contact zones<sup>82</sup>. TCRs not engaged will diffuse out of the contact and will be dephosphorylated before any downstream signalling can occur. To ensure this the close contact zones must be of small enough size (contact radius < 220 nm) as large areas will cause ligand independent signalling<sup>82,92</sup> which could lead to aberrant signalling and autoimmune disease. TCRs bound to agonist-peptide MHC molecules, however, stay sufficiently long in the contact to become phosphorylated, recruit ZAP-70 and cause T-cell activation. The potency of the TCR-MHC interaction is therefore related to both its half-life (lifetime) and its affinity which determine whether the TCR stays in the contact zone or diffuses out abrogating signalling.

Important to keep in mind is that the formation of close contacts occurs before the formation of an immunological synapse (see Introductory Chapter) and is triggering independent. Thus, no signalling dependent processes such as cytoskeletal rearrangement are involved in the initiation of TCR triggering by CD45 exclusion. In addition, the KS model requires that the excluded CD45 molecules possess a large and rigid extracellular domain to allow for steric effects causing exclusion. However, only parts of the full-length CD45 have been structurally resolved as the N-terminal mucin-like segment cannot be crystallised or clearly visualised using currently



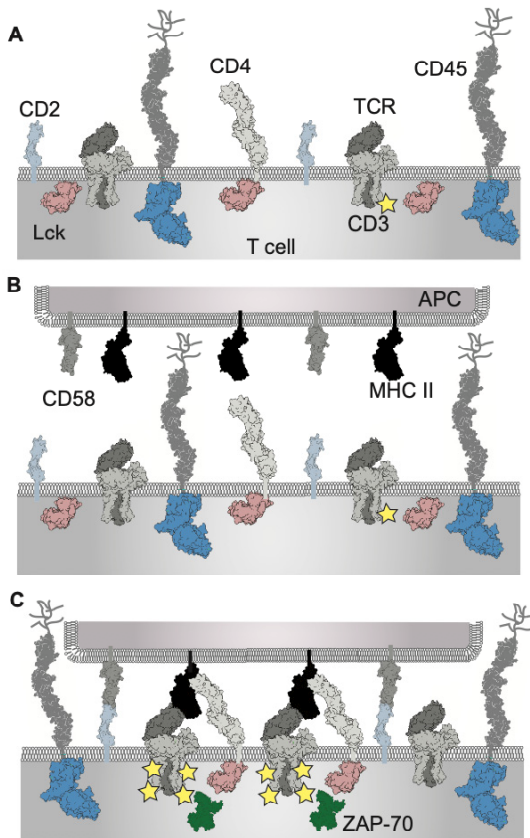


**Figure 2.1.2. The kinetic segregation model.**

**(A)** Random distribution of T cell membrane proteins. The kinase, Lck (pink), and the phosphatase domain of CD45 (blue, PDB: 1ygr)<sup>95</sup> are localised intracellularly. They cause a constant phosphorylation (yellow star) and dephosphorylation of the TCR-CD3 complex. **(B)** An APC, which contains adhesion molecules like CD58 and the MHC class II molecule, is approaching. The glycoprotein CD45 is taller than all the other immune-cell proteins. **(C)** Binding of an APC to a T cell via CD2-CD58 and TCR-MHC. The large CD45 molecules are excluded from the contact area (extracellular domain (dark grey), cytoplasmic phosphatase domains (blue), O-linked oligosaccharides are shown as lines at the N-terminus of CD45). The balance of kinases to phosphatases is changed and sufficient phosphorylation of TCR-CD3 complexes occurs upon binding of an agonist-peptide MHC. ZAP-70 is recruited and causes downstream signalling. Non-bound TCRs can freely diffuse out of the contact and get dephosphorylated by CD45.

available methods such as electron microscopy (EM)<sup>24</sup>. Thus, only an approximation of the full-length protein's dimensions on the cell surface can be made (see **Paper II**) and a summary of these will be given below. Despite the absence of detailed structural insights at the cell surface, several studies have shown that glycoproteins like CD45 are excluded from areas of TCR triggering as well as that a truncation of CD45's extracellular domain inhibits TCR triggering supporting the KS model<sup>93,94</sup>. This effect was reversed by replacing the truncated domain of CD45 with the large extracellular domain of CD43<sup>94</sup>. Moreover, elongation of peptide MHCs in complex with TCRs have been shown to inhibit TCR triggering by diminished CD45 exclusion<sup>96,97</sup>. By mimicking TCR triggering in a reconstituted system, using non-immune cells transfected with key molecules involved in T-cell activation such as Lck, ZAP-70, TCR-CD3 and CD45, it has been shown that ZAP-70 recruitment

was connected to CD45 exclusion and that neither conformational changes nor actin had essential roles in initial T-cell activation<sup>27</sup>. All these studies offer support for the KS model<sup>24,27,93,94,96-98</sup>. However, the uncertainty about the structural properties of the extracellular region of CD45 at the cell surface remain and resolving these is important to better understand the feasibility of the KS model and the protein organisation in a cell-cell contact as a whole.

## 2.2 Large Glycoproteins

### 2.2.1 CD45 and its Isoforms

CD45 is one of the most abundant glycoproteins comprising up to 10% of the cell surface area. It is a type-I transmembrane protein containing two cytoplasmic tyrosine phosphatase domains, one transmembrane domain and a highly glycosylated extracellular region<sup>24,99</sup>. The extracellular region consists of four membrane-proximal domains that belong to the type III fibronectin domain family characterised by a  $\beta$ -sandwich structure (domain D1-D4). The most membrane distal domain is rich in cysteines and connects the fibronectin domains to the N-terminal region that does not have a domain structure but exists in an extended polypeptide sequence bearing O-linked glycan side chains (**Figure 2.2.1**). Of the CD45 domains only the cytoplasmic membrane proximal domain is enzymatically active. The cysteine-rich domain is likely to stabilise the protein by forming inter- and intradomain disulphide bonds and the N-terminal or mucin-like region is the source of various CD45 isoforms arising from alternative splicing varying the length of this region<sup>24,29,30,99</sup>. Which isoform is expressed depends on the cell type, the development stage and the activation stage of the cell<sup>29,30</sup>. So far at least five different isoforms have been identified in humans and EM measurements revealed that CD45R0 is the shortest (~20 nm) and CD45RABC the largest (~40 nm) isoform (**Figure 2.2.1**)<sup>24,29,30,99</sup>. There is little to no evidence for a clear functional difference between these isoforms, but it is suggested that the expression level of the CD45 isoforms is a critical parameter<sup>29,30</sup>. Moreover, it has been argued that CD45R0 forms homodimers in greater proportion than CD45RABC does, which can be accounted

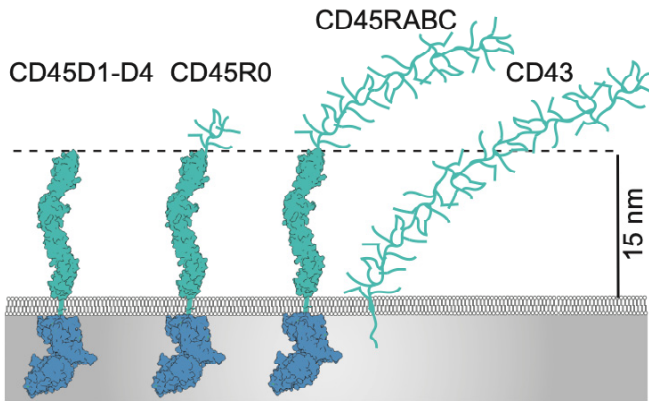


**Figure 2.2.1. Dimensions and structure of various forms of CD45 and CD43.**

Schematic representation of the glycoprotein phosphatase CD45. All versions possess the cytoplasmic tandem phosphatase domains (*blue*). CD45D1-D4 denotes the rigid domain region of the extracellular part of the full-length protein. CD45R0 and CD45RABC contain the domain region as well as 41 or 202 residues at the N-terminus, respectively. The residues are a highly glycosylated primary structure. CD43 is highly glycosylated and extended (no domain structure) extracellularly as well as intracellularly. The CD45D1-D4 region is 15 nm in height<sup>24</sup>. The height of CD45RABC and CD43 is suggested to be 40 nm<sup>99,101,102</sup>.

for by a lower amount of charged carbohydrate repulsion due to a shorter mucin-like region<sup>29,30</sup>. It is controversial whether these dimers exist *in vivo* and if they form *via* an interaction of the intra- or extracellular domains<sup>29,30,100</sup>. Since, in regard to the KS model, only the largest and smallest isoform are of interest the other isoforms will not be further considered.

### 2.2.2 CD43

CD43 is an abundant glycoprotein on most hematopoietic cells. It comprises a cytoplasmic domain, a transmembrane domain and an extracellular domain<sup>103</sup>. However, it does not contain any phosphatase function and the extracellular region is characterised only by an elongated, unfolded, mucin-like structure (**Figure 2.2.1**)<sup>103,104</sup>. The carbohydrates contribute up to 50-60% to the molecular weight. Despite its high abundance the precise function of CD43 has not been resolved. However, CD43 exclusion from the immune synapse has been observed<sup>105</sup> and several studies have shown that inefficient exclusion of CD43 results in the

inhibition of IL-2 production, a marker of activated T cells<sup>106,107</sup>. Therefore, CD43 has been suggested to function as a negative regulator in T-cell activation. It was initially assumed that CD43's extracellular domain acts as a barrier for cell-cell contacts due to the high amount of negative charges<sup>108</sup> but newer data suggest instead that the cytoplasmic domain has a role in the active transport of CD43 away from the cell-cell contact area<sup>109</sup>. The existing functional studies are controversial and an uncertainty about the role of the extracellular domain remains. Structural and functional analyses would help to resolve these uncertainties.

### 2.2.3 Structural Studies Using Microscopy

Several studies have investigated the height of the extracellular region of CD45RABC (40-50 nm)<sup>99,101</sup> and CD45R0 (22 nm)<sup>24</sup> as well as of CD43 (45 nm)<sup>102</sup> using EM. These measurements consider the orientation and dimensions of the protein in solution but not their orientation on the membrane or what effective height they possess in a cellular context. Using other microscopy techniques based on fluorescence bypasses this problem by allowing the investigation of proteins attached to a surface while achieving high axial resolution. An overview of the microscopy methods used to obtain structural insights together with some of the recent findings from their application will be given.

#### Protein Height Measurements

One of the above mentioned fluorescence microscopy techniques is called variable-angle TIRF (VA-TIRF) (**Figure 2.2.2A**) and has been used to determine the relative heights of different CD45 isoforms on an SLB showing a similar relation between CD45RABC and R0<sup>24</sup>. In VA-TIRF the position of a fluorophore attached to for example the N-terminus of the studied protein can be determined by varying the angle of the incident light and translating the subsequent changes in the emitted fluorescence intensity to the distance between the surface and the fluorophore<sup>110</sup>. Despite being a versatile method VA-TIRF is experimentally difficult to apply. Fluorescence interference contrast microscopy (FLIC) is a wide-field microscopy technique just like TIRF but has a greater range providing more topographic

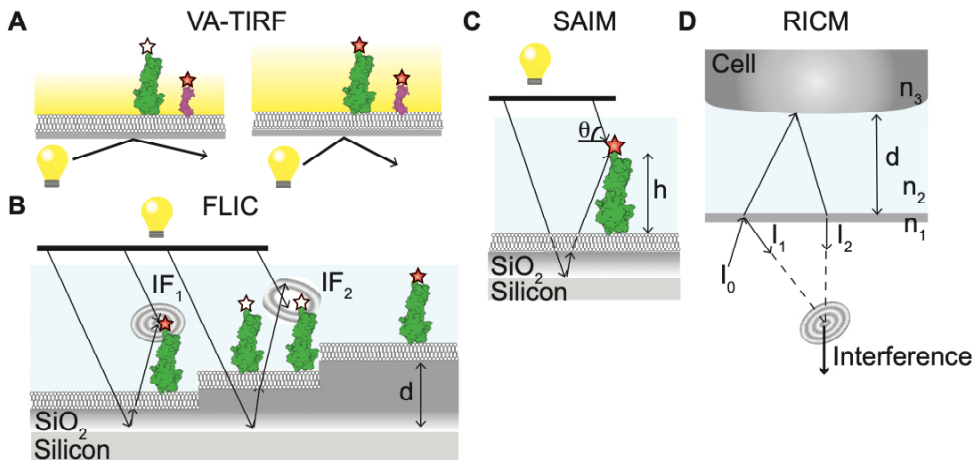


**Figure 2.2.2. Sketch of microscopy techniques to measure protein heights.**

(A) The principle of VA-TIRF. The incident light hits the sample at different angles and excites the fluorophores differently depending on the depth of the evanescent wave. The orientation of the studied proteins at the SLBs are approximated from the fluorescence intensity in relation to the incident angle. (B) In FLIC several silicon oxide terraces are used to create a difference in the interferences ( $IF_1$  and  $IF_2$ ) of the incident and reflected (emitted) light exciting the fluorophore.  $d$  is the terrace distance. (C) SAIM uses instead of different sized terraces variable angles ( $\theta$ ) of the incident light causing different interferences and height-dependent,  $h$ , excitation of the fluorophore. (D) RICM measures the distance between the support and an object at distance,  $d$ , by reflection of the incident beam ( $I_0$ ) at the first interface ( $I_1$ ) and at the second interface ( $I_2$ ). Both rays ( $I_1$  and  $I_2$ ) interfere and the interference pattern depends on the distance of the second interface. The refractive indices ( $n_1$ ,  $n_2$ ,  $n_3$ ) of the three materials must be known.

information (Figure 2.2.2B)<sup>111</sup>. It was used to gain information about the orientation of rod-like polymers mimicking mucin-like glycoproteins bound to a lipid membrane<sup>112</sup> but could be applied to CD45 or CD43 measurements. FLIC is based on the principle that incident light will be reflected by the surface and emitted by the fluorophore attached to the object of interest, *i.e.*, a protein, causing a specific interference pattern and height dependent intensity that is measured. Scanning angle interference microscopy, SAIM<sup>113</sup> (Figure 2.2.2C) uses the same principle as FLIC but the structure of the interference pattern can be controlled by varying the incident angle of the excitation light as in VA-TIRF<sup>114</sup>. This technique is powerful in distinguishing differences in thin structures due to a high axial resolution. However, calibration and image analysis in SAIM are complex and it has so far only been used in a limited number of studies. One of those studies has shown that CD45RABC

and R0 are excluded from contact areas formed between a giant unilamellar vesicle (GUV) and an SLB. The contact formation was studied using either a strong binding receptor-ligand pair, called FRB-FKBP, or the weaker interaction pair, TCR-MHC. Both were able to initiate an SLB-GUV contact but caused a difference in the percentage of excluded CD45 showing a dependence of CD45 exclusion on the affinity of the receptor-ligand pair<sup>98</sup>. Moreover, it has been observed that in the presence of TCR-MHC complexes (the weaker binding pair) the amount of CD45R0 exclusion was lower compared to CD45RABC with 15% vs 40% exclusion, respectively<sup>98</sup>. The estimated size of CD45R0 on the GUV was in agreement with the height of an extended protein structure (~22 nm) and thus suggests an upright orientation of CD45R0 on the membrane, which was also predicted by another study using VA-TIRF<sup>24,98</sup>. The size of CD45R0 was estimated from the membrane distance of the GUV to the SLB using SAIM. Another, more common, method to measure this distance is RICM, reflection interference contrast microscopy, which is able to measure membrane distances in the absence of fluorophores (**Figure 2.2.2D**)<sup>115</sup>. It has previously been used to measure distances of membrane contacts formed by two interacting proteins and contains information about the axial dimensions of these proteins<sup>116,117</sup>. RICM is physically similar to FLIC and can be used for absolute height measurements but results in images of lower contrast compared to the images obtained with FLIC<sup>111</sup>. Additionally, this method cannot be used for non-interacting, free molecules in the SLB since it is dependent on the presence of a second surface above the first one.

To summarise, these studies revealed structural insights into the (upright) orientation of CD45RABC and R0 on the membrane and estimated the height of the short isoform CD45R0 to be ~22 nm<sup>24,98</sup>. CD45RABC seemed to be of similar height as CD45R0 but was not directly measured in any of the cases. Moreover, CD43 was not addressed in those studies and information about CD43's structure at the cell membrane is lacking.

### **Orientation of Proteins**

Experiments have shown that membrane anchored molecules can adopt different surface heights depending on the orientation and/or free rotation around their

anchoring point at the membrane indicating that height measurements need to be obtained in an environment affecting the orientation and rotational freedom of the proteins<sup>112</sup>. This environment likely includes lateral protein crowding on the surface or in the cell contact which was not considered in the above-mentioned studies. Schmid and colleagues approached this issue by studying differently sized proteins of binding or non-binding character in contacts between SLBs and GUVs using RICM<sup>117</sup>. They showed that the organisation at the membrane interface was dependent on the protein size (as suggested by other studies<sup>24,98</sup>) but also on lateral crowding<sup>117</sup>. While no information about how this affects the orientation of the protein was obtained it was shown that lateral crowding resulted in the exclusion of non-binding proteins from the contact area regardless of their height. This protein exclusion was further affected by axial crowding which considers a steric effect with proteins on the opposing membrane<sup>117</sup>. A similar effect was seen by James and Vale in a reconstituted cell system, however, the investigated protein density was much lower (50 molecules/ $\mu\text{m}^2$ ) than that of Schmid *et al.* who had a protein density (at the interface between the SLB and the GUV) ranging from 1 000 – 11 000 molecules/ $\mu\text{m}^2$  showing that the crowding effect is system dependent and probably of different nature in the two experiments<sup>27,117</sup>. Whereas the crowding effect observed by James and Vale is comparable to what we and others have seen and most likely accounted for by the interaction with the contacting cell expressing naturally high levels of various membrane proteins<sup>27,118,119</sup> the crowding effect observed by Schmid *et al.* is mainly due to lateral crowding<sup>117</sup>. Thus, the exclusion of non-binding proteins such as CD43 and CD45 during cell-cell contact formation might not be solely size-dependent but can also be affected by protein crowding on the surface. Whether protein crowding affects the relative height of these tall or flexible molecules is unknown. A new technique called hydrodynamic trapping, that has been used in this thesis, allowed investigation of the dimensions of membrane bound proteins as well as the interaction-potential between them over a wide range of concentrations and provided the possibility to answer some of the remaining questions<sup>120,121</sup>. Hydrodynamic trapping has here been used to characterise CD45, the adhesion molecule CD2 and the T-cell co-receptor CD4 (**Paper I**) as well as CD45R0, CD45D1-D4 and CD43 (**Figure 2.2.1**).

## 2.3 Trapping of CD2, CD4 and CD45RABC

The main aim of the study in **Paper I** was to investigate the dimension and orientation of the large isoform CD45RABC on a model membrane. It has been shown that the folded part of CD45, which comprises the four domains D1-D4, as well as CD45R0 are rather rigid and both proteins were suggested to orient upright from the membrane<sup>24,98</sup>. Nevertheless, structural information about CD45RABC at the cell surface is missing. Hydrodynamic trapping was here used to obtain further structural information about CD45RABC and to relate those findings to previous observations made in cell-contact assays.

### 2.3.1 Principle of Hydrodynamic Trapping

In hydrodynamic trapping a micropipette is placed in a fixed position above an SLB anchoring fluorescently-labelled proteins (**Figure 2.3.1A**). Applying a negative pressure through the micropipette causes an inward flow which drags on the proteins moving them towards the area beneath the pipette where the proteins accumulate (**Figure 2.3.1B**). A higher pressure results in greater protein accumulation which continues until steady state is reached (**Figure 2.3.1C**). The hydrodynamic force that is acting on the molecules is dependent on (i) the size and geometry of the protein and on the surface concentration of the protein all summarised by the hydrodynamic area,  $A_{hydro}$ , as well as on (ii) the shear force (or the force that drags on the molecules) which is defined by the dimensions of the pipette, the applied pressure and the distance between the pipette and the SLB (**Figure 2.3.1D**). The thermodynamic effect this has on the molecules is described by  $\varepsilon_{hydro}$  which is a measure of the work required to move one membrane bound molecule from infinite distance to a radial distance,  $r$ , from the center of the trap (**Figure 2.3.1C**). At steady state the resulting force can be related to the concentration of the molecules *via* their chemical potential,  $\mu(c)$ , at the distance  $r$  by:

$$\mu(c) = \mu(c_0) + \int_0^{\varepsilon_{hydro}} A_{hydro}(c) d\varepsilon_{hydro} \quad \text{Eq. 2.1}$$



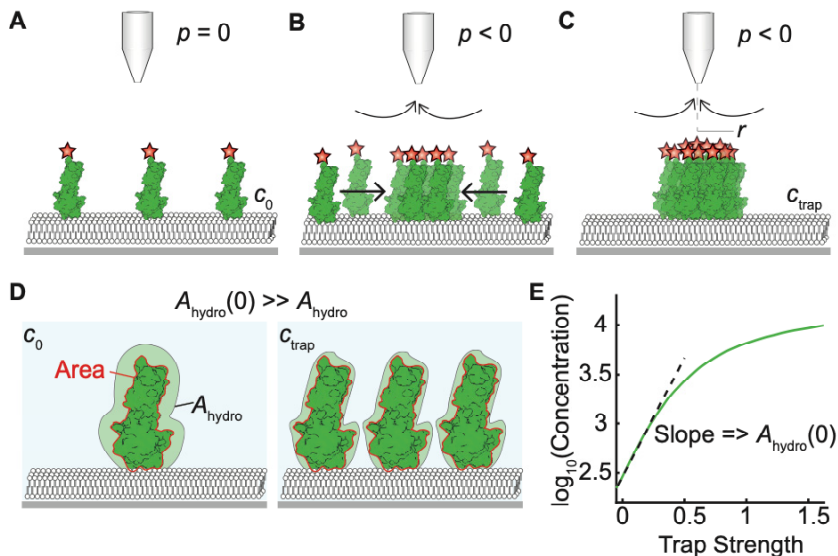


**Figure 2.3.1. Principle of hydrodynamic trapping.**

(A) A micropipette is positioned above an SLB functionalised with fluorescent proteins at dilute concentrations,  $c_0$  (not drawn to scale). (B, C) Negative pressure is applied through the micropipette causing the accumulation of the proteins in the SLB beneath the micropipette. The accumulation of the molecules depends on the applied pressure and the distance between the pipette and the SLB. The radial distance,  $r$ , from the center of the trap is shown in C. (D) The relation between the hydrodynamic area,  $A_{\text{hydro}}$  (light green shade), and the protein area (red line). At high surface concentrations in the trap,  $c_{\text{trap}}$ ,  $A_{\text{hydro}}$  is smaller than at dilute concentrations. (E) Interaction curves are obtained and relate the concentration of accumulated proteins to the strength of the trap. The slope of this curve is used to calculate  $A_{\text{hydro}}(0)$  and thus the height of the protein on the SLB at dilute concentrations.

At low surface coverage,  $c_0$  (the dilute regime at which the concentration of the molecules equals the concentration before trapping), the chemical potential is equal to  $\mu(c_0)$  and  $A_{\text{hydro}}$  will change to  $A_{\text{hydro}}(0)$  which is the hydrodynamic area the molecule experiences at dilute conditions,  $c_0$ . For this situation, Eq. 2.1 simplifies to:

$$\ln(c) = \ln(c_0) + A_{\text{hydro}}(0) \varepsilon_{\text{hydro}} / k_B T \quad \text{Eq. 2.2}$$

where  $k_B$  is the Boltzmann constant and  $T$  the temperature. By plotting  $\ln(c)$  vs  $\varepsilon_{\text{hydro}}$  information about the hydrodynamic dimensions of the molecule at low surface coverage can be obtained from the slope  $A_{\text{hydro}}(0)/k_B T$  of the so-called interaction curve (Figure 2.3.1E). Each protein has its own characteristic interaction curve

which contains information about the hydrodynamic area as well as existing intermolecular forces between the studied molecules, *i.e.*, if the proteins are attracted or repulsed by each other.

To verify the method of hydrodynamic trapping it was initially tested on the structurally well-studied protein streptavidin bound to biotinylated SLBs. The data obtained were in good agreement with the crystallographic data confirming the applicability of the method. The findings regarding streptavidin will not be further discussed here (see **Paper I** for more details).

### 2.3.2 Considerations of the Method

The effective height of proteins can be estimated using hydrodynamic trapping. The measurements contain crucial information about how the proteins orient on the SLB as well as how they interact over a wide range of concentrations, which is hard to measure with other methods. The here studied immune-cell proteins were not incorporated into the SLB as full-length proteins since they are transmembrane proteins *in vivo* and generally difficult to work with in SLB studies (see Chapter 1). Thus, only the extracellular region of each protein was anchored to the membrane and measured using hydrodynamic trapping. From this, no definitive conclusions on how these proteins behave *in vivo* can be drawn as no transmembrane or intracellular interactions are accounted for. However, the effective dimensions, effect of glycosylation or molecular flexibility are not expected to be significantly different.

In order for hydrodynamic trapping to produce reliable data there are many important, success rate determining, steps (see **Figure 2.3.2** for the experimental setup). This starts with a clean environment in which the experiment is conducted since the pipette can easily block hampering the outcome of the experiment. Another important step is to make sure that the buffer in the pipette and in the sample-holder are filtered and exactly the same. The electrode in the micropipette must be chlorinated to avoid fluctuations in the measured resistance, as this must be stable for estimating the distance to the SLB. Additionally, the applied pressure needs to be constant for at least 30 minutes and hence, the air-tube system should not leak at any connecting point between the pump and the pipette. While acquiring the images

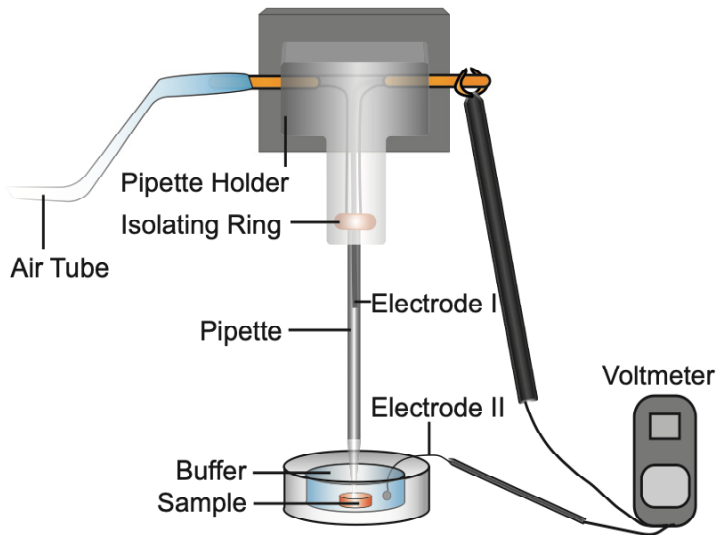


**Figure 2.3.2. Experimental setup of hydrodynamic trapping.**

A micropipette is mounted above a sample in a pipette holder connected to an air-pressure system and an electrode (Electrode I). The isolating ring in the pipette holder assures that the air-pressure system is tight. A second electrode (Electrode II) is introduced in the buffer solution filling the sample holder. The ion current between the two electrodes is measured with a voltmeter. The resistance increases when the micropipette approaches the surface and was used as a reference for how far the pipette is above the surface.

a steady stage and focus is of immense value since a drift in the focus can induce significant errors into the measurements. Regarding the bilayer preparation it was always made sure that, besides a high fluidity of the proteins, all unbound vesicles and proteins in the bulk are washed off since they can block the pipette. A blocked pipette is usually the end of the experiment and can only infrequently be saved by exchanging a blocked pipette with a fresh one. Generally, a quick but precise and accurate handling of the pipette and the trapping system as a whole is important to guarantee a successful experimental outcome.

### 2.3.3 The Measured Proteins

CD45 is, as described above, a rather structurally complex molecule comprising the rigid domains (D1-D4) and a large mucin-like region. It differs strongly from the globular model protein streptavidin and thus two, structurally more similar,

immune-cell proteins, CD2 and CD4 were additionally studied. CD2 and CD4 are, like CD45, suggested to be rod-like proteins protruding upright from the membrane but are smaller in size and do not contain any mucin-like regions (**Figure 2.3.3**)<sup>20,23,122</sup>. The crystal structures of these two proteins show a typical Ig  $\beta$ -sheet structure for each of the extracellular domains with CD2 comprising two Ig domains (7.5 nm tall) and CD4 consisting of four Ig domains (11 nm tall) (**Figure 2.3.3**). Both proteins play an important part in APC-T cell contacts, but it is not well defined how they orient on the membrane or how these glycosylated proteins interact laterally. Hence, they were included in the present study.

### 2.3.4 Dimensions and Orientations of CD2, CD4 and CD45RABC

#### CD2 and CD4

The obtained slopes and thus  $A_{\text{hydro}}(0)$  values from the interaction curves of CD2, CD4 and CD45RABC attached to an SLB are in good agreement with their respective protein size. CD45RABC, being the tallest molecule, possessed the steepest slope and highest  $A_{\text{hydro}}(0)$  value followed by CD4 and then CD2 (**Figure 2.3.4A**). The effective protein heights were estimated from the measured  $A_{\text{hydro}}(0)$  values with  $8 \pm 0.3$  nm for CD2 and  $11 \pm 0.6$  nm for CD4 and are well in line with the protein heights obtained from their crystal structures, suggesting that the proteins orient in an upright position on the SLB<sup>24,98</sup>. The CD4 accumulation levelled off at a higher concentration in the trap than that for CD2 which could be aided by a higher glycosylation of CD2 with four N-linked oligosaccharides on the protein compared to two on CD4 (**Figure 2.3.3**). To obtain information about the protein's intermolecular interactions and thus, the effect of glycosylation, the excess chemical potential,  $\mu^{\text{ex}}$ , was calculated with the values obtained from the interaction curves. The excess chemical potential is mainly dependent on the concentration of the studied protein and would be zero for non-interacting and infinitely small molecules. As soon as molecules start to interact the system can be characterised with  $\mu^{\text{ex}}$  which is negative if the molecules are attractive to each other and positive if they are repulsive. In simple terms it describes if an interaction is energetically favoured or not. Both, CD2 and CD4 are highly repulsive observed by an increase in  $\mu^{\text{ex}}$  with increasing protein concentration in the trap (**Figure 2.3.4B**). Thus, the more

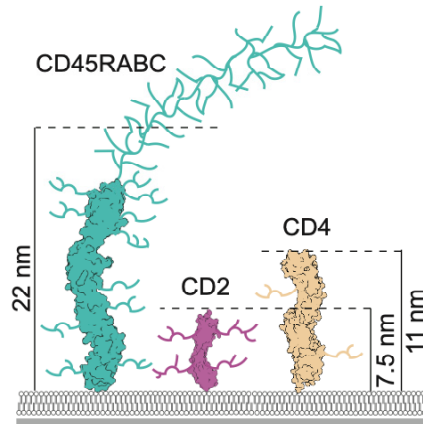


**Figure 2.3.3. Structure of the studied proteins.**

Extracellular domains of CD45RABC, CD2 and CD4 attached to a 5% NTA-chelated SLB. N-linked oligosaccharides are indicated as linear chains extruding laterally from the crystal structure.

proteins accumulated in the trap the harder it was to trap further proteins. A high amount of glycosylation would cause the molecule to take up more lateral space, which increases the intermolecular repulsion. Indeed, CD2 is more repulsive than CD4 (**Figure 2.3.4B**). Therefore, CD2 molecules cannot be ‘packed’ as closely as CD4 resulting in a lower concentration of accumulated CD2 in the trap (**Figure 2.3.4A**). The lower glycosylation and decreased repulsion observed for CD4 is in line with its suggested ability to freely diffuse within the cell-cell contact providing the TCR with Lck. Moreover, it has been previously shown that non-binding proteins are, independent of their size, excluded from cell-cell contact areas (see above: Orientation of Proteins). It is possible that this is partly aided by the glycosylation levels of the binding proteins in the contact area increasing lateral repulsion. CD2 is one of the main binding proteins causing the adhesion of T cells and APCs and is suggested to have a key role in initiating close contacts, which leads to CD45 exclusion and subsequent TCR triggering. It is not clear if and what role glycosylation has in this system, but it could act as a repulsive force increasing the lateral crowding effect. Thus, it might ‘help’ to regulate the initial protein segregation following close contact formation.

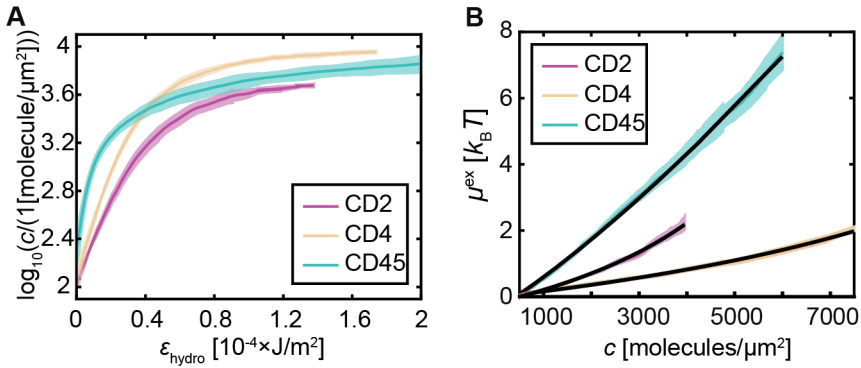


**Figure 2.3.4. Hydrodynamic trapping of CD2, CD4 and CD45RABC.**

(A) Interaction curves for CD2, CD4 and CD45RABC (mean  $\pm$  SD). (B) The experimentally obtained excess chemical potential for the three proteins (mean  $\pm$  SD). The black lines are theoretical fits assuming 'hard disks' for CD2 and CD4 and a ' $\pm 90^\circ$ ' rotating rod' for CD45RABC.

Monte Carlo simulations were used to further investigate the impact of protein glycosylation on the protein's interaction potential. Varying amounts of sugars were therefore added as side chains ('arms') to a theoretical protein model by adding small beads-on-a-string-structures extruding laterally from the protein simulated as a 'three-beads-on-string' structure (see **Paper I**). These 'proteins' were studied theoretically on a surface with increasing surface coverage of the same type of protein from which the theoretical  $\mu^{\text{ex}}$  was calculated (**Figure 2.3.5A**). For rigid and upright standing 'proteins', the effect of glycosylation on the intermolecular repulsion was relatively high at already small numbers of added sugars supporting the observation of highly repulsive CD2 and CD4 molecules possessing only few glycosylation sites and the idea that this might have an effect on cell-cell contact formation (**Figure 2.3.5A**).

## CD45

Despite having the steepest slope and thus highest  $A_{\text{hydro}}(0)$  value CD45RABC had an effective calculated height of 22 nm, which is roughly half the size observed for CD45RABC's extended structure in EM (40 nm)<sup>99</sup>. Moreover, the excess chemical potential and consequently the repulsion was much higher for CD45RABC than for CD2 or CD4 and  $\mu^{\text{ex}}$  changed almost linearly with an increasing amount of

accumulated CD45RABC which was not observed for CD2 and CD4 (**Figure 2.3.4B**). Whereas the obtained data for CD2 and CD4 could be fitted to a 'hard-disk' model describing the protein structure in a simplified form as a cylinder, it did not describe the excess chemical potential curve of CD45RABC accurately. There are two possible explanations for this finding. One is that the mucin-like region did not experience the same hydrodynamic drag force as the more rigid folded region (D1-D4) due to a more extended structure (no folding). However, this would mainly explain the difference in height but not necessarily why CD45RABC is highly repulsive. The other possibility is that CD45RABC has a much higher flexibility than the other two molecules which can cause the molecule to rotate around its anchoring point at a low surface coverage (higher free space per molecule). This was further investigated using Monte Carlo simulation. Hereby, a bead-on-a-string structure including either three or six beads represent two different sized protein species such as CD2 and CD45RABC. Investigating the behaviour of these 'proteins' on a theoretical surface assuming rotational freedom of the protein showed that with increasing surface coverage the rotational freedom decreased. This occurs due to steric hindrance which also forces the proteins to be in an upright position (**Figure 2.3.5B**). The obtained theoretical excess chemical potential for the 'six-beads-on-a-string' structure increased linearly with the surface coverage which is in line with the  $\mu^{\text{ex}}$  behaviour observed for CD45RABC's. Thus, CD45RABC's behaviour at the membrane was well described with a ' $\pm 90^\circ$  rotating rod' model fit and explains why it differs from what has been found for CD2 and CD4 which could be better described with a 'hard-disk' model (**Figure 2.3.5C**). The flexibility of CD45RABC could affect either the protein as a whole or the mucin-like region only. Independent of what exactly is affected by this flexibility it causes the protein to have a lower effective height (22 nm), similar to what has been measured by others, and could explain why CD45RABC is not fully excluded from close-contact areas<sup>24,98</sup>. Nevertheless, this effect might be reduced on the crowded cell membrane (high protein surface coverage) since close packing of various proteins including CD45RABC and other tall glycoproteins could cause an upright position of CD45RABC due to steric limitations of its rotational freedom. Indeed, by using Monte Carlo simulation a 5 nm increase in the effective height of CD45RABC was observed in a crowded environment of 2000 molecules/ $\mu\text{m}^2$ . The assumed density is

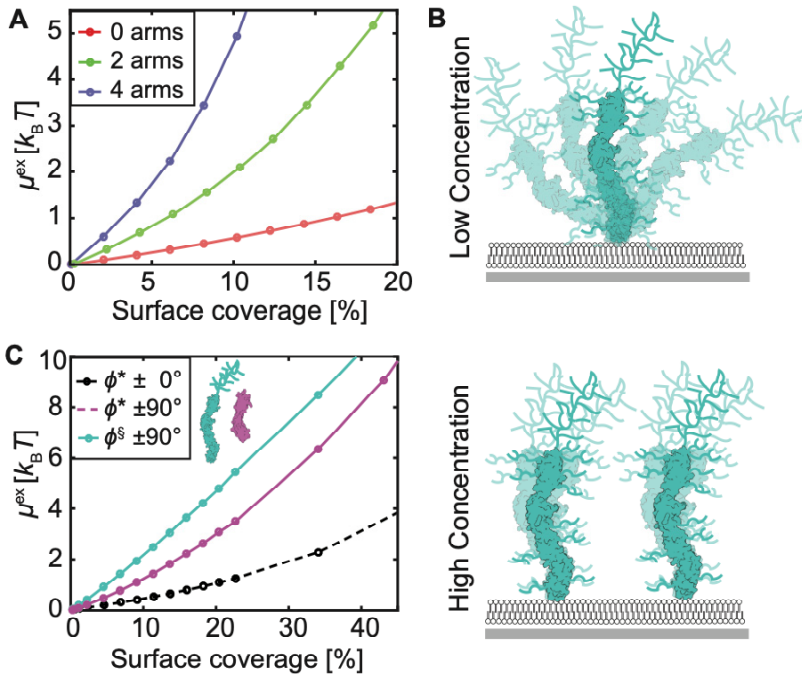


**Figure 2.3.5. The effect of protein glycosylation and flexibility on intermolecular interactions.** (A) Theoretical excess chemical potential,  $\mu^{\text{ex}}$ , calculated for a three-beads-on-a-string structure with and without sugars (4, 2 and 0 arms, respectively) at  $\pm 10^\circ$  rotational angle. (B) At low surface coverage the flexible protein CD45RABC takes up space and can have a lower effective height. At a high surface concentration, the flexibility of the protein decreases and the protein orients more upright. (C) Theoretical  $\mu^{\text{ex}}$  at high rotational freedom ( $\pm 90^\circ$ ) for three (solid purple line) or six beads-on-a-string (cyan solid line) structured molecules similar to CD2 and CD45RABC, respectively. The theoretical  $\mu^{\text{ex}}$  for a three-beads-on-a-string structure or 'CD2' at no rotational freedom is shown as a comparison (dashed black line). Of note, this is identical to  $\mu^{\text{ex}}$  of a six-beads-on-a-string structure resembling 'CD45' at no rotational freedom.

however much lower than the physiological density at the cell surface with roughly  $30\,000 \text{ molecules}/\mu\text{m}^2$ <sup>117,123</sup> predicting a stronger effect of crowding *in vivo*. Thus, exclusion depends not only on the relative protein height but also on the protein's glycosylation and the protein density on the membrane.

### CD45RABC trapped with CD2 or CD4

The trapping of two proteins at the same time showed their height dependent separation in the trap, with the taller molecule accumulating in the center of the trap



and the small molecule orienting around it (**Figure 2.3.6**). This effect was more significant for CD2 than for CD4 trapped together with CD45RABC (**Figure 2.3.6**). Thus, the force acting on the molecules is higher for taller proteins and shows an inside-out segregation process emphasising that protein size is an important property of the trapping results. Under any of the examined conditions neither of the studied proteins formed dimers or bigger aggregates as previously argued<sup>100,124–128</sup>. Whereas CD2 is generally believed to be in monomeric form, CD4 and CD45 are more controversially discussed. Nevertheless, the obtained data here are in line with the previous observations that (i) CD4 exists in a monomeric form binding to MHC and TCR as seen in the crystal structure<sup>20,122</sup> as well as that (ii) only monomeric CD45 molecules have been found in solution and that the crystal structure of CD45D1-D4 did not reveal any important oligomerisation interfaces<sup>24</sup>.

### 2.3.5 Conclusion

In conclusion, the dimensions as well as the orientations of the three immune-cell proteins, CD2, CD4 and CD45RABC were estimated using hydrodynamic trapping. The obtained sizes for CD2 and CD4 were well in agreement with the crystal structure's top-to-bottom heights. For CD45RABC this value was smaller than the estimated height from EM measurements and was attributed to a higher flexibility of the protein at low surface coverage at the SLB. A higher flexibility could also explain the similar height values observed for CD45R0 and CD45RABC in other studies<sup>24,98</sup>. The flexibility of CD45RABC, however, is reduced on the crowded cell membrane causing it to orient in a more upright position. All three measured proteins were highly repulsive which is attributed to their glycosylated side chains, which are further suggested to counteract dimer or aggregate formation. Interestingly, already a low amount of carbohydrates on the molecules did have a significant effect on their intermolecular interaction. Thus, studies of protein binding behaviour comparing the glycosylated to the non-glycosylated protein would be valuable and could give further insights into the organisation of proteins in a cell-cell contact.

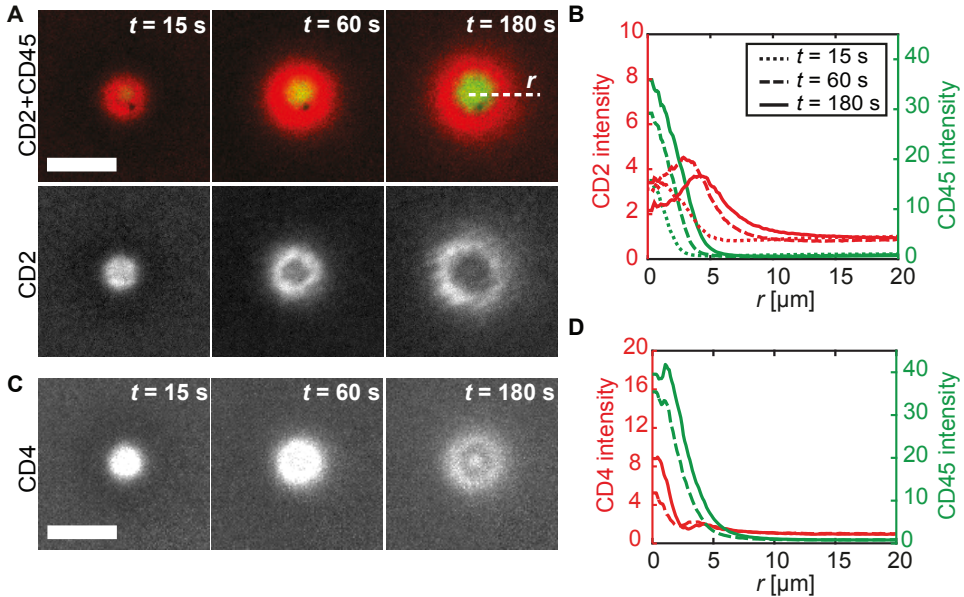


**Figure 2.3.6. Double trapping of CD45RABC with CD2 or CD4.**

(A) *Top panel:* Merged images of the intensity of CD45RABC and CD2 after negative pressure was applied,  $t=0$ . *Bottom panel:* Intensity signal of CD2 alone. The white dashed line represents the radial distance,  $r$ . Scale bar 10  $\mu\text{m}$ . (B) Radial line profiles of CD2 (red lines) and CD45RABC (green lines) from the data in A. (C) Images of CD4 in the double trap with CD45RABC at various times after pressure has been applied. (D) Radial line profiles of CD4 (red lines) and CD45RABC (green lines) at two different applied pressures (dashed lines: -10 kPa, solid lines: -20 kPa).

## 2.4 Dimensional Studies of CD45 and CD43

The dimensions of CD45R0 and CD45RABC on membranes as well as their exclusion from cell-contacts have been investigated in several studies using various microscopy techniques. Only few structural data exist for CD45D1-D4 and CD43 and contain mainly solution-based information. Evidence about their organisation, orientation and dimensions on SLBs are missing. Thus, the studies of CD45RABC using hydrodynamic trapping were extended by including the rigid domain part of CD45, *i.e.*, CD45D1-D4, the shortest isoform CD45R0 and the tall glycoprotein CD43. To complement these studies all four proteins were further investigated with scattering techniques characterising their dimensions in solution. This work was done together with Amélie Fuentes, who did the trapping experiments and Dr. Luigi

Gentile who measured and analysed the soluble unlabelled proteins with dynamic light scattering and small angle x-ray scattering.

### 2.4.1 Trapping of CD45D1-D4, CD45R0 and CD43

The trapping experiments were conducted the same way as described in **Paper I** with either CD45D1-D4, CD45R0 or CD43 on the SLB. All three proteins were, like CD45RABC, labelled with Alexa Fluor® 488 which allowed for a better comparison to the previously measured CD45RABC (**Paper I**). Furthermore, an initial trapping experiment was done on CD45RABC to compare the newly obtained with the previous trapping results. The slope of the measured interaction curve was almost identical to the previous results (see above and **Paper I**). The next step was to obtain the interaction curves for CD45D1-D4 and CD45R0 to estimate their respective  $A_{\text{hydro}}(0)$  values. As expected, CD45D1-D4, being the smallest protein, had the lowest  $A_{\text{hydro}}$  value with  $450 \text{ nm}^2$ , and CD45R0, which is size-wise between CD45D1-D4 and CD45RABC, had an  $A_{\text{hydro}}$  value of  $890 \text{ nm}^2$ . The estimated heights of these two proteins, 10 nm and 16 nm, were, however, lower than their expected heights from crystallography and EM measurements with 15.2 nm and 22 nm, respectively. One explanation could be that these two molecules rotate around their anchor point similar to what has been described for CD45RABC decreasing their effective height on the SLB. However, it could also be that the observed initial concentrations on the bilayer were too high ( $c_0 = 300 \text{ molecules}/\mu\text{m}^2$ ) compared to what has been used for CD45RABC with  $c_0 = 100 \text{ molecules}/\mu\text{m}^2$ . It is possible that the proteins start shielding each other at this higher surface concentration decreasing their effective  $A_{\text{hydro}}$  values. This would cause a change in the initial slope of the interaction curve and consequently in the calculated height. The here obtained height shall therefore be seen as a lower limit value. The concentrations of accumulated CD45RABC and CD45R0 in the trap seem to level off at a similar value of around  $6000 \text{ molecules}/\mu\text{m}^2$  (**Figure 2.4.1**). CD45D1-D4 follows this trend but at much higher trapping strengths. This suggests that all three proteins eventually orient upright and have, at  $6000 \text{ molecules}/\mu\text{m}^2$ , a similar effective cross-sectional area as non-trapped CD2. Interaction curves for CD43 were harder to obtain than for the other proteins, which was mainly accounted for by the poor labelling

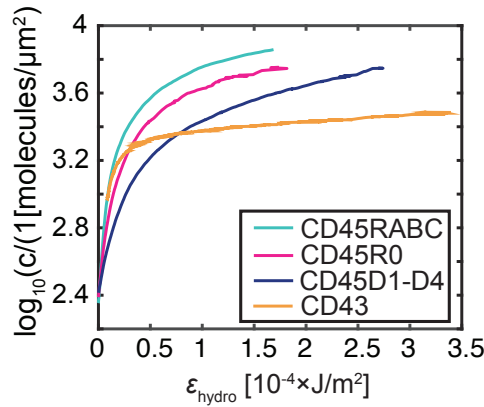


**Figure 2.4.1. Interaction curves for three CD45 versions and CD43.**

The interaction curves for CD45R0, CD45D1-D4 and CD43 are shown in comparison to the previously obtained interaction curve for CD45RABC. The slope for CD43 is missing and hence the 'beginning' of the CD43 interaction curve could start at higher or lower  $\epsilon_{\text{hydro}}$  values.

efficiency of the protein resulting in very dim fluorescence at the SLB. This was compensated for by the addition of large amounts of CD43 to be able to visualise protein binding to the SLBs. However, the used concentration was too high to measure a prominent slope in the interaction curves and thus, no  $A_{\text{hydro}}$  value, *i.e.*, height for CD43 could be calculated. In addition, CD43 accumulation in the trap levels off at a concentration of 2000 molecules/ $\mu\text{m}^2$ , a third of what has been found for the trapped CD45 versions, suggesting that CD43 has a higher effective cross-sectional area than any of the other tested proteins (Figure 2.4.1). One other possibility for this behaviour could be that the protein collapsed on the bilayer increasing its intermolecular repulsion and decreasing its maximum 'packing' density. A third possibility is that due to the poor labelling efficiency some of the CD43 are unlabelled which might have falsified the calculated protein concentration at the SLB. The next step was to use fluorescence independent scattering methods to analyse the structure of the glycoproteins. These measurements, similar to EM, are done on proteins in solution but give, together with the results obtained on SLBs, a broad picture of important structural features of the here studied glycoproteins.

## 2.4.2 Dimensions in Solution

### Dynamic Light Scattering

Neither of the CD45 isoforms nor the CD43 extracellular domains have, to the best of my knowledge, been structurally analysed in solution using dynamic light scattering (DLS) or small angle x-ray scattering (SAXS). However, both techniques are powerful tools to measure the size of molecules in the submicron region ( $< 1 \mu\text{m}$ ). In DLS a light ray is focussed onto a spot illuminating a delimited part of the molecules in solution. The molecules move randomly in and out of this volume, due to Brownian motion, and scatter the light leading to a fluctuating intensity signal captured by a detector (**Figure 2.4.2A**). Small proteins generally diffuse quicker out of the detection volume than large ones causing more rapid fluctuations in the scattered light (**Figure 2.4.2B**). How the signals correlate at different times thus gives a measure of how fast the molecules diffuse (**Figure 2.4.2C**). This is represented in an autocorrelation function from which the translational diffusion coefficient,  $D$ , is obtained and used to calculate the hydrodynamic diameter,  $d_{\text{hydro}}$ , of the protein assuming a spherical shape *via* the Stokes-Einstein equation given by:

$$d_{\text{hydro}} = \frac{k_B T}{3\pi\eta D} \quad \text{Eq. 2.3}$$

where  $T$  is the temperature,  $k_B$  the Boltzmann constant and  $\eta$  the viscosity of the system. The hydrodynamic radius ( $d_{\text{hydro}}/2$ ) and calculated protein length of the four measured proteins can be found in Table 2.1. The length of the proteins was estimated assuming a linear chain of domains (similar to the bead-on-string-structure) in which the orientation of two consecutive domains towards each other follow a gaussian distribution<sup>129</sup>. The estimated height of CD45D1-D4 with 15.5 nm, of CD45R0 with 19.2 nm and of CD45RABC with 38 nm were in line with previous findings (**Table 2.1**)<sup>24,98,99</sup>. The protein length found for CD43 is almost half of what would have been expected from EM measurements (**Table 2.1**)<sup>102</sup>. Small-angle x-ray scattering was used to better characterise the structure of CD43 and to obtain information about the size and the flexibility of CD43 as well as CD45D1-D4, CD45R0 and CD45RABC.

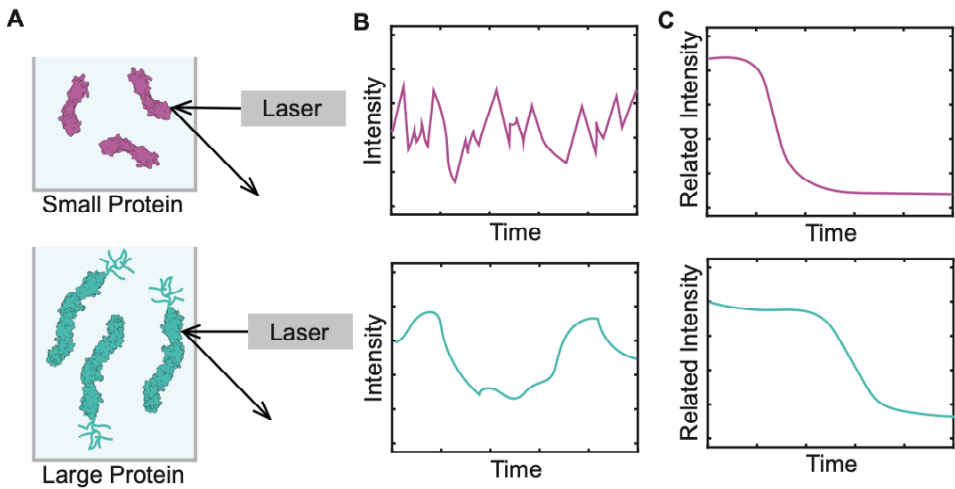


**Figure 2.4.2. Principle of DLS.**

(A) Small and large proteins are freely diffusing in solution. A laser beam is illuminating a small volume in the sample and the scattered light is detected. (B) The intensity change in a delimited volume of the sample over time is recorded. The intensity profile shows fast fluctuations for small and slow fluctuations for large proteins. (C) The initial intensities are related to the intensities at later time points and the results are presented in an autocorrelation function. The decay is fast for small proteins and slow for large proteins.

### Small-Angle X-Ray Scattering

In SAXS a highly focussed x-ray beam is directed onto the sample containing the soluble protein of interest. The proteins in the sample scatter the x-rays at small angles onto a detector and produce a scattering pattern that contains information about the structure of the protein. The SAXS pattern obtained for the three CD45 molecules and CD43 was fitted to a model describing a flexible cylinder<sup>130,131</sup> and was in good agreement with the data observed in the DLS measurements (Figure 2.4.3). From the fit, information about the total length or contour length,  $L$ , can be obtained (Figure 2.4.3 and Table 2.2). The contour length in the flexible-cylinder model describes the number of locally stiff segments of a certain length,  $l_p$ , *i.e.*, the persistence length, in the protein chain not assuming any folding. High values like those seen for CD45RABC can for example occur due to a fully extended protein (Table 2.2). Thus, the displacement length,  $\langle R \rangle$ , the distance between one end to the other end ('top-to-bottom') of the coiled protein, is a better description of the actual protein height.  $\langle R \rangle$  is also called the end-to-end distance and is calculated

**Table 2.1. The hydrodynamic radius and length of the protein estimated with DLS.**

Protein	Hydrodynamic Radius [nm]	Protein Length [nm]
CD45D1-D4	4.2	15.5
CD45R0	5.7	19.2
CD45RABC	10.3	38.0
CD43	7.0	26.0

with  $\langle R^2 \rangle \approx l_k \times L$  (Figure 2.4.3A), where  $l_k$  is the Kuhn length which is two times  $l_p$ . Both,  $l_p$  and/or  $l_k$  are used to describe the stiffness of the protein chain (Table 2.2). However, a large Kuhn length does not automatically mean that the protein is stiff because the flexibility also depends on the contour length of the protein. The more similar the Kuhn length and the contour length are the more rigid the protein is. For CD45D1-D4  $l_k$  is very similar to the contour length (Table 2.2) suggesting a rigid molecule as shown previously<sup>24</sup>. The end-to-end distance was 15.4 nm for CD45D1-D4 which is in well agreement with what has been found here using DLS and from the crystal structure<sup>24</sup>. CD45R0 has a slightly smaller  $l_k$  in respect to CD45D1-D4, whereas  $L$  is larger, thus, CD45R0 is slightly more flexible than CD45D1-D4 and could explain the observed lower height of CD45R0 using hydrodynamic trapping. Whether the apparent flexibility originates solely from the mucin-like region as well as why the herein estimated height of CD45R0 is slightly smaller than what has been shown previously is unknown<sup>24,98</sup>. An explanation could be that the assumed mathematical model in both methods is not the best-fitting model to describe the molecule. CD45RABC is among all proteins the most flexible one and spans an end-to-end distance of 42 nm, which is in agreement with what was measured in DLS herein and in EM by others<sup>99</sup>. Concluding, CD45RABC has an extended structure in solution and most likely also on the SLBs but due to its high flexibility acquires a smaller effective height (see Paper I). Interestingly, the estimated height of CD43 using SAXS was comparable to the height measured in DLS but was only half the size of what has been found in EM<sup>102</sup>. The estimated Kuhn length to contour length ratio for CD43 describes a structure that is less pronounced in flexibility than CD45RABC but more flexible than CD45R0. A possible explanation could be that the protein is aggregated or collapsed on itself forming a rather globular structure similar to a polymer in a theta solvent<sup>129</sup>. This is

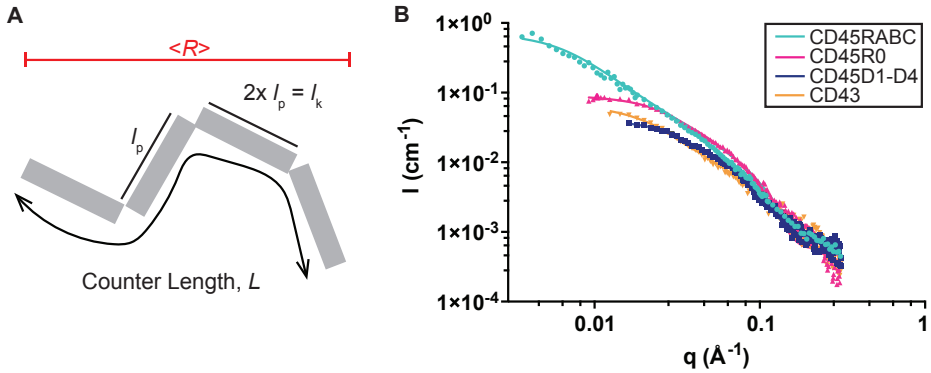


**Figure 2.4.3. Model and SAXS profiles for CD45 and CD43.**

(A) Sketch of the applied flexible polymer chain model with a polymer chain in *grey* and the representation of the counter length,  $L$ , the persistence length,  $l_p$ , and the Kuhn length,  $l_k$ , in *black*. The end-to-end distance,  $\langle R \rangle$ , is shown in red. (B) The SAXS profiles for CD45RABC, CD45R0, CD45D1-D4 and CD43. The data were fitted to a flexible cylinder model<sup>130,131</sup>.

also supported by the fact that the ratio between the radius of gyration and the hydrodynamic radius is approximately 0.77 (typical of spherical objects). The radius of gyration,  $r_g$ , which is the root-mean-square distance of the molecule's segments from its center of mass can be estimated by using the Guinier approximation (Table 2.2)<sup>132</sup>. This approximation is valid for any particle shape, which means that no assumptions are made on the structure of the molecule<sup>132</sup>. To note is that the here denoted 'globular' structure of CD43 is still of 20 nm in height and thus very similar to the upright oriented CD45R0 shown to be excluded from contact regions. It could be that the globular structure resembles a bent over protein chain. The 'globular' structure could also explain the poor labelling quality since CD43 does not have many lysines (5% lysine content) necessary for the ester reaction with the fluorophore and hence, could easily be buried within the aggregated molecule decreasing the labelling outcome. It needs to be investigated if the 'globular' structure of CD43 is an artefact of the preparation or purification process of the protein or whether the structure for CD43 also deviates from an extended rod-like structure *in vivo* which could have significant consequences on the cell-cell contact organisation.



**Table 2.2. Characterisation of the dimensions of CD45 and CD43 by SAXS.**

Protein	$L$ [nm]	$l_k$ [nm]	$\langle R \rangle$ [nm]	$r_g$ [nm]
CD45D1-D4	15.7	15.2	15.4	4.2
CD45R0	20.8	14.5	17.4	4.9
CD45RABC	235.9	7.5	42	5.4
CD43	31.6	11.3	18.9	16.6

$L$  is the contour length of the protein,  $l_k$  the Kuhn length,  $\langle R \rangle$  the end-to-end distance and  $r_g$  the radius of gyration.

### 2.4.3 Summary

Overall, the new data support the previous findings of this work and of others suggesting a dominantly flexible structure of CD45RABC which could affect its effective height on the membrane. Moreover, CD45D1-D4 and CD45R0 seem to be rather rigid molecules with CD45R0 possessing some flexibility in itself as suggested by SAXS. In contrast, CD43 appears to be ‘globular’ in structure and of moderate flexibility in solution. Information about CD43’s dimension and orientation on a model or cell membrane however are still missing.

### 2.4.4 Outlook

More insights into how the glycoproteins orient and interact on model membranes could be obtained by repeating the hydrodynamic trapping measurements with a lower surface coverage of the proteins. This would be especially interesting for CD43 since it seems to be in a globular or collapsed shape in solution. An alternative approach to estimate the height of CD43 could be to compare its exclusion to the exclusion level of different sized proteins on a model membrane in contact with a cell since protein exclusion has been shown to be size dependent<sup>117</sup>. For this the comparison to CD45RABC would be particularly interesting as their reported height in solution is similar. It can further be tested how the exclusion depends on the densities of the contact forming receptor-ligand pair such as CD2-CD58. Both could answer some remaining questions about the effective height of CD43 on the bilayer and how glycoproteins in general affect and are affected by cell-cell or cell-SLB contact formation.

## Chapter 3

*Knowing is better than wondering, making is better than sleeping and even the biggest failure, even the worst, beats the hell out of never trying.*

-Shonda Rhimes-



# 3

## Affinity Measurements of Immune-Cell Proteins

### Contents

---

3.1 Introduction.....	78
3.2 Dissociation Constants and Affinity.....	79
3.2.1 Three-Dimensional Affinities.....	80
3.2.2 Two-Dimensional Affinities.....	82
3.3 The Zhu-Golan Method.....	87
3.4 The Study of an Agonistic TCR-MHC Affinity.....	90
3.4.1 Receptor Pairs.....	90
3.4.2 Changes to the Zhu-Golan Method.....	91
3.4.3 Single Ligand Affinities.....	93
3.4.4 Multiple Ligand Affinities.....	94
3.4.5 Contact Size and High Ligand Densities.....	96
3.4.6 High-Binding Interaction.....	97
3.4.7 Conclusion.....	99
3.5 TCR Binding to Self-Peptide MHC – a Measurable Affinity?...99	
3.5.1 HLA-DQ8 and L3-12 TCR.....	100
3.5.2 HLA-A02 and 1G4 TCR.....	101
3.5.3 Summary.....	103
3.5.4 Outlook.....	104

---

Chapter 3 gives an introduction into the field of 3D and 2D affinities and the methods used in the literature to obtain these values. A strong focus will be on the Zhu-Golan method used in **Paper III** and a summary of the findings in **Paper III** will follow in section 3.4. The chapter will finish with the most recent observations in studying self-peptide MHC-TCR interactions in section 3.5.

### 3.1 Introduction

A crucial step in initiating an immune response is the activation or triggering of TCRs upon binding to MHC molecules presenting agonist peptides. However, in the presence of self peptides, TCRs typically do not trigger. This phenomenon is described as self-tolerance. Self-tolerance is ensured by negative selection of T-cell precursors during thymic development in which T cells are screened for recognition of self-peptide MHCs (positive selection) and are eliminated when they bind those too strongly (negative selection)<sup>133</sup>. Most T cells undergoing the selection process die by controlled apoptosis leaving a pool of mature T cells which can distinguish between self-peptide and foreign-peptide MHCs. This guarantees that mature T cells leaving the thymus are not self-reactive against the body's own antigens which would result in autoimmune diseases, *i.e.*, harmful chronic attacks against the body's own tissue. However, not all self peptides are presented in the thymus and a few autoreactive T cells can complete their maturation and migrate to the periphery. Those cells are naturally destroyed or inactivated due to varying mechanisms of peripheral tolerance such as activation-induced cell death or anergy (functional unresponsiveness). It is believed that the distinction between positive and negative selection is merely based on the affinity differences between TCRs binding self-peptide MHCs<sup>76,133</sup>. Where this cut-off is and how the binding or affinity differs in the periphery when mature T cells meet an actual (non-self) antigen is not fully understood and has been the subject of extensive studies for decades<sup>9,12,19,134-139</sup>. An approach early on to shed some light onto this conundrum was to measure the affinity of various peptide TCR-MHC interaction pairs in solution (ranging from agonistic to antagonistic interactions) with one receptor bound to a surface and one freely diffusing in solution. However, the obtained three-dimensional affinities cannot be translated to the more complex cellular environment in which the TCR and MHC receptors are laterally confined by cell membranes and subject to cellular mechanisms and other proteins such as CD2, ICAM-1 and cell-specific co-receptors. If, and how, the binding of these other molecules in the contact area affect TCR-MHC binding has not been studied. This is because binding or affinity studies of membrane-proteins are generally difficult to conduct, even more so when considering more than one binding pair. Two-dimensional affinities are therefore

also much harder to measure than 3D affinities but crucial for understanding key interactions in a cell-cell contact. To date only a few studies have succeeded in measuring 2D affinities of TCR-MHC interactions but information about different parameters in the cell-cell contact such as the role of auxiliary proteins are mostly lacking. The aim of the work summarised in this chapter was therefore to measure the 2D affinity of a TCR-agonist MHC interaction using fluorescence microscopy and to investigate parameters that could affect the affinity such as the presence of the auxiliary binding protein CD2 and high ligand densities. The results will help to understand how to measure binding affinities between TCR and 'self' or weak agonist-peptide MHCs and what needs to be done to achieve this. The concept of affinity, how to measure it and what is known so far with the main focus on CD2 and TCR will be discussed first, after which I will move on to summarise the main findings of the work in this chapter, including the data from **Paper III**.

### 3.2 Dissociation Constants and Affinity

A general description of a non-covalent ligand-receptor interaction is given by:



where square brackets denote the concentration of the ligand (L), the receptor (R) and the ligand-receptor complex (LR). The ratio of the reactants to the product is, at equilibrium, a constant defined as the dissociation constant ( $K_d$ ) of the reaction. The  $K_d$  is a measure of how strongly the ligand binds to the receptor. It is usually presented in molar units (M) and corresponds to the ligand concentration at which half of the receptors are bound. Thus, small  $K_d$  values represent strong binding of the LR complex, *i.e.*, high affinity (*e.g.*, pM-nM), and larger values signify weak binding and hence low affinities (*e.g.*,  $\mu\text{M}$  and larger). The dissociation constant can also be calculated from the association constant ( $K_a$ ) as well as by the ratio of the on-rate ( $k_{\text{on}}$ , how fast the LR complex forms) to the off-rate ( $k_{\text{off}}$ , how fast LR dissociates):

$$K_a = \frac{[LR]}{[L][R]} = \frac{k_{on}}{k_{off}} = \frac{1}{K_d} \quad \text{Eq. 3.2}$$

A high affinity is usually associated with a fast on-rate ( $k_{on}$ ) and a slow off-rate ( $k_{off}$ ). Thus, a large association constant reflects strong binding as does a small dissociation constant.

### 3.2.1 Three-Dimensional Affinities

One of the earliest technologies to shed some light on the characteristics of TCR-MHC binding was surface plasmon resonance (SPR). SPR is an optical technique that can be used to measure kinetics and affinities of interacting proteins (ligands and receptors)<sup>140,141</sup>. The ligands (*e.g.*, MHC) are immobilised adjacent to a metal surface on a sensor chip, over which the receptors (*e.g.*, TCR) are passed in solution. Binding of the receptors to the ligands is detected as energy taken from reflected light under conditions of total internal reflection (**Figure 3.2.1A**). The incident light causes the electrons in the sensor chip to resonate. At a specific incident angle determined by the refractive index of the solution adjacent to the metal strip, this resonance frequency is the same as the light, causing it to be absorbed. This leads to a loss of intensity (a dip) in the reflected light that is recorded by a detector. Once the receptors bind to the ligand the refractive index of the solution containing them changes, causing a shift in the angle at which the intensity dip occurs. It is this change in angle that the detector records. Thus, the change in depletion angle is a direct measure of the changes in mass on the surface, *i.e.*, the amount of binding. These changes are visualised in sensograms where the signal is quantified as arbitrary response units (RU) vs time (**Figure 3.2.1B**). Once steady-state or an equilibrium of binding and dissociation is reached the maximum RU is measured for binding at the conditions studied. These graphs can also give the 3D kinetics, *i.e.*,  $k_{on}$  and  $k_{off}$ , which can along with the affinity be obtained after fitting the data to an appropriate binding model (**Figure 3.2.1B**).

Initial studies using SPR have shown that the affinities of TCR-MHC interactions were rather low (ranging from 1 to 100  $\mu\text{M}$ ), which was associated with fast off-rates (receptor-ligand complex half-life,  $t_{1/2} < 10$  seconds)<sup>9,137,142</sup>. Moreover, it has been

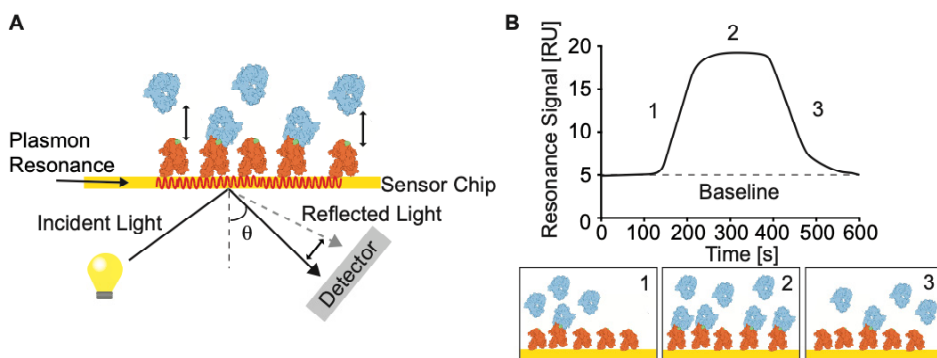


**Figure 3.2.1. Principle of surface plasmon resonance.**

(A) An incident light hits a sensor chip (yellow) on which ligands (orange) are bound. The light gets reflected towards a detector and experiences a loss in intensity at the point where the electrons in the sensor chip resonate at the same frequency as the light. The resonance of the electrons in the sensor chip and the angle of reflection ( $\theta$ ) changes upon binding of the receptors in solution (blue) and is monitored by the detector. (B) A sensogram of receptor binding to the ligands on the sensor chip. Initially the sensor chip is at baseline resonance which increases upon binding events between receptors and ligands occurring after loading the soluble receptors onto the chip (1). At the point when all receptors are in equilibrium with the ligand (2) the resonance signal reaches steady-state. Washing the chip leads to a decrease in soluble receptors and detaching of bound receptors (3) that is monitored as a decrease in response signal back to the baseline. Information of the association rate can be obtained from step 1 and the dissociation rate from step 3. Step 2 contains information about the affinity of the receptor-ligand complex.

shown that there is generally a good correlation between the strength of the TCR-MHC interaction (T-cell activation) and the off-rate<sup>9,137,142</sup>, meaning that T cell activating peptide-MHCs bind longer to the TCRs. However, several exceptions have been reported over the years<sup>138,139,143</sup>. Additionally, studies that measured binding affinities between strong activating (agonist) peptides and inhibitory (antagonist) peptides showed that the differences in 3D  $K_d$ s were rather small (e.g., 52  $\mu$ M vs 62  $\mu$ M, respectively)<sup>143,144</sup>. This makes it more complicated to draw decisive conclusions about function based TCR binding kinetics in solution. Besides, TCR and MHC molecules are laterally confined molecules *in vivo* and dissociation constants presented as a solution concentration (in molar) are generally hard to interpret and to translate into 2D affinities (in molecules/ $\mu$ m<sup>2</sup>). The important parameter to determine is therefore ideally the 2D  $K_d$  of these interactions. However, as mentioned above, measurements of 2D  $K_d$ s are difficult to obtain and have only



been generated for a few cases, which will be summarised in the next section<sup>12,18,19,118,136,145</sup>.

### 3.2.2 Two-Dimensional Affinities

Early 2D  $K_d$  studies were done by Dustin and colleagues for the human CD2-CD58 adhesion pair<sup>119,145,146</sup>. This was done by incorporating various amounts of GPI-anchored human CD58 molecules in SLBs and adding CD2-expressing T cells. The fluorescently-labelled CD58 molecules accumulate in the cell-SLB contact upon binding to CD2, observed by fluorescence microscopy as an intensity increase inside compared to outside of the contact. The principle was based on the study by McCloskey and Poo where fluorescently-labelled antibodies were observed to bind and accumulate locally in a cell-vesicle contact<sup>147</sup>. The main difference between these two approaches was how the two opposing membranes were brought into contact, with McCloskey and Poo<sup>147</sup> aspirating vesicles onto micropipettes contacting surface immobilised cells and Dustin *et al.*<sup>145</sup> using cells contacting functionalised SLBs. Micropipettes have later been used to measure 2D affinities in a mechanical-based approach that differs from fluorescence-based methods in which functionalised SLBs are used. Both methods will be described in detail below.

#### Mechanical-Based Methods

The initial idea to measure two-dimensional affinities and kinetics was based on mechanical studies investigating the adhesion behaviour of two cells or a cell and a surface *via* ligand-receptor binding. Various methods developed since the 1990s utilise this (in detail reviewed in references<sup>22,135</sup>). (i) In the flow-chamber method cells continuously flow over a ligand-functionalised surface to which they can randomly adhere<sup>148,149</sup>. While adhering, the cells experience an observable change in velocity which is recorded as a successful binding event. (ii) In the centrifugation method radiolabelled cells are brought into contact with a ligand-functionalised surface, incubated and subsequently centrifuged in an inverted configuration<sup>150</sup>. The adherence is measured through 'left-over' radioactive signals on the surface. (iii) In the micropipette method two cells are aspirated on a micropipette and are brought

periodically in and out of contact to measure adhesion events<sup>12,134</sup>. Since the latter approach became the most applied method over the last few years this section will focus on the principle of the micropipette approach.

The micropipette technique allows the formation of transient adhesive interactions at the interface of a red blood cell (RBC) placed in close proximity to a nucleated cell (**Figure 3.2.2A**). The RBC and nucleated cell can be modified or genetically engineered to present the ligand and receptor of interest, respectively. Both cells are aspirated on micropipettes and are micromanipulated to touch allowing receptor-ligand binding (**Figure 3.2.2B**). Increasing the distance between the micropipettes is used to break that bond by retracting the RBC from the brief contact (**Figure 3.2.2C**). If binding between the ligand and the receptor occur the retracted RBC changes shape to an elongated instead of spherical form (**Figure 3.2.2C**). This elongation, reflecting adhesion, is visually observed and can be translated into an adhesion frequency curve by repeatedly moving the RBC in and out of the contact, thus increasing the total contact duration and chance of binding. The off-rate,  $k_{\text{off}}$  is determined from the time that is required to reach half of the steady-state binding<sup>22</sup>. The steady-state binding can be translated into the association constant,  $K_{\text{a}}$ , that together with  $k_{\text{off}}$  can be used to determine  $k_{\text{on}}$  which is proportional to the initial slope of the adhesion frequency curve<sup>22</sup>. A more specific method was achieved by using beads attached to the RBC, which allowed for a precise tracking of the bead position and thus a higher spatial and temporal resolution<sup>12,151</sup>. Additionally, it ensures ligand-specific binding, *i.e.*, no unspecific binding between endogenously expressed proteins on the cells (**Figure 3.2.2D**)<sup>135</sup>. This approach is commonly known as the thermal fluctuation assay using a biomembrane force probe (BFP).

Both the RBC- and the bead-based methods have been used to study the 2D  $K_{\text{d}}$ s of TCRs that bind to MHC class I molecules (**Table 3.1**). The measured 2D affinities were in the same range as the high affinity interaction pair LFA-1/ICAM-1 and consequently suggested to be of higher affinity than what is conveyed by SPR measurements (**Table 3.1**)<sup>12,152</sup>. In addition, the off-rates were considerably faster in 2D than in solution implying that the apparent ligand potency will differ depending on whether 2D and 3D measurements are made<sup>12</sup>. The study showed further that the on-rate and therefore also contact formation was highly dependent on the

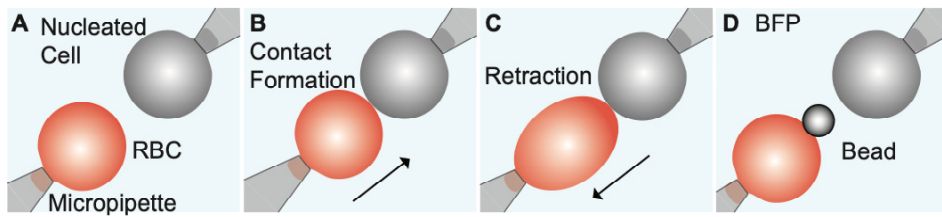


**Figure 3.2.2. Adhesion frequency assay.**

(A) A red blood cell (RBC) and a nucleated cell are aspirated on two micropipettes. (B) The RBC is moved towards the nucleated cell for contact formation. (C) The RBC is retracted from the contact area after a certain contact time and changes shape upon receptor-ligand binding. If no binding occurred the cell keeps its spherical shape (not shown). B and C are repeated several times for the adhesion frequency assay. (D) Attaching a bead to the RBC allows for precise tracking of the bead position and is used in the thermal fluctuation assay.

presented peptide supporting this as being an important source of peptide specific TCR-MHC recognition<sup>12</sup>. The observed fast off-rates, however, were inconsistent with the finding of a  $\sim 100$ -fold slower off-rate in 2D vs 3D measured using a fluorescence-based method<sup>12,153</sup>. What effect the micropipette aspiration has on the cells and how these observations would translate *in vivo* is not known. Furthermore, while the micropipette approach is very useful in determining the  $k_{\text{off}}$ , affinities (and  $k_{\text{on}}$  values) are harder to obtain and appear always as the product of the contact area,  $A_c$ , which cannot be accurately defined and thus determined for the single bonds formed using this approach. The difficulty to measure the contact area is also based on the unpredictable orientation of this area to the microscope's field of view as well as irregular contact sites that cannot yet be resolved with current microscopy methods<sup>22</sup>. The affinities measured in the mechanical approach are generally lower compared to affinities measured in fluorescence-based methods in which contact areas are easier to define since they are formed by multiple protein bonds<sup>22,156</sup>. In addition, the adhesion frequency method is best used for one receptor-ligand pair interaction (single-bond interaction) and is not a suitable approach for studying two different receptor-ligand pairs since the individual contributions to the adhesion would be difficult to discriminate. Alternative approaches to study this problem are fluorescence-based methods.

**Table 3.1. Summary of 3D and 2D affinities and off-rates measured in the literature.**

Protein* Complex	SPR			Mechanical-based			Fluorescence-based			Ref.
	3D $K_d$ ( $\mu\text{M}$ )	$k_{\text{off}}$ ( $\text{s}^{-1}$ )	$t_{1/2}$ (s)	2D $K_d$ ( $\mu\text{m}^4$ )	$k_{\text{off}}$ ( $\text{s}^{-1}$ )	$t_{1/2}$ (s)	2D $K_d$ ( $\text{mol.}/\mu\text{m}^2$ )	$k_{\text{off}}$ ( $\text{s}^{-1}$ )	$t_{1/2}$ (s)	
2B4 – MCC/E <sup>k</sup>	40-90	0.06	11.5				10			9,19,137
OT1 – OVA/H- 2K <sup>b</sup>	6	0.02	33	$1.7 \times 10^{-4}$	7	0.1				13,142
ICAM-1/ LFA-1	0.26	0.05	20	$8.6 \times 10^{-3}$	0.2	3.5				152
5c.c7 – MCC/E <sup>k</sup>	40	0.6	1.2				39	0.19-6	0.1-3.6	136,154, 155
CD2/ CD58	2-20	5	0.1				1-7	0.07	9	23,119,1 45,153
CD4/ MHC II	>2500						4800			118

\* TCR-MHC complexes are presented with the name of the TCR first followed by the peptide and the MHC name.

## Fluorescence-Based Methods

The main fluorescence-based method is the one described above where cells are attached to protein-functionalised SLBs and from which 2D affinities can be calculated using *the Zhu-Golan method*<sup>19</sup> (this will be described in detail below, see Section 3.3). As introduced earlier, advantages of the Zhu-Golan method are: (i) the contact area can be determined separately thus allowing estimates of the  $K_d$  value, and (ii) auxiliary binding proteins can be introduced into the system and easily distinguished from the main binding pair by labelling the ligands with different fluorophores. This allows for measurements of very weakly interacting proteins as has been shown by Jönsson *et al.* where the 2D  $K_d$  of the weakly interacting co-receptor CD4 to MHC II was estimated to be  $\sim 4800$  molecules/ $\mu\text{m}^2$  (Table 3.1)<sup>118</sup>. A similar approach was used by Grakoui *et al.* to estimate the 2D  $K_d$  of the MHC class II restricted 2B4 TCR<sup>19</sup>. The obtained two-dimensional 2B4 TCR-MHC affinity (2D  $K_d = 10$  molecules/ $\mu\text{m}^2$ )<sup>19</sup> is twice that of the moderate 2D affinity of the human CD2-CD58 interaction pair (average 2D  $K_d = 5$  molecules/ $\mu\text{m}^2$ )<sup>119,145</sup> (Table 3.1). In contrast, the average 3D  $K_d$  of the 2B4 TCR-MHC interaction pair in solution ( $\sim 65$   $\mu\text{M}$ )<sup>9,137</sup> was six-fold higher than the average 3D  $K_d$  of human CD2-CD58 ( $\sim 11$   $\mu\text{M}$ )<sup>23,145</sup> (Table 3.1). Thus, the TCR seemed to bind with weaker

affinity in solution than in 2D when compared to the respective values for human CD2-CD58. This observation is similar to the findings by Huang *et al.* on comparable protein systems using the micropipette approach<sup>12</sup>. It has been suggested that the depth of the third dimension is small when two cell-membranes are in close proximity supporting the interaction or adhesion of laterally confined proteins<sup>22,145</sup>. This leads, in effect, to a higher concentration of molecules in the contact area which favours bond formation and alignment of the opposing membranes, facilitating receptor-ligand binding<sup>22,145,156</sup>.

The trade-off with this method is that absolute  $k_{\text{on}}$  and  $k_{\text{off}}$  values are not directly obtainable. Nevertheless, other techniques such as FRAP or single molecule measurements including fluorescence resonance energy transfer (FRET) can be used to measure  $k_{\text{off}}$  values<sup>136,153,154</sup>. Using single-molecule FRET the off-rate as well as the 2D  $K_{\text{d}}$  of a TCR-MHC class II system, 5c.c7 TCR/MCC/E<sup>k</sup>, similar to the 2B4 TCR investigated previously, have been measured (Table 3.1). The off-rate was found to be ~12-fold faster compared to the off-rate in solution and the effective 2D  $K_{\text{d}}$  was 39 molecules/ $\mu\text{m}^2$  (Table 3.1)<sup>136</sup>. Faster off-rates in 2D have also been observed in the mechanical-based measurement by Huang *et al.* (see above)<sup>12</sup>. However, other studies have shown that 2D off-rates are in line with the off-rates obtained by SPR measurements emphasising the apparent discrepancy between measurements<sup>77,154</sup>.

## Conclusion

To conclude this section, several 2D  $K_{\text{d}}$  values have been reported in the literature using various techniques (Table 3.1). However, the obtained 2D affinities and kinetics varied between the applied 2D methods. The off-rates, which have the same units of measure (time), also varied between 2D and 3D measurements and showed by comparison that the half-lives in 2D can be faster than the respective half-lives in 3D when measuring on living cells<sup>156</sup>. This might be facilitated by cellular mechanisms regulating bond dissociation<sup>156</sup>. Moreover, affinities measured using mechanical-based methods can be up to five orders of magnitude lower than when measured using fluorescence-based methods (see Figure 2C in Zhu *et al.*<sup>156</sup>) a difference that might, at least partly, be accounted for by the effective contact area

formed which varies between these two methods. Therefore, a broader range of 2D  $K_d$ s needs to be measured to allow for a better comparison between the proteins and the applied methods. These  $K_d$  measurements need to be further extended to the multi-protein setting since TCR and MHC interact in an environment containing adhesion molecules and co-receptors.

### 3.3 The Zhu-Golan Method

2D dissociation constants of a ligand-receptor complex can be obtained by analysing the binding behaviour of receptor-expressing cells in contact with fluorescently-labelled ligand functionalised SLBs<sup>119</sup>. Initially, the receptors on the cell bind to few ligands on the SLB leading to a decrease of free ligands in the contact. Consequently, due to the law of mass action, free ligands diffuse into the contact area increasing the number of receptor-ligand interactions. The accumulation of the ligand in the contact can be observed as a fluorescence intensity increase beneath the cell and continues until steady state (equilibrium) is reached (see Eq. 3.1) (Figure 3.3.1). The affinity of a ligand binding to a receptor was commonly analysed using the Scatchard analysis<sup>140,144,146</sup>, given by:

$$\frac{[LR]}{[L]} = \frac{[LR]_{max}}{K_d} - \frac{[LR]}{K_d} \quad \text{Eq. 3.3}$$

with [LR] being the concentration of receptor-ligand complexes at equilibrium and  $[LR]_{max}$  the maximum concentration of receptor-ligand complexes. This expression assumes that the ligand is monovalent and that  $[LR]_{max}$  is constant. Applying this equation to the above described system and substituting [LR] by the amount of bound ligands in the contact,  $B$ , and [L] by the amount of free ligands,  $F$ , on the SLB (Figure 3.3.1) gives:

$$\frac{B}{F} = \frac{B_{max}}{K_d} - \frac{B}{K_d} \quad \text{Eq. 3.4}$$

Plotting  $B/F$  vs  $B$  allows fitting of the data by linear regression. The negative reciprocal slope of this curve equals the 2D  $K_d$  and the intercept with the  $x$ -axis equals the total number of binding sites,  $B_{max}$ . However, the Scatchard analysis assumes that

the receptor concentration in the contact area is constant, which is not the case for cell-cell or cell-SLB contacts, where the receptors are mobile and can diffuse into the contact from the outside.

To account for this lateral mobility Zhu *et al.* introduced the Zhu-Golan analysis which considers the total amount of mobile receptors,  $N_{tot} \times f$ , where  $N_{tot}$  is the total amount of cell surface receptors and  $f$  is the mobile fraction of these<sup>119</sup>. Zhu and colleagues further introduced the dimensionless factor  $p$  to account for the amount of receptors in the contact by incorporating the total cell surface area,  $S_{cell}$ , as well as the contact area,  $S_b$ , as variables in the analysis<sup>119</sup>. This resulted in the Zhu-Golan equation:

$$\frac{B}{F} = \frac{N_{tot} \times f}{K_d \times S_{cell}} - \frac{B \times p}{K_d} \quad \text{Eq. 3.5}$$

where  $p = S_b/S_{cell}$ . The contact area is obtained by visible differences in the intensity beneath and outside the cell using RICM or fluorescence microscopy and the total cell surface area is estimated by:

$$S_{cell} = 4\pi r^2 \times 1.8 \quad \text{Eq. 3.6}$$

where  $r$  is the measured radius of the cells in bright field and 1.8 is a correction factor for the cell's surface roughness<sup>157</sup> (Figure 3.3.1B and D).

Note, that for the Zhu-Golan equation to be true, it was assumed that the free receptor number in the contact area is, at equilibrium, equal to the receptor number outside the contact area and that only the laterally mobile receptors are capable of migrating into the contact area, binding to their respective ligand<sup>119</sup>. In addition, the measured  $B$  values are the sum of mobile and immobile receptors. Since the number of bound immobile receptors is not measurable the Zhu-Golan analysis is an approximation. Errors introduced by this approximation have however been shown to be small for most practical situations<sup>118,119</sup>. Similar to the Scatchard analysis the 2D  $K_d$  can be obtained from the negative reciprocal of the slope in the  $B/F$  vs  $B \times p$  plot. This plot is henceforth referred to as a Zhu-Golan plot (Figure 3.3.1E). The intercept with the  $x$ -axis,  $X$ , where  $B/F = 0$ , gives the total amount of mobile receptors on the cell by:

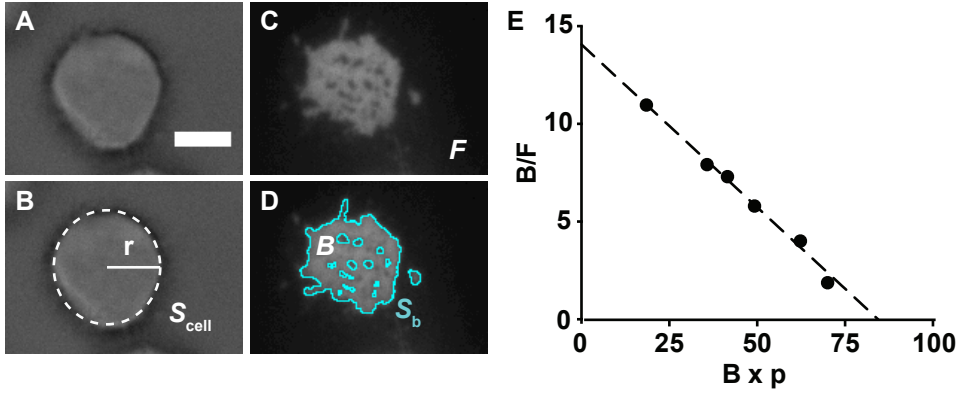


**Figure 3.3.1. The Zhu-Golan analysis in images.**

(A) A bright field image of a cell that is in contact with an SLB functionalised with a fluorescently-labelled TCR. (B) The total area of the cell,  $S_{\text{cell}}$ , is calculated from the radius of the spherical contour of the cell (*white dashed circle*) according to Eq. 3.6. (C) Accumulated TCR beneath the cell is visible as an intensity increase inside compared to outside the cell contact. The intensity outside the cell contact resembles the free ligand density,  $F$ . (D) The contact area,  $S_b$ , is the area of higher intensity (*cyan contour*). The amount of bound ligands,  $B$ , can be extracted from the average of the intensity over  $S_b$ . (E) Zhu-Golan plot with the fraction of bound to free ligand density on the y-axis and the amount of bound ligands times  $p$ , which is the ratio of  $S_b$  to  $S_{\text{cell}}$ , on the x-axis.

$$X = \frac{N_{\text{tot}} \times f}{S_{\text{cell}}} \quad \text{Eq. 3.7}$$

$f$  can be independently determined by FRAP and together with  $S_{\text{cell}}$  and  $X$  be used to estimate the total amount of receptors given by:

$$N_{\text{tot}} = \frac{X \times S_{\text{cell}}}{f} \quad \text{Eq. 3.8}$$

Determined  $N_{\text{tot}}$  values can be further compared to the actual total number of receptors on the cell measured in flow cytometry, briefly explained in the next section.

## Flow Cytometry

Flow cytometry is a technique used to analyse specific characteristics of cells. The cells are typically labelled with a fluorescently-tagged antibody against a specific antigen, in this case the receptor, and injected into the flow cytometer. While injecting, the cells pass through a laser cell by cell. The light scattering and emission



profile of the labelled cells are visualised in so called dot-plots. This allows sorting of the cells by size, granularity, and fluorescence intensity. These intensities can be transformed into actual receptor numbers using calibration beads (QuantiBrite Beads, BD Bioscience). The calibration beads contain four different levels (pre-calibrated) of a specific fluorophore and each level has a known number of fluorescent molecules per bead. Relating the four measured intensities of the beads in the flow cytometer to the known number of fluorophores per bead gives a calibration curve used to determine the receptor number on the cell.

### 3.4 The Study of an Agonistic TCR-MHC Affinity

As discussed above only a few 2D  $K_{ds}$  of membrane-proteins that play key roles in immune-cell contacts have been obtained using fluorescence-based methods. Most of these studies measured the  $K_{ds}$  in the presence of an additional ligand such as ICAM-1 or CD2. Whether the auxiliary proteins had any effect on the measured 2D  $K_d$  values, however, was thereby not addressed<sup>19,118,136,154</sup>. Moreover, it is unknown if the high protein densities commonly occurring in a contact affect receptor-ligand binding. The main aim of my study and thus **Paper III** was therefore to investigate the affinity of a TCR specific for an agonist-peptide MHC class II molecule using the Zhu-Golan method, and to understand if this affinity is affected by the two following parameters: (i) high ligand densities and (ii) the presence of an auxiliary binding molecule, which here was rat CD2 (rCD2). The affinities of rCD2 and the L3-12 TCR were analysed separately first and then together by having both ligands on the same SLB. This was done at low and high ligand densities for both proteins. The obtained results showed that the amount of auxiliary proteins can affect the 2D  $K_d$  which is further discussed in context with recent data studying 'self' interactions in Section 3.5.

#### 3.4.1 Receptor Pairs

The here chosen TCR-MHC system was an agonistic interaction between the L3-12 TCR and the human leukocyte antigen DQ8 presenting a peptide derived from

digested wheat gluten, gliadin- $\alpha$ 1 (HLA-DQ8-glia- $\alpha$ 1) with HLA-DQ8 denoting an MHC class II molecule found in humans. The L3-12 TCR has been found in celiac disease patients binding to HLA-DQ8-glia- $\alpha$ 1 and is a particularly interesting TCR since it is directly related to an autoimmune disorder and has been well characterised in 3D but not in 2D<sup>158</sup>. The 2D  $K_d$  was here measured with the Zhu-Golan method. However, differently to other studies, in which the SLBs were functionalised with the MHC molecules<sup>19,136,154</sup>, the SLBs in this study were functionalised with the L3-12 TCR and the MHCs (here HLA-DQ8) were expressed on the added cells. This was done in part to minimise signalling effects that result in cellular alterations such as cytoskeletal rearrangements which might in turn affect the 2D kinetics. That was also the determining factor for the choice of the second (adhesion) protein pair. rCD2 binding to rat CD48T92A (rCD48T92A), a high affinity mutant of the wild type rCD48, has been shown to have no signalling characteristics when transfected in Jurkat T cells<sup>24</sup>. In addition, this interaction has a similar 3D affinity and molecular size as the human CD2-CD58 interaction pair which has been argued to align opposing cell membranes supporting TCR-MHC binding<sup>145,159</sup>. Thus, rCD2 was used as a non-signalling substitute for human CD2.

### 3.4.2 Changes to the Zhu-Golan Method

#### Cell Binding to Bilayers

The original approach of the Zhu-Golan analysis is to use several bilayers that are functionalised with various (increasing) initial ligand densities. This can range from three to five or more bilayers per experiments to which the cells are added and incubated for contact formation. However, the added cells on each bilayer are 'different' (not the exact same) cells and might display binding behaviour that would be different from that observed if the exact same cells experienced increasing ligand densities. It has been shown that cells expressing higher receptor numbers also have a higher tendency to bind to low amounts of ligand on SLBs, affecting the cell pool that binds to low versus high ligand density SLBs<sup>119,145</sup>. Thus, for this study an experiment was conducted on the same bilayer with one initial ligand concentration

to which the cells bound. After washing non-bound cells off more ligand was added and incubated. This was repeated three to four times. By doing so the binding behaviour of the same cells was observable as the amount of ligand increased. It was also tested if the results from this approach differed to the ‘classic’ Zhu-Golan method and the same experiments were conducted using both approaches. No difference was observed indicating that the effect of biased cell binding is minimal at the ligand densities used here (see Supplementary Figure 1, **Paper III**). However, the new approach allows for Zhu-Golan measurements in cases of observably biased cell binding or when the receptor number on the cells can vary considerably from experiment to experiment.

### Free Ligand Density in the Contact

The fluorescence intensity in the cell-SLB contact contains information about the bound as well as the free ligands in the contact. To obtain the number of bound ligands, the intensity needs to be corrected by the intensity of the free ligands in the contact. In the Zhu-Golan method it is generally approximated that the amount of free ligands in the contact is the same as the free ligand density outside the contact (see Subchapter 3.3 ‘The Zhu-Golan Method’). This assumption is however not considering possible steric effects occurring in the contact area upon ligand binding and accumulation which can reduce the free ligand density in the contact<sup>27,117,119</sup>. The more ligands bind the more likely it is that the amount of free ligands will decrease in the contact area<sup>117</sup>. If that is true, then assuming that the free ligand density in the contact is the same as outside would cause an error by estimating a too low number of bound receptors in the contact. To test this SLBs containing either rCD2 and a non-binding TCR (1G4 TCR labelled with Alexa Fluor® 488) or the L3-12 TCR and the non-binding TCR (1G4 TCR labelled with Alexa Fluor® 647) were studied at different ligand densities (**Figure 3.4.1**). The binding densities of rCD2 varied from 300 to 550 molecules/ $\mu\text{m}^2$  causing a decrease, ranging from 15-30%, in the intensity of the 1G4 TCR in the contact compared to outside the contact. The densities of the bound L3-12 TCRs varied from 400-1600 molecules/ $\mu\text{m}^2$  which were up to three-fold higher than the ones obtained for rCD2. However, a similar level of 1G4 TCR exclusion (20-40%) was seen. Thus, an average

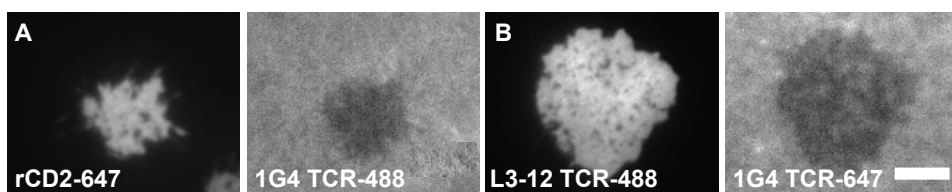


**Figure 3.4.1. Exclusion of free ligand from the contact area.**

(A) A cell binding to rCD2 (*left panel*) and 1G4 TCR (*right panel*) functionalised SLBs. (B) A cell binding to L3-12 TCR (*left panel*) and 1G4 TCR (*right panel*) functionalised SLBs. The proteins were labelled either with Alexa Fluor® 488 or 647. Black or dark grey areas indicate a decrease in intensity compared to the surrounding. Scale bar 10  $\mu\text{m}$ .

value of the fraction of free ligand density inside versus outside the contact of all obtained data was estimated and found to be 0.75. To correct for the observed decrease in free ligand density inside the contact the free ligand density outside the contact,  $F$ , was multiplied with the average value 0.75 obtaining  $F^*$  which was the ‘real’ free ligand density in the contact. This number was subtracted from the amount of apparent ‘bound’ molecules to obtain the number of actual bound ligands,  $B$ .

### 3.4.3 Single Ligand Affinities

Initially the accumulation of the single ligands, the L3-12 TCR or rCD2, beneath the cells was analysed and the 2D  $K_d$ s estimated to be  $14 \pm 5$  molecules/ $\mu\text{m}^2$  for the L3-12 TCR and  $6 \pm 1$  molecules/ $\mu\text{m}^2$  for rCD2 (Figure 3.4.2). The 2D  $K_d$  of rCD2 was similar to the 2D  $K_d$  of the human CD2-CD58 interaction, as expected from the 3D affinities (with 2-20  $\mu\text{M}$  for human CD2-CD58 and 11  $\mu\text{M}$  for the rCD2 binding CD48T92A<sup>23,119,145,153,160</sup>), and thus rCD2 seems to be a good non-signalling substitute for human CD2<sup>24,119,145,160</sup>. The affinity of the L3-12 TCR was two times lower than the affinity of rCD2 but similar to the affinity of the 2B4 TCR measured by Grakoui *et al.* with a 2D  $K_d$  of 10 molecules/ $\mu\text{m}^2$ <sup>19</sup>. However, the 3D  $K_d$  of the 2B4 TCR at 40-90  $\mu\text{M}$  is much higher than the 3D  $K_d$  of the L3-12 TCR at 7  $\mu\text{M}$ <sup>158</sup> demonstrating that the L3-12 TCR has a much stronger affinity in solution than the 2B4 TCR, but interestingly a slightly weaker one in 2D. This correlation represents a non-linear relationship between 2D and 3D measurements and underlines the lack

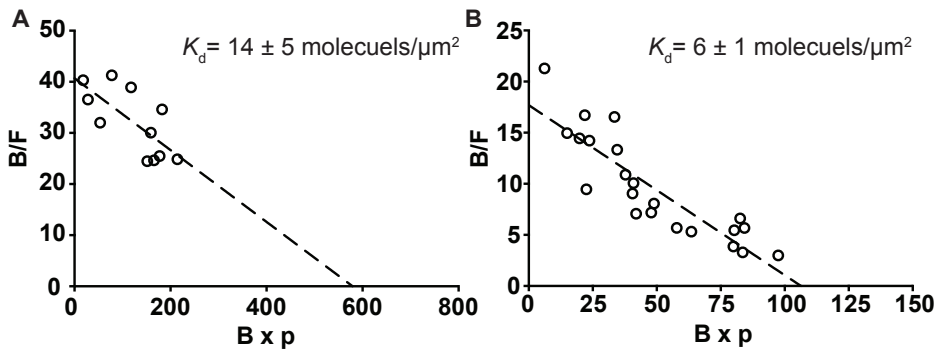


**Figure 3.4.2. Zhu-Golan plots for the L3-12 TCR and rCD2.**

(A) Zhu-Golan plot for the L3-12 TCR binding HLA-DQ8. (B) Zhu-Golan plot for the rCD2-rCD48 interaction. The dashed lines are fits to Eq. 3.5. The data points represent an average value over 50-100 analysed cells per  $F$ -value.

of understanding of how 3D values should be translated into 2D affinities. Moreover, it is hard to tell of what strength an affinity with a 2D  $K_d$  of 14 molecules/ $\mu\text{m}^2$  is since there are not many comparable studies, and IL-2 activation assays for the L3-12 TCR are missing.

### 3.4.4 Multiple Ligand Affinities

The effect of auxiliary ligands on the affinity of the studied ligand-receptor pair was investigated next. For that either (i) rCD2 was added as the auxiliary ligand to the L3-12 TCR-MHC interaction or (ii) the L3-12 TCR was the auxiliary ligand to the rCD2-CD48 interaction pair on the SLB. At low ligand densities of the auxiliary ligand in the system ( $B_{\text{rCD2}} < 200 \text{ molecules}/\mu\text{m}^2$  and  $B_{\text{TCR}} = 700 \text{ molecules}/\mu\text{m}^2$ ) no significant change in the binding density or affinity of rCD2 or the L3-12 TCR was seen (Figure 3.4.3 - red line). This low density was similar to the average density of the counter-receptors at the surface of the modified Jurkat T cells in an unbound state, with 143 molecules/ $\mu\text{m}^2$  for rCD48 and 647 molecules/ $\mu\text{m}^2$  for HLA-DQ8. Moreover, the free ligand density,  $F$ , was below 60 molecules/ $\mu\text{m}^2$  which is similar to the endogenous expression level of CD2<sup>161</sup> and TCR<sup>1,162</sup> on naïve (inactivated) T cells with 20-50 molecules/ $\mu\text{m}^2$ . However, the expression level of rCD48 and even MHC class II with 30 to 200 molecules/ $\mu\text{m}^2$ , respectively, on APCs is at least three-

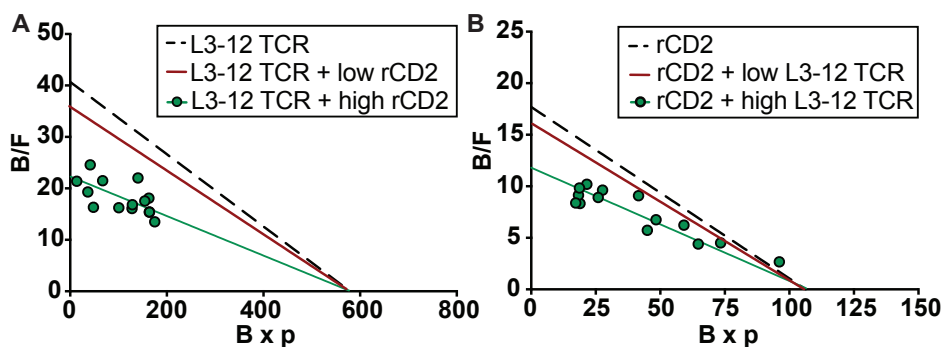


**Figure 3.4.3. Effect of auxiliary ligands on the affinity of the studied ligand.**

(A) Zhu-Golan plots of the L3-12 TCR binding HLA-DQ8 in absence of rCD2 (dashed line) and in presence of low (red line) or high amounts of rCD2 (green circles). The dashed line is a fit to the Zhu-Golan plot for the L3-12 TCR only and the solid lines to the mixture with rCD2. (B) Zhu-Golan plots of rCD2 in absence (dashed line) and in presence of low (red line) or high amounts of the L3-12 TCR (green circles). The dashed line is a fit to the Zhu-Golan plot for the rCD2 only and the solid lines to the mixture with the L3-12 TCR. Each point represents an average value for 50-100 analysed cells per  $F$ -value.

fold lower than the expression level on the here used Jurkat T cells. Thus, it would also be important to measure on cells expressing physiological receptor levels, *i.e.*, rCD48 and HLA-DQ8, to see whether the binding behaviour differs.

Increasing the ligand density of the auxiliary proteins, rCD2 or L3-12 TCR, in the cell-SLB contact above 300 and 900 molecules/ $\mu\text{m}^2$ , respectively, affected both the bound ligand density,  $B$ , and the 2D  $K_d$  of the studied proteins. This was observed by a decrease in  $B$  (data not shown, see Paper III) as well as a shift to the left in the Zhu-Golan plot at high bound densities of the auxiliary ligand in the contact (Figure 3.4.3 - green line). Under these conditions, the affinity decreased by almost 40% for both tested ligands but what exactly drives this change in affinity is not clear. One explanation could be that the increased density of the auxiliary ligand decreases the free density of the studied ligand and its counter receptor in the contact due to steric effects. If the repulsive forces are strong enough for this to occur or if the two proteins undergo some kind of competition for binding sites in the contact, which in turn could have an effect on the affinities, is unknown. It remains to be seen how common this effect is among other receptor-ligand pairs and whether it is of significance *in vivo*. Furthermore, this finding raises the question what actually defines the ‘true’

affinity of a receptor-ligand pair. Is it the binding strength of the single receptor-ligand interaction or more likely the strength of that interaction in concert with the multiple proteins important in a cell-cell contact? Thus, the observation shows, together with studies like the one by Jönsson *et al.* where the 2D affinity of CD4 could only be measured upon the addition of rCD2 in the SLB which promoted contact formation, the knife-edge between the advantage and ‘disadvantage’ of auxiliary binding molecules<sup>118</sup>. Attention must therefore be given in future experiments to what extent auxiliary protein densities are added and what  $K_d$  is aimed to be measured, the single interaction dependent affinity or the affinity influenced by the presence of the auxiliary ligand at physiological conditions.

### 3.4.5 Contact Size and High Ligand Densities

While analysing the single proteins it became apparent that the binding behaviour of the cells was different on the two studied ligands. The cells tended to form larger contact areas on L3-12 TCR than on rCD2 functionalised SLBs due to the formation of prominent lamellipodia, *i.e.*, thin membrane structures, on the L3-12 TCR. At high L3-12 TCR densities ( $F > 100$  molecules/ $\mu\text{m}^2$ ) the cell-SLB contact sizes could reach up to 40% of the total cell surface area (**Figure 3.4.4A**). High amounts of the L3-12 TCR on the SLB also caused high binding densities which were shifted to the right in the Zhu-Golan plot (at high  $B \times p$  values) (**Figure 3.4.4B**). However, at similar free ligand densities of rCD2 the cell contact size reached only a maximum of 15% of the total cell surface area (**Figure 3.4.4A**) and no stronger binding of rCD2 in the contact was observed (see **Paper III**). A reason for this difference could be that four times more HLA-DQ8 molecules than rCD48 molecules are expressed on the surface of the Jurkat T cells. Thus, care was taken about which binding densities,  $B$ -values, to include in the Zhu-Golan plot since strong binding and lamellipodia formation would increase the estimated 2D  $K_d$ . This was only necessary for the L3-12 TCR for which high ligand densities were excluded from the Zhu-Golan analysis. Upon adding both ligands on the SLB large contact formation and high binding densities were also seen for rCD2 which was explained by the presence of the L3-12 TCR dominating contact formation.

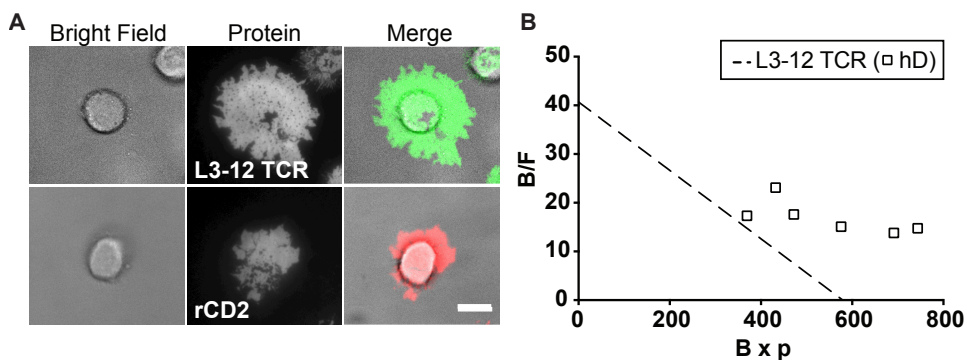


**Figure 3.4.4. High ligand density binding.**

(A) *Top panel:* Bright field image of a cell binding to the L3-12 TCR; accumulated L3-12 TCR beneath that cell at high free ligand density,  $F$ , and the merge of both channels. *Bottom panel:* Bright field image of a cell binding to rCD2, accumulated rCD2 beneath that cell at high  $F$ , and the merge of both channels. Scale bar is 10  $\mu\text{m}$ . (B) Zhu-Golan plot for the L3-12 TCR at high values of  $B \times p$ . The dashed line is a linear fit to Eq. 3.5 for the L3-12 TCR alone on the SLB at low ligand densities. Squares represent values at high ligand densities (hD). Each point represents an average value for 50-100 analysed cells per  $F$ -value.

### 3.4.6 High-Binding Interaction

Large contact areas and high free ligand densities led to strong binding (see Section 3.4.5). This could either be due to an increase in receptor-ligand complexes or trapped ligands in the contact. However, FRAP analysis revealed  $\sim 90\%$  ligand recovery within 40 seconds, showing an almost complete exchange and thus no trapping of the ligands in the contact area (Figure 3.4.5A and B). Moreover, the two complexes were estimated to have short to intermediate half-lives of 7-9 seconds or faster based on the FRAP measurements. These are comparable to what has been measured in 3D for similar soluble interactions<sup>158,163-165</sup>. Consequently, the high binding densities are more likely to appear due to an increase in receptors on the cell surface. The syntheses of new receptors within the cell is, however, questionable since high binding densities were observed using the ‘classic’ Zhu-Golan method. In this approach, the cells had been added directly to high free ligand densities and images were captured within 30 minutes, a too-short time window for the production of new receptors<sup>166</sup>. The next step was to investigate if the formation of prominent lamellipodia affected the ligand binding. Therefore, the active polymerisation



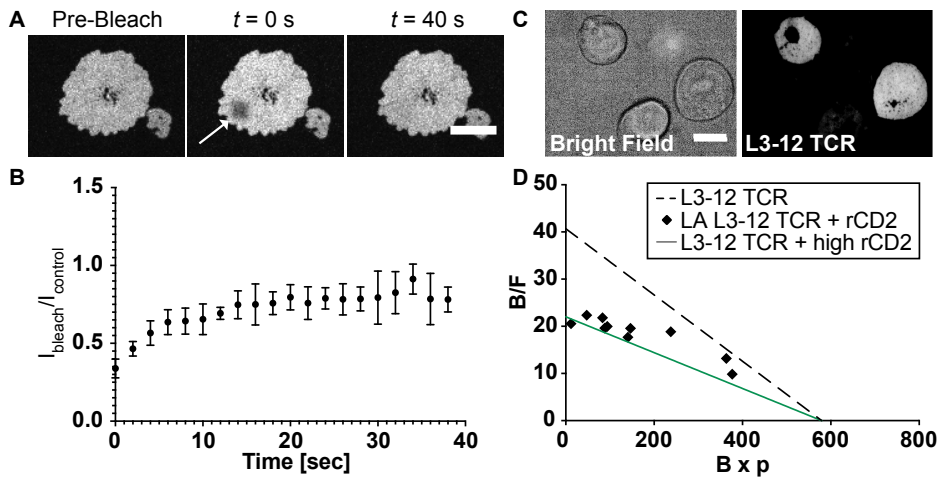


**Figure 3.4.5. FRAP and latrunculin A measurements.**

(A) Confocal images of the L3-12 TCR in the contact area of a Jurkat T cell interacting with an SLB containing both proteins, the L3-12 TCR and rCD2. Images were taken before (*pre-bleach*) and after local bleaching (indicated by a white arrow,  $t = 0$  s) as well as after recovery ( $t = 40$  s). Scale Bar 10  $\mu\text{m}$ . (B) Recovery curve of the L3-12 TCR with  $I_{\text{bleach}}$  being the intensity in the center of the bleached spot and  $I_{\text{control}}$  the intensity outside the bleached spot. Error bars are in  $\pm$  one SD. (C) Images of latrunculin A treated cells. *Left panel*: Bright field image. *Right panel*: Accumulated L3-12 TCR beneath the cells. Scale bar is 10  $\mu\text{m}$ . (D) Zhu-Golan plots for the L3-12 TCR at high amounts (*green solid line*) or in the absence of the auxiliary ligand rCD2 (*dashed lines*) for untreated cells. *Black diamonds* are for latrunculin A treated cells on SLBs containing both rCD2 and the L3-12 TCR. Each point represents an average value for 30-100 analysed cells per  $F$ -value.

of actin was inhibited by treating the cells with latrunculin A minimising lamellipodia formation (Figure 3.4.5C and D). This treatment caused a decrease in the amount of bound ligands in the contact and apparent high binding densities were no longer observed. It has previously been shown that cell activation can lead to an increase of cell surface receptors by 1.5-fold, originating from a receptor pool stored in cytoplasmic vesicles<sup>167,168</sup>. Lamellipodia might be a more active site of vesicular fusion from the cytoplasm or have, due to their thin structure, a lower receptor recycling rate. Both could account for an increased ligand density in the contact in a T-cell activation independent manner. Disrupting the actin cytoskeleton and lamellipodia formation might inhibit the vesicle transport to the cell surface and hence prevent stronger binding.

### 3.4.7 Conclusion

Taken together, I have measured 2D  $K_d$ s of the celiac disease related L3-12 TCR binding HLA-DQ8 as well as of the high affinity rCD2-rCD48T92A interaction. Cells that bound to the ligand present in high amounts at the SLBs formed contact areas that were larger than physiological sizes. Adding auxiliary proteins enhanced this effect by increasing lamellipodia formation. Moreover, high amounts of the auxiliary ligand affected the binding affinities of the studied protein by decreasing its effective 2D  $K_d$ . If this is representing the 'true'  $K_d$  *in vivo* or if it is an artefact of the *in vitro* experiment is unknown. However, the findings have important implications for future 2D  $K_d$  studies especially of weak binding interactions since, although auxiliary proteins are essential for the cell-SLB contact formation<sup>118</sup>, care needs to be taken to keep the amounts to a minimum.

### 3.5 TCR Binding to Self-Peptide MHC – a Measurable Affinity?

It has so far not been possible to measure the affinity of TCRs binding to self-peptide MHCs accurately. SPR measurements have shown that any binding of a TCR to a self-peptide MHC is below the measurable limit, which is around 300  $\mu$ M, for molecules with the size and solubility of TCRs or MHCs<sup>169</sup>. However, some studies have shown that strong T cell responses to agonist peptides can occur even at measured solution affinities > 200  $\mu$ M suggesting that 'self' should have a measurable affinity but its determination is limited by the current available methods<sup>169</sup>. A good example is the weak binding co-receptor CD4 whose lower limit for SPR-based-affinity was estimated to be 2.5 mM. Nevertheless, CD4 binding to MHC class II molecules has been proven in a cell-SLB contact where it binds with a 2D affinity of  $\sim$ 4800 molecules/ $\mu$ m<sup>2</sup>, the to date lowest ever measured affinity of a transmembrane protein<sup>118</sup>. This study gave hope to being able to measure an affinity for 'self' too. Thus, the second main aim of this Chapter's work was to investigate if the affinity of a TCR to a self-peptide presenting MHC can be measured using the Zhu-Golan method. For this, I have studied two different TCR-MHC systems and the focus was then set on the better working, 1G4 TCR-HLA-A02, system (Figure 3.5.1). A

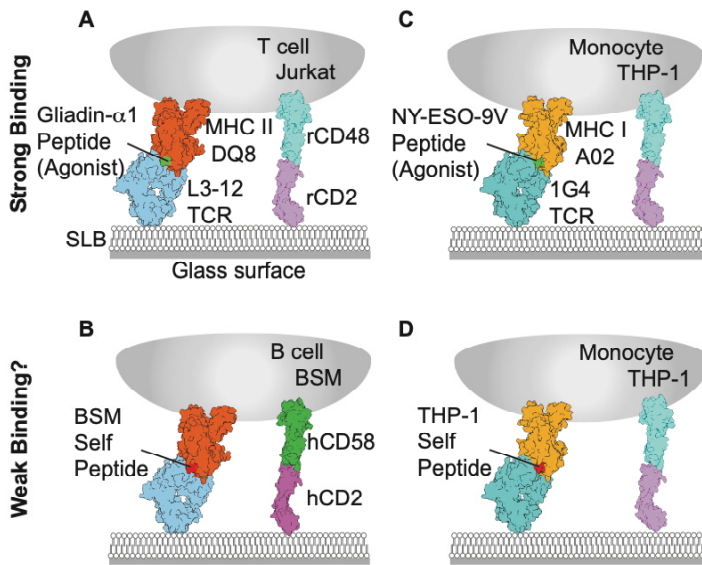


**Figure 3.5.1. Schematic representation of the agonist and self-peptide MHC-TCR systems used.**

Various TCR-MHC interactions between different cells and ligand functionalised SLBs. Strong binding is induced *via* TCR binding to agonist-peptide MHC molecules (*top panel*). Assumed weak binding is expected for TCRs binding to self-peptide MHC molecules (*bottom panel*). **(A)** Jurkat T cells expressing transfected rCD48T92A and the MHC class II molecules HLA-DQ8-gliadin- $\alpha$ 1 binding to L3-12 TCR and rCD2 functionalised SLBs. **(B)** The self-system of the HLA-DQ8 molecules is mimicked by the BSM B cell line expressing endogenous HLA-DQ8 and human CD58 binding to L3-12 TCR and human CD2 (hCD2), respectively. **(C)** THP-1 monocyte cells expressing endogenous HLA-A02 loaded with the NY-ESO 9V peptide and rCD48T92A binding to 1G4 TCR and rCD2 at the SLB, respectively. **(D)** The HLA-A02 molecules presenting only self peptides that can bind to 1G4 TCR at the SLB with rCD2-rCD48T92A as accessory proteins.

short summary about the different systems will be given below and the most important results are presented.

### 3.5.1 HLA-DQ8 and L3-12 TCR

For the self-peptide TCR-MHC system B cells of the BSM cell line have been used. These cells are expressing self-peptide presenting, endogenous, HLA-DQ8 molecules and human CD58 and were added to L3-12 TCR and human CD2 functionalised SLBs (**Figure 3.5.1B**). However, only weak contacts were formed between human CD2 and CD58 (at maximum a 2.5 increase of bound vs free molecules/ $\mu\text{m}^2$  and a

*p*-value of 0.025) and no binding was seen for the L3-12 TCR to HLA-DQ8. Moreover, the cells were sensitive to the environment resulting in inefficient culture growth and dying on the SLB, which made them particularly difficult to work with. Thus, I turned to investigate a second TCR-MHC system.

### 3.5.2 HLA-A02 and 1G4 TCR

#### The system

The next system tested was the well-studied interaction of the 1G4 TCR binding to the MHC class I molecule HLA-A02. HLA-A02 is a widely distributed allele in the population and has been found to present the tumour related peptide NY-ESO-1<sup>170</sup>. This peptide is not expressed in normal, non-germline tissues but in the testis and many tumour types such as breast and melanoma tumors<sup>171,172</sup>. The 1G4 TCR binds to NY-ESO presenting HLA-A02 with a 3D affinity of 13.3  $\mu$ M and a half-life of 4 seconds<sup>173</sup>. An even higher affinity (5  $\mu$ M) was found for the modified NY-ESO peptide 9V in which the ninth amino acid of the peptide (originally a cysteine) was exchanged with a valine<sup>173</sup>. As for most TCRs, 2D affinity information for both interactions, the agonist and 'self' 1G4 TCR-HLA-A02, are lacking. To measure 2D affinities THP-1 cells expressing HLA-A02 were bound to 1G4 TCR (16 mg/ml kindly provided by Jamie Rossjohn, Monash University, Australia) and rCD2 functionalised SLBs. THP-1 cells are a monocyte cell line, and monocytes are a type of leukocyte cell that can differentiate into for example DCs. To create an analogues system as to what has been used in **Paper III**, THP-1 cells were stably transfected with rCD48T92A.

#### The results

The THP-1 cell line was easy to handle and did not show any sensitivity or apoptosis when bound to SLBs. Moreover, a strong accumulation of rCD2 beneath the cells was observed (**Figure 3.5.2**). However, similar to the previous system, no accumulation of the 1G4 TCR was seen (**Figure 3.5.2**). It could be possible that the strong binding of rCD2 affected the weak binding interaction of the 1G4 TCR to the HLA molecules due to a steric effect decreasing the free ligand density

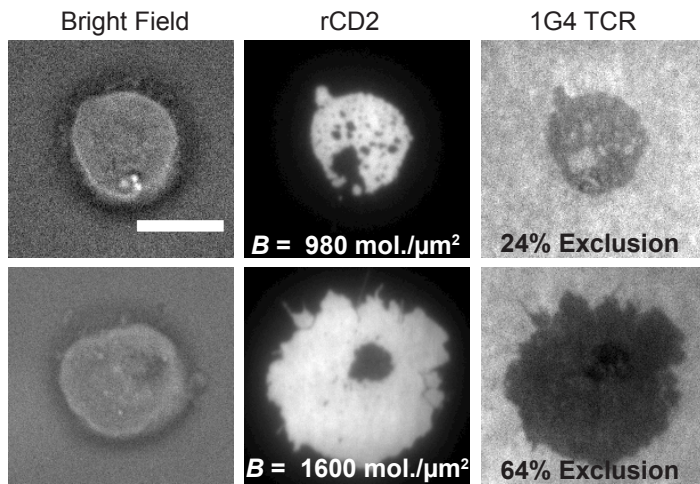


**Figure 3.5.2. Free ligand exclusion from the contact is dependent on ligand binding densities.** THP-1 cells binding to 1G4 TCR and rCD2 functionalised SLBs. *Top panel:* One cell in bright field bound to the SLB; accumulated fluorescently-labelled rCD2 beneath the cells; exclusion of the 1G4 TCR from the contact area. The free ligand density is 24% lower inside compared to outside the contact area. *Bottom panel:* Another cell bound to a higher ligand density at the SLB; accumulated rCD2; excluded 1G4 TCR from the contact area. The free ligand density inside the contact is now 64% lower than outside the contact.

of the TCR (and thus the affinity) in the contact area (see above or Conclusions **Paper III**). Indeed, increasing the ligand density ( $> 1000$  molecules/ $\mu\text{m}^2$ ) of the auxiliary protein led to a higher exclusion of the 1G4 TCR in the contact from initially 20% to more than 50% (**Figure 3.5.2**). A stronger exclusion than what was found for the non-binding 1G4 TCR in contact with the L3-12 TCR at similar  $B$  values studying Jurkat T cells (see Section 3.4.2). A decrease in free ligand density in the contact by more than 50% shows a strong steric effect and supports the conclusions drawn in **Paper III**. This observation underlines the significance of using low amounts of auxiliary protein to allow for sufficient contact formation but limited exclusion of the weaker binding protein from the contact area.

The next step was to investigate if the 1G4 TCR binds to the agonist HLA-A02. Thus, the THP-1 cells were pulsed for two hours with 100  $\mu\text{M}$  NY-ESO-9V peptide (henceforth called 9V peptide) to load the HLA-A02 molecules with the agonist peptide. This changes the self-system to an agonist-system and accumulation of the 1G4 TCR beneath the cell was expected. However, no binding to the 1G4 TCR was

seen. This could have had two reasons: either the recombinant 1G4 TCR is misfolded or not correctly bound at the SLB, or the peptide loading was not successful. The latter was investigated by flow cytometry using an HLA-A02-9V specific ImmTac (kindly provided by David Cole, ImmunoCore). An ImmTac is a T-cell receptor with a high (picomolar) affinity against the antigen of interest and is usually connected to an anti-CD3 single fragment antibody chain. In this case however, the antibody fragment was exchanged with biotin. Adding streptavidin bound to the fluorophore phycoerythrin (PE) allows for visualising of the ImmTac binding to the peptide loaded THP-1 cells. The intensities can further be related to the number of molecules per cell (see Section 3.5.1 Flow Cytometry). The number of HLA-A02 molecules presenting the 9V peptide was around 3000 molecules per cell which was 4% of the total amount of HLA-A02 on the cell surface (**Figure 3.5.3**). This number is lower than the minimum receptor number necessary to see accumulation of weak binding ligands in a cell-SLB contact<sup>145</sup> and could explain the non-binding phenomenon. This becomes even more apparent when estimating the maximum B/F-value with:

$$\left(\frac{B}{F}\right)_{max} = \frac{N_{tot} \times f}{S_{cell} \times K_d} \quad \text{Eq. 3.9}$$

The values for  $N_{tot} \times f$  and  $S_{cell}$  were measured and found to be 3000 molecules/ $\mu\text{m}^2$  and 900  $\mu\text{m}^2$ , respectively. Assuming a 2D  $K_d$  of 10 molecules/ $\mu\text{m}^2$ , the estimated  $(B/F)_{max}$  was 0.33, a low B/F-value that is difficult to detect. This value will be further lowered by high amounts of rCD2 in the system. An improved peptide loading protocol could increase the number of agonist-peptide presenting MHC molecules and thus sufficient binding of the 1G4 TCR which will be investigated in the future. If no binding can be observed, then the reason for non-binding is most likely due to a dysfunctional 1G4 TCR, which can be tested using SPR.

### 3.5.3 Summary

Two different TCR-MHC systems have been studied to measure 2D affinities of TCRs to self-peptide MHCs. It has not been possible yet to estimate a 2D affinity to 'self'. However, a promising system involving the 1G4 TCR binding to HLA-A02

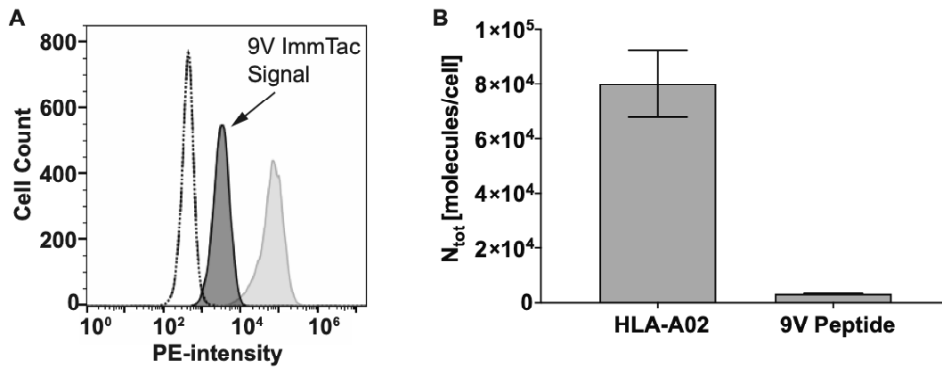


**Figure 3.5.3. Low 9V peptide loading of HLA-A02 on THP-1 cells.**

**(A)** Histogram of the measured PE-intensity of an anti-HLA-A02 (*light grey*); the ImmTac anti-9V HLA-A02 (*dark grey*); the isotype control anti-mouse IgG1  $\kappa$  (*dashed line*) and the ImmTac anti-9V HLA A02 on unloaded THP-1 cells (*dotted line*). **(B)** Via quantification beads calculated total numbers,  $N_{\text{tot}}$ , of HLA-A02 self-peptide or 9V peptide loaded molecules per cell.

has been identified. To allow for ‘self’ measurements to take place both the amount of auxiliary binding protein and the method of the 1G4 TCR binding to agonist HLA-A02-9V require optimisation.

### 3.5.4 Outlook

Once an accumulation of the 1G4 TCR beneath the cells expressing agonist-peptide MHCs is obtained the next step is to try measuring ‘self’ again considering the use of low amounts of auxiliary proteins. In case ‘self’ cannot be measured directly, one could estimate the minimum threshold for the weakest measurable interaction and thus, set an upper limit on the self-interaction without measuring ‘self’. This can be done by loading peptides of various 2D affinities ranging from strong (agonist peptide NY-ESO-9V) to very weak (null peptide) affinities onto the HLA-A02 molecules presented by the THP-1 cells and following the accumulation of the 1G4 TCR beneath the cells to estimate the 2D affinities using the Zhu-Golan method. In the case that an affinity of the 1G4 TCR to self-peptide MHCs can be measured these experiments would be complemented by investigating how other auxiliary proteins, of lower and higher affinity than the rCD2-rCD48 interaction, can affect this binding. In addition, it would be interesting to test if this behaviour is similar

when testing primary cells and under physiological levels of protein expression. Of course it would be of immense value to then move on to measure a known TCR-MHC interaction involved in an autoimmune disease such as diabetes or arthritis and see if that is related to a difference in binding affinities to 'self' and '*self*'.





## Conclusion

*Zum Abschied habe ich noch drei gut gemeinte Worte für euch.*

*Werdet. Er. Wachsen.*

*Was meint er?*

*Keine Ahnung.*

*-Tino Hanekamp, SO WAS VON DA, 2012-*



## Conclusion

The main aim of this thesis was to better understand the dimensions, lateral interactions and binding of key proteins involved in T-cell activation. I focussed first on the dimensions and lateral protein interactions of the adhesion molecule CD2, the co-receptor CD4 and tall glycoproteins such as CD45 (Chapter 2). I then moved on to have a closer look at binding affinities of TCR and rCD2 in a cell-SLB contact (Chapter 3). It was previously difficult to measure the dimensions of highly glycosylated mucin-like proteins as the sugars interfere with crystal formation. In this work, by using the hydrodynamic trapping method, more information about the dimensions and thus orientation of CD45 on the membrane was obtained. CD45RABC was found to be extended but flexible around its anchor point on the membrane causing it to have a lower effective height than what was expected for the full-length protein. This observation is a plausible explanation to why similar heights for CD45RABC and R0 were found in the literature using different microscopy techniques<sup>24,98</sup>. CD45R0 and CD45D1-D4 were also studied and showed a qualitative height difference with CD45D1-D4 being the shortest and CD45RABC the tallest molecule among these three versions. The dimensions of CD2 and CD4 were also measured and are well in agreement with the heights obtained from their crystal structures. Additionally, these proteins were highly repulsive, with CD2 more so than CD4, which was accounted for by the difference in number of glycosylation sites. CD43 has also been tested and appeared to be 'globular' in solution. Information about the orientation of CD43 on the membrane is still lacking and will be the focus of future experiments. In conclusion, I showed by using hydrodynamic trapping that the lateral interaction between proteins is affected by their glycosylation and flexibility validating this technique for further studies of membrane protein characteristics such as aggregation and dimensions. These studies will give us important insights into key membrane proteins and their behaviour in crucial cellular processes.

It seems very likely that the affinity of TCR to agonist or self-peptide MHCs differs. However, to measure two-dimensional affinities has been quite challenging, especially for weak binding interactions such as self-binding. Thus, crucial information about the suggested difference is lacking. In this work a step in the

direction of measuring 'self' was taken by investigating an agonist TCR-MHC interaction and how it depends on auxiliary proteins such as CD2. The affinity of the here tested L3-12 TCR to the HLA-DQ8 molecule was with 14 molecules/ $\mu\text{m}^2$  within the range of previously measured TCR affinities<sup>12,19</sup> and was not affected by low densities ( $B < 200$  molecules/ $\mu\text{m}^2$ ) of the auxiliary protein rCD2. However, in the presence of high amounts of rCD2 the L3-12 TCR affinity to HLA-DQ8 was two times lower. The L3-12 TCR had a similar effect on the binding of rCD2 to rCD48. The reason for this is unclear. It could be that several protein species in the contact are affected by steric hindrance or there is some kind of competition for binding sites. In addition, the cell binding behaviour varied on the two tested interaction pairs especially at high ligand densities. Larger contact areas and stronger ligand binding due to lamellipodia formation was observed on L3-12 TCR functionalised SLBs. A similar effect was seen if both proteins were on the same SLB but not for rCD2 alone. Lamellipodia formation caused more ligand binding which was attributed to increased vesicular transport from the cytoplasm to the membrane. In conclusion, strong lamellipodia formation affected the binding behaviour of the cell and the presence of high amounts of auxiliary proteins, *i.e.*, rCD2 and the L3-12 TCR, decreased the affinity of the studied ligand. The latter finding raises the question of what the true affinity of an interaction is and gives important implications for future studies. For measurements aiming to obtain 2D  $K_{ds}$  of the 'single' protein interaction Zhu-Golan measurements should be conducted without or with low amounts of the auxiliary protein. This would also be true for weak interactions such as measuring 'self', which has been tried in this work. The high amount of rCD2 which has been used to promote contact formation could explain a decrease in the binding strength of the self-binding TCR-MHC interaction to an undetectable limit and could be circumvented in future by decreasing the amount of bound rCD2 in the contact. This would allow to measure an affinity for 'self' that is currently missing.

## References

*You are a little scary sometimes, you know that?*

*Brilliant...but scary!*

-Ron Weasley, *Harry Potter and the Philosopher's Stone*, 1997-



## References

1. Murphy, K. & Weaver, C. *Janeway's Immunobiology*. (2017).
2. Harris, L. J., Skaletsky, E. & McPherson, A. Crystallographic structure of an intact IgG1 monoclonal antibody. *J. Mol. Biol.* (1998). doi:10.1006/jmbi.1997.1508
3. Dong, D. *et al.* Structural basis of assembly of the human T cell receptor–CD3 complex. *Nature* (2019). doi:10.1038/s41586-019-1537-0
4. Artyomov, M. N., Lis, M., Devadas, S., Davis, M. M. & Chakraborty, A. K. CD4 and CD8 binding to MHC molecules primarily acts to enhance Lck delivery. *Proc. Natl. Acad. Sci. U. S. A.* (2010). doi:10.1073/pnas.1010568107
5. Bosselut, R., Feigenbaum, L., Sharrow, S. O. & Singer, A. Strength of signaling by CD4 and CD8 coreceptor tails determines the number but not the lineage direction of positively selected thymocytes. *Immunity* (2001). doi:10.1016/S1074-7613(01)00128-5
6. Koretzky, G. A. Multiple Roles of CD4 and CD8 in T Cell Activation. *J. Immunol.* (2010). doi:10.4049/jimmunol.1090076
7. Glassman, C. R., Parrish, H. L., Lee, M. S. & Kuhns, M. S. Reciprocal TCR-CD3 and CD4 Engagement of a Nucleating pMHCII Stabilizes a Functional Receptor Macrocomplex. *Cell Rep.* (2018). doi:10.1016/j.celrep.2017.12.104
8. Shaw, A. S. & Dustin, M. L. Making the T cell receptor go the distance: A topological view of T cell activation. *Immunity* (1997). doi:10.1016/S1074-7613(00)80279-4
9. Matsui, K., Boniface, J. J., Steffner, P., Reay, P. A. & Davis, M. M. Kinetics of T-cell receptor binding to peptide/I-E(k) complexes: Correlation of the dissociation rate with T-cell responsiveness. *Proc. Natl. Acad. Sci. U. S. A.* (1994). doi:10.1073/pnas.91.26.12862
10. Wu, L. C., Tuot, D. S., Lyons, D. S., Garcia, C. & Davis, M. M. Two-step binding mechanism for T-cell receptor recognition of peptide-MHC. *Nature* (2002). doi:10.1038/nature00920
11. Rudolph, M. G., Stanfield, R. L. & Wilson, I. A. HOW TCRS BIND MHCS, PEPTIDES, AND CORECEPTORS. *Annu. Rev. Immunol.* (2006). doi:10.1146/annurev.immunol.23.021704.115658
12. Huang, J. *et al.* The kinetics of two-dimensional TCR and pMHC interactions determine T-cell responsiveness. *Nature* (2010). doi:10.1038/nature08944
13. Huang, J. *et al.* A Single peptide-major histocompatibility complex ligand triggers digital cytokine secretion in CD4+ T Cells. *Immunity* (2013). doi:10.1016/j.immuni.2013.08.036
14. Purbhoo, M. A., Irvine, D. J., Huppa, J. B. & Davis, M. M. T cell killing does not require the formation of a stable mature immunological synapse. *Nat. Immunol.* (2004). doi:10.1038/ni1058
15. Irvine, D. J., Purbhoo, M. A., Krosgaard, M. & Davis, M. M. Direct observation



- of ligand recognition by T cells. *Nature* **419**, 845–849 (2002).
16. Courtney, A. H., Lo, W. L. & Weiss, A. TCR Signaling: Mechanisms of Initiation and Propagation. *Trends in Biochemical Sciences* (2018). doi:10.1016/j.tibs.2017.11.008
  17. Dustin, M. L. The immunological synapse. *Cancer immunology research* (2014). doi:10.1158/2326-6066.CIR-14-0161
  18. Bromley, S. K. *et al.* The immunological synapse and CD28-CD80 interactions. *Nat. Immunol.* **2**, 1159–1166 (2001).
  19. Grakoui, A. *et al.* The immunological synapse: A molecular machine controlling T cell activation. *Science (80-. )*. **285**, 221–227 (1999).
  20. Yin, Y., Wang, X. X. & Mariuzza, R. A. Crystal structure of a complete ternary complex of T-cell receptor, peptide-MHC, and CD4. *Proc. Natl. Acad. Sci. U. S. A.* (2012). doi:10.1073/pnas.1118801109
  21. Yan, Q. *et al.* Structural Basis for Activation of ZAP-70 by Phosphorylation of the SH2-Kinase Linker. *Mol. Cell. Biol.* (2013). doi:10.1128/mcb.01637-12
  22. Dustin, M. L., Bromley, S. K., Davis, M. M. & Zhu, C. Identification of Self Through Two-Dimensional Chemistry and Synapses. *Annu. Rev. Cell Dev. Biol.* (2001). doi:10.1146/annurev.cellbio.17.1.133
  23. Davis, S. J. & Van Der Merwe, P. A. The structure and ligand interactions of CD2: Implications for T-cell function. *Immunology Today* (1996). doi:10.1016/0167-5699(96)80617-7
  24. Chang, V. T. *et al.* Initiation of T cell signaling by CD45 segregation at “close contacts.” *Nat. Immunol.* **17**, 574–582 (2016).
  25. Jones, E. Y., Davis, S. J., Williams, A. F., Harlos, K. & Stuart, D. I. Crystal structure at 2.8 Å resolution of a soluble form of the cell adhesion molecule CD2. *Nature* **360**, 232–239 (1992).
  26. Ikemizu, S. *et al.* Crystal structure of the CD2-binding domain of CD58 (lymphocyte function-associated antigen 3) at 1.8-Å resolution. *Proc. Natl. Acad. Sci. U. S. A.* (1999). doi:10.1073/pnas.96.8.4289
  27. James, J. R. & Vale, R. D. Biophysical mechanism of T-cell receptor triggering in a reconstituted system. *Nature* (2012). doi:10.1038/nature11220
  28. Brittain, W. J. & Minko, S. A structural definition of polymer brushes. *J. Polym. Sci. Part A Polym. Chem.* (2007). doi:10.1002/pola.22180
  29. Holmes, N. CD45: All is not yet crystal clear. *Immunology* (2006). doi:10.1111/j.1365-2567.2005.02265.x
  30. Hermiston, M. L., Xu, Z. & Weiss, A. CD45: A Critical Regulator of Signaling Thresholds in Immune Cells. *Annu. Rev. Immunol.* (2003). doi:10.1146/annurev.immunol.21.120601.140946
  31. Alberts, B. *et al.* *Molecular Biology of the Cell.* (2017). doi:10.1201/9781315735368
  32. Watson, H. Biological membranes. *Essays Biochem.* (2015). doi:10.1042/BSE0590043

33. Singer, S. J. & Nicolson, G. L. The fluid mosaic model of the structure of cell membranes. *Science* (80-. ). (1972). doi:10.1126/science.175.4023.720
34. Alenghat, F. J. & Golan, D. E. Membrane protein dynamics and functional implications in mammalian cells. in *Current Topics in Membranes* (2013). doi:10.1016/B978-0-12-417027-8.00003-9
35. Winterhalter, M. Black lipid membranes. *Current Opinion in Colloid and Interface Science* (2000). doi:10.1016/S1359-0294(00)00063-7
36. Castellana, E. T. & Cremer, P. S. Solid supported lipid bilayers: From biophysical studies to sensor design. *Surface Science Reports* (2006). doi:10.1016/j.surfrep.2006.06.001
37. Tamm, L. K. & McConnell, H. M. Supported phospholipid bilayers. *Biophys. J.* (1985). doi:10.1016/S0006-3495(85)83882-0
38. Khan, M. S., Dosoky, N. S. & Williams, J. D. Engineering lipid bilayer membranes for protein studies. *International Journal of Molecular Sciences* (2013). doi:10.3390/ijms141121561
39. McConnell, H. M., Watts, T. H., Weis, R. M. & Brian, A. A. Supported planar membranes in studies of cell-cell recognition in the immune system. *BBA - Rev. Biomembr.* (1986). doi:10.1016/0304-4157(86)90016-X
40. Mennicke, U. & Salditt, T. Preparation of solid-supported lipid bilayers by spin-coating. *Langmuir* (2002). doi:10.1021/la025863f
41. Brian, A. A. & McConnell, H. M. Allogeneic stimulation of cytotoxic T cells by supported planar membranes. *Proc. Natl. Acad. Sci. U. S. A.* (1984). doi:10.1073/pnas.81.19.6159
42. Andrecka, J., Spillane, K. M., Ortega-Arroyo, J. & Kukura, P. Direct observation and control of Supported lipid bilayer formation with interferometric scattering Microscopy. *ACS Nano* (2013). doi:10.1021/nn403367c
43. Thompson, N. L., Brian, A. A. & McConnell, H. M. Covalent linkage of a synthetic peptide to a fluorescent phospholipid and its incorporation into supported phospholipid monolayers. *BBA - Biomembr.* (1984). doi:10.1016/0005-2736(84)90512-1
44. Sackmann, E. Supported membranes: Scientific and practical applications. *Science* (80-. ). (1996). doi:10.1126/science.271.5245.43
45. Salafsky, J., Groves, J. T. & Boxer, S. G. Architecture and function of membrane proteins in planar supported bilayers: A study with photosynthetic reaction centers. *Biochemistry* (1996). doi:10.1021/bi961432i
46. Medof, M. E., Nagarajan, S. & Tykocinski, M. L. Cell-surface engineering with GPI-anchored proteins. *FASEB Journal* (1996).
47. Chan, P. Y. *et al.* Influence of receptor lateral mobility on adhesion strengthening between membranes containing LFA-3 and CD2. *J. Cell Biol.* (1991). doi:10.1083/jcb.115.1.245
48. Groves, J. T., Wülfing, C. & Boxer, S. G. Electrical manipulation of glycan-

- phosphatidyl inositol-tethered proteins in planar supported bilayers. *Biophys. J.* (1996). doi:10.1016/S0006-3495(96)79462-6
49. Hafeman, D. G., Von Tscharner, V. & McConnell, H. M. Specific antibody-dependent interactions between macrophages and lipid haptens in planar lipid monolayers. *Proc. Natl. Acad. Sci. U. S. A.* (1981). doi:10.1073/pnas.78.7.4552
  50. Kitch Humphries, G. M. & McConnell, H. M. Antigen mobility in membranes and complement mediated immune attack. *Proc. Natl. Acad. Sci. U. S. A.* (1975).
  51. Liu, Z. *et al.* Specific binding of avidin to biotin containing lipid lamella surfaces studied with monolayers and liposomes. *Eur. Biophys. J.* (1995). doi:10.1007/BF00216828
  52. Green, N. M. Avidin. 3. The Nature of the Biotin-Binding Site. *Biochem. J.* (1963). doi:10.1042/bj0890599
  53. Piran, U. & Riordan, W. J. Dissociation rate constant of the biotin-streptavidin complex. *J. Immunol. Methods* (1990). doi:10.1016/0022-1759(90)90328-S
  54. Werner, A. Beitrag zur Konstitution anorganischer Verbindungen. *Zeitschrift für Anorg. Chemie* (1893). doi:10.1002/zaac.18930030136
  55. Porath, J., Carlsson, J., Olsson, I. & Belfrage, G. Metal chelate affinity chromatography, a new approach to protein fractionation. *Nature* (1975). doi:10.1038/258598a0
  56. Schmitt, L., Dietrich, C. & Tampé, R. Synthesis and Characterization of Chelator-Lipids for Reversible Immobilization of Engineered Proteins at Self-Assembled Lipid Interfaces. *J. Am. Chem. Soc.* (1994). doi:10.1021/ja00098a008
  57. Dietrich, C., Schmitt, L. & Tampé, R. Molecular organization of histidine-tagged biomolecules at self-assembled lipid interfaces using a novel class of chelator lipids. *Proc. Natl. Acad. Sci. U. S. A.* **92**, 9014–9018 (1995).
  58. Celia, H., Wilson-Kubalek, E., Milligan, R. A. & Teyton, L. Structure and function of a membrane-bound murine MHC class I molecule. *Proc. Natl. Acad. Sci. U. S. A.* (1999). doi:10.1073/pnas.96.10.5634
  59. Kim, T. K. & Eberwine, J. H. Mammalian cell transfection: The present and the future. *Anal. Bioanal. Chem.* (2010). doi:10.1007/s00216-010-3821-6
  60. Nye, J. A. & Groves, J. T. Kinetic control of histidine-tagged protein surface density on supported lipid bilayers. *Langmuir* (2008). doi:10.1021/la703788h
  61. Sydor, A. M., Czymmek, K. J., Puchner, E. M. & Mennella, V. Super-Resolution Microscopy: From Single Molecules to Supramolecular Assemblies. *Trends in Cell Biology* (2015). doi:10.1016/j.tcb.2015.10.004
  62. Vangindertael, J. *et al.* An introduction to optical super-resolution microscopy for the adventurous biologist. *Methods and Applications in Fluorescence* (2018). doi:10.1088/2050-6120/aae0c
  63. E.M., B. Fluorescence microscopy of biological objects using light from above. *Biophysics (Oxf)*. 97–104 (1959).
  64. Ploem, J. S. The use of a vertical illuminator with interchangeable dichroic mirrors

- for fluorescence microscopy using incident light. *Z. Wiss. Mikrosk.* **68**, 129–42 (1967).
65. Masters, B. R. The Development of Fluorescence Microscopy. in *Encyclopedia of Life Sciences* (2010). doi:10.1002/9780470015902.a0022093
  66. Axelrod, D. Cell-substrate contacts illuminated by total internal reflection fluorescence. *J. Cell Biol.* (1981). doi:10.1083/jcb.89.1.141
  67. Axelrod, D. Total internal reflection fluorescence microscopy in cell biology. *Traffic* (2001). doi:10.1034/j.1600-0854.2001.21104.x
  68. Axelrod, D., Burghardt, T. P. & Thompson, N. L. Total internal reflection fluorescence. *Annual review of biophysics and bioengineering* (1984). doi:10.1146/annurev.bb.13.060184.001335
  69. Minsky, M. Microscopy Apparatus. *US Pat. 3013467* (1957). doi:US3013467A
  70. Fellers, M. & Davidson, T. Introduction to Confocal Microscopy. *Olympus* Available at: <https://www.olympus-lifescience.com/en/microscope-resource/primer/techniques/confocal/confocalintro/>. (Accessed: 5th September 2019)
  71. Cox, G. *Optical Imaging Techniques in Cell Biology. Optical Imaging Techniques in Cell Biology* (CRC Press, 2006). doi:10.1201/9781420005615
  72. Andor. An Overview of Spinning Disk Confocal Microscopy. *Oxford Instruments* Available at: <https://andor.oxinst.com/learning/view/article/spinning-disk-confocal>. (Accessed: 5th September 2019)
  73. Petráň, M., Hadravský, M., Egger, M. D. & Galambos, R. Tandem-Scanning Reflected-Light Microscope\*. *J. Opt. Soc. Am.* (1968). doi:10.1364/josa.58.000661
  74. Gräf, R., Rietdorf, J. & Zimmermann, T. Live cell spinning disk microscopy. *Advances in Biochemical Engineering/Biotechnology* (2005). doi:10.1007/b102210
  75. Axelrod, D., Koppel, D. E., Schlessinger, J., Elson, E. & Webb, W. W. Mobility measurement by analysis of fluorescence photobleaching recovery kinetics. *Biophys. J.* (1976). doi:10.1016/S0006-3495(76)85755-4
  76. Mckeithan, T. W. Kinetic proofreading in T-cell receptor signal transduction. *Proc. Natl. Acad. Sci. U. S. A.* (1995). doi:10.1073/pnas.92.11.5042
  77. Pielak, R. M. *et al.* Early T cell receptor signals globally modulate ligand: receptor affinities during antigen discrimination. *Proc. Natl. Acad. Sci. U. S. A.* (2017). doi:10.1073/pnas.1613140114
  78. Rossy, J., Williamson, D. J. & Gaus, K. How does the kinase Lck phosphorylate the T cell receptor? Spatial organization as a regulatory mechanism. *Frontiers in Immunology* (2012). doi:10.3389/fimmu.2012.00167
  79. Au-Yeung, B. B., Shah, N. H., Shen, L. & Weiss, A. ZAP-70 in Signaling, Biology, and Disease. *Annu. Rev. Immunol.* (2018). doi:10.1146/annurev-immunol-042617-053335
  80. Morris, G. P. & Allen, P. M. How the TCR balances sensitivity and specificity for the recognition of self and pathogens. *Nature Immunology* (2012).

doi:10.1038/ni.2190

81. Gaud, G., Lesourne, R. & Love, P. E. Regulatory mechanisms in T cell receptor signalling. *Nature Reviews Immunology* (2018). doi:10.1038/s41577-018-0020-8
82. Davis, S. J. & van der Merwe, P. A. The kinetic-segregation model: TCR triggering and beyond. *Nature Immunology* (2006). doi:10.1038/ni1369
83. Chakraborty, A. K. & Weiss, A. Insights into the initiation of TCR signaling. *Nature Immunology* (2014). doi:10.1038/ni.2940
84. Garcia, K. C. Molecular interactions between extracellular components of the T-cell receptor signaling complex. *Immunol. Rev.* (1999). doi:10.1111/j.1600-065X.1999.tb01357.x
85. Kuhns, M. S. & Davis, M. M. TCR signaling emerges from the sum of many parts. *Frontiers in Immunology* (2012). doi:10.3389/fimmu.2012.00159
86. Wucherpfennig, K. W., Gagnon, E., Call, M. J., Huseby, E. S. & Call, M. E. Structural biology of the T-cell receptor: insights into receptor assembly, ligand recognition, and initiation of signaling. *Cold Spring Harbor perspectives in biology* (2010). doi:10.1101/cshperspect.a005140
87. Lee, M. S. *et al.* A Mechanical Switch Couples T Cell Receptor Triggering to the Cytoplasmic Juxtamembrane Regions of CD3 $\zeta$ . *Immunity* (2015). doi:10.1016/j.immuni.2015.06.018
88. Brazin, K. N. *et al.* Structural features of the  $\alpha\beta$ TCR mechanotransduction apparatus that promote pMHC discrimination. *Frontiers in Immunology* (2015). doi:10.3389/fimmu.2015.00441
89. Kim, S. T. *et al.* The  $\alpha\beta$  T cell receptor is an anisotropic mechanosensor. *J. Biol. Chem.* (2009). doi:10.1074/jbc.M109.052712
90. Liu, B., Chen, W., Evavold, B. D. & Zhu, C. Accumulation of dynamic catch bonds between TCR and agonist peptide-MHC triggers T cell signaling. *Cell* (2014). doi:10.1016/j.cell.2014.02.053
91. Feng, Y. *et al.* Mechanosensing drives acuity of  $\alpha\beta$  T-cell recognition. *Proc. Natl. Acad. Sci. U. S. A.* (2017). doi:10.1073/pnas.1703559114
92. Fernandes, R. A. *et al.* A cell topography-based mechanism for ligand discrimination by the T cell receptor. *Proc. Natl. Acad. Sci. U. S. A.* (2019). doi:10.1073/pnas.1817255116
93. Irlles, C. *et al.* CD45 ectodomain controls interaction with GEMs and Lck activity for optimal TCR signaling. *Nat. Immunol.* (2003). doi:10.1038/ni877
94. Cordoba, S. P. *et al.* The large ectodomains of CD45 and CD148 regulate their segregation from and inhibition of ligated T-cell receptor. *Blood* 121, 4295–4302 (2013).
95. Nam, H. J., Poy, F., Saito, H. & Frederick, C. A. Structural basis for the function and regulation of the receptor protein tyrosine phosphatase CD45. *J. Exp. Med.* (2005). doi:10.1084/jem.20041890
96. Choudhuri, K. *et al.* Peptide-major histocompatibility complex dimensions control

- proximal kinase-phosphatase balance during T cell activation. *J. Biol. Chem.* (2009). doi:10.1074/jbc.M109.039966
97. Choudhuri, K., Wiseman, D., Brown, M. H., Gould, K. & Van Der Merwe, P. A. T-cell receptor triggering is critically dependent on the dimensions of its peptide-MHC ligand. *Nature* (2005). doi:10.1038/nature03843
  98. Carbone, C. B. *et al.* In vitro reconstitution of T cell receptor-mediated segregation of the CD45 phosphatase. *Proc. Natl. Acad. Sci.* 201710358 (2017). doi:10.1073/pnas.1710358114
  99. Symons, A., Willis, A. C. & Barclay, A. N. Domain organization of the extracellular region of CD45. *Protein Eng. Des. Sel.* **12**, 885–892 (1999).
  100. James, J. R. *et al.* The T cell receptor triggering apparatus is composed of monovalent or monomeric proteins. *J. Biol. Chem.* (2011). doi:10.1074/jbc.M111.219212
  101. McCall, M. N., Shotton, D. M. & Barclay, a N. Expression of soluble isoforms of rat CD45. Analysis by electron microscopy and use in epitope mapping of anti-CD45R monoclonal antibodies. *Immunology* **76**, 310–317 (1992).
  102. Cyster, J. G., Shotton, D. M. & Williams, a F. The dimensions of the T lymphocyte glycoprotein leukosialin and identification of linear protein epitopes that can be modified by glycosylation. *EMBO J.* **10**, 893–902 (1991).
  103. Shelley, C. S., Remold-O'Donnell, E., Rosen, F. S. & Whitehead, A. S. Structure of the human sialophorin (CD43) gene. Identification of features atypical of genes encoding integral membrane proteins. *Biochem. J.* (1990). doi:10.1042/bj2700569
  104. Walker, J. & Green, J. M. Structural requirements for CD43 function. *J. Immunol.* (1999).
  105. Sperling, A. I. *et al.* Cutting edge: TCR signaling induces selective exclusion of CD43 from the T cell-antigen-presenting cell contact site. *J. Immunol.* (1998).
  106. Tong, J. *et al.* CD43 Regulation of T Cell Activation Is Not through Steric Inhibition of T Cell-APC Interactions but through an Intracellular Mechanism. *J. Exp. Med.* (2004). doi:10.1084/jem.20021602
  107. Delon, J., Kaibuchi, K. & Germain, R. N. Exclusion of CD43 from the immunological synapse is mediated by phosphorylation-regulated relocation of the cytoskeletal adaptor Moesin. *Immunity* (2001). doi:10.1016/S1074-7613(01)00231-X
  108. Manjunath, N., Correa, M., Ardman, M. & Ardman, B. Negative regulation of T-cell adhesion and activation by CD43. *Nature* (1995). doi:10.1038/377535a0
  109. Mody, P. D. *et al.* Signaling through CD43 regulates CD4 T-cell trafficking. *Blood* (2007). doi:10.1182/blood-2007-01-065276
  110. Stock, K. *et al.* Variable-angle total internal reflection fluorescence microscopy (VA-TIRFM): Realization and application of a compact illumination device. *J. Microsc.* (2003). doi:10.1046/j.1365-2818.2003.01200.x
  111. Groves, J. T., Parthasarathy, R. & Forstner, M. B. Fluorescence Imaging of Membrane Dynamics. *Annu. Rev. Biomed. Eng.* **10**, 311–338 (2008).

112. Godula, K. *et al.* Control of the Molecular Orientation of Membrane-Anchored Biomimetic Glycopolymers. *J. Am. Chem. Soc.* **131**, 10263–10268 (2009).
113. Paszek, M. J. *et al.* Scanning angle interference microscopy reveals cell dynamics at the nanoscale. *Nat. Methods* **9**, 825–827 (2012).
114. Ajo-Franklin, C. M., Ganesan, P. V. & Boxer, S. G. Variable incidence angle fluorescence interference contrast microscopy for *Z*-imaging single objects. *Biophys. J.* **89**, 2759–2769 (2005).
115. Limozin, L. & Sengupta, K. Quantitative reflection interference contrast microscopy (RICM) in soft matter and cell adhesion. *ChemPhysChem* **10**, 2752–2768 (2009).
116. Fenz, S. F., Merkel, R. & Sengupta, K. Diffusion and intermembrane distance: Case study of avidin and E-cadherin mediated adhesion. *Langmuir* (2009). doi:10.1021/la803227s
117. Schmid, E. M. *et al.* Size-dependent protein segregation at membrane interfaces. *Nat. Phys.* **12**, 704–711 (2016).
118. Jönsson, P. *et al.* Remarkably low affinity of CD4/peptide-major histocompatibility complex class II protein interactions. *Proc. Natl. Acad. Sci. U. S. A.* (2016). doi:10.1073/pnas.1513918113
119. Zhu, D.-M., Dustin, M. L., Cairo, C. W. & Golan, D. E. Analysis of Two-Dimensional Dissociation Constant of Laterally Mobile Cell Adhesion Molecules. *Biophys. J.* **92**, 1022–1034 (2007).
120. Jönsson, P. & Jönsson, B. Hydrodynamic Forces on Macromolecules Protruding from Lipid Bilayers Due to External Liquid Flows. *Langmuir* **31**, 12708–12718 (2015).
121. Jönsson, P. *et al.* Hydrodynamic trapping of molecules in lipid bilayers. *Proc. Natl. Acad. Sci. U. S. A.* **109**, 10328–33 (2012).
122. Li, Y., Yin, Y. & Mariuzza, R. A. Structural and biophysical insights into the role of CD4 and CD8 in T cell activation. *Frontiers in Immunology* (2013). doi:10.3389/fimmu.2013.00206
123. Guigas, G. & Weiss, M. Effects of protein crowding on membrane systems. *Biochim. Biophys. Acta - Biomembr.* (2016). doi:10.1016/j.bbamem.2015.12.021
124. Murray, A. J., Lewis, S. J., Barclay, A. N. & Brady, R. L. One sequence, two folds: A metastable structure of CD2. *Proc. Natl. Acad. Sci. U. S. A.* (1995). doi:10.1073/pnas.92.16.7337
125. Moldovan, M.-C. *et al.* CD4 Dimers Constitute the Functional Component Required for T Cell Activation. *J. Immunol.* (2002). doi:10.4049/jimmunol.169.11.6261
126. Desai, D. M., Sap, J., Schlessinger, J. & Weiss, A. Ligand-mediated negative regulation of a chimeric transmembrane receptor tyrosine phosphatase. *Cell* **73**, 541–554 (1993).
127. Majeti, R., Bilwes, A. M., Noel, J. P., Hunter, T. & Weiss, A. Dimerization-induced inhibition of receptor protein tyrosine phosphatase function through an inhibitory

- wedge. *Science* (80- ). 279, 88–91 (1998).
128. Xu, Z. & Weiss, A. Negative regulation of CD45 by differential homodimerization of the alternatively spliced isoforms. *Nat. Immunol.* 3, 764–771 (2002).
  129. Teraoka, I. *Polymer Solutions*. (John Wiley & Sons, Inc., 2002).
  130. Chen, W. R., Butler, P. D. & Magid, L. J. Incorporating intermicellar interactions in the fitting of SANS data from cationic wormlike micelles. *Langmuir* (2006). doi:10.1021/la0530440
  131. Pedersen, J. S. & Schurtenberger, P. Scattering functions of semiflexible polymers with and without excluded volume effects. *Macromolecules* (1996). doi:10.1021/ma9607630
  132. Guinier, A. & Fournet, G. *Small-angle scattering of X-rays. Small-Angle Scattering of X-Rays* (John Wiley & Sons, Inc., 1955).
  133. Murphy, K. & Weaver, C. *Janeway's immunobiology*. (Garland Science, Taylor&Francis Group, LLC, 2017).
  134. Chesla, S. E., Selvaraj, P. & Zhu, C. Measuring two-dimensional receptor-ligand binding kinetics by micropipette. *Biophys. J.* (1998). doi:10.1016/S0006-3495(98)74074-3
  135. Depoil, D. & Dustin, M. L. Force and affinity in ligand discrimination by the TCR. *Trends in Immunology* (2014). doi:10.1016/j.it.2014.10.007
  136. Huppa, J. B. *et al.* TCR-peptide-MHC interactions in situ show accelerated kinetics and increased affinity. *Nature* (2010). doi:10.1038/nature08746
  137. Lyons, D. S. *et al.* A TCR binds to antagonist ligands with lower affinities and faster dissociation rates than to agonists. *Immunity* (1996). doi:10.1016/S1074-7613(00)80309-X
  138. Rosette, C. *et al.* The Impact of duration versus extent of TCR occupancy on T cell activation: A revision of the kinetic proofreading model. *Immunity* (2001). doi:10.1016/S1074-7613(01)00173-X
  139. Stone, J. D., Chervin, A. S. & Kranz, D. M. T-cell receptor binding affinities and kinetics: impact on T-cell activity and specificity. *Immunology* (2009). doi:10.1111/j.1365-2567.2008.03015.x
  140. Merwe, P. A. Van Der. Surface plasmon resonance GENERAL PRINCIPLES OF BIACORE EXPERIMENTS. *Physics (College. Park. Md)*. (2010). doi:10.1007/978-1-60761-670-2
  141. Van Der Merwe, P. A. & Barclay, A. N. Analysis of cell-adhesion molecule interactions using surface plasmon resonance. *Curr. Opin. Immunol.* 8, 257–261 (1996).
  142. Alam, S. M. *et al.* T cell-receptor affinity and thymocyte positive selection. *Nature* (1996). doi:10.1038/381616a0
  143. Gascoigne, N. R. J., Zal, T. & Alam, S. M. T-cell receptor binding kinetics in T-cell development and activation. *Expert Rev. Mol. Med.* (2001). doi:10.1017/S1462399401002502



144. Kersh, G. J., Kersh, E. N., Fremont, D. H. & Allen, P. M. High- and low-potency ligands with similar affinities for the TCR: The importance of kinetic in TCR signaling. *Immunity* (1998). doi:10.1016/S1074-7613(00)80647-0
145. Dustin, M. L. *et al.* Low affinity interaction of human or rat T cell adhesion molecule CD2 with its ligand aligns adhering membranes to achieve high physiological affinity. *J. Biol. Chem.* 272, 30889–30898 (1997).
146. Dustin, M. L., Ferguson, L. M., Chan, P. Y., Springer, T. A. & Golan, D. E. Visualization of CD2 interaction with LFA-3 and determination of the two-Dimensional dissociation constant for adhesion receptors in a contact area. *J. Cell Biol.* (1996). doi:10.1083/jcb.132.3.465
147. McCloskey, M. A. & Poo, M. M. Contact-induced redistribution of specific membrane components: Local accumulation and development of adhesion. *J. Cell Biol.* (1986). doi:10.1083/jcb.102.6.2185
148. Kaplanski, G. *et al.* Granulocyte-endothelium initial adhesion. Analysis of transient binding events mediated by E-selectin in a laminar shear flow. *Biophys. J.* (1993). doi:10.1016/S0006-3495(93)81563-7
149. Pierres, A., Benoliel, A. M. & Bongrand, P. Measuring the lifetime of bonds made between surface-linked molecules. *J. Biol. Chem.* (1995). doi:10.1074/jbc.270.44.26586
150. Piper, J. W., Swerlick, R. A. & Zhu, C. Determining force dependence of two-dimensional receptor-ligand binding affinity by centrifugation. *Biophys. J.* (1998). doi:10.1016/S0006-3495(98)77807-5
151. Chen, W., Zarnitsyna, V. I., Sarangapani, K. K., Huang, J. & Zhu, C. Measuring Receptor–Ligand Binding Kinetics on Cell Surfaces: From Adhesion Frequency to Thermal Fluctuation Methods. *Cell. Mol. Bioeng.* 1, 276–288 (2008).
152. Zhang, F. *et al.* Two-dimensional kinetics regulation of  $\alpha$  L  $\beta$  2 -ICAM-1 interaction by conformational changes of the  $\alpha$  L -inserted domain. *J. Biol. Chem.* (2005). doi:10.1074/jbc.M510407200
153. Tolentino, T. P. *et al.* Measuring Diffusion and Binding Kinetics by Contact Area FRAP. *Biophys. J.* 95, 920–930 (2008).
154. O'Donoghue, G. P., Pielak, R. M., Smoligovets, A. A., Lin, J. J. & Groves, J. T. Direct single molecule measurement of TCR triggering by agonist pMHC in living primary T cells. *Elife* (2013). doi:10.7554/eLife.00778
155. Axmann, M., Huppa, J. B., Davis, M. M. & Schütz, G. J. Determination of interaction kinetics between the T cell receptor and peptide-loaded MHC class II via single-molecule diffusion measurements. *Biophys. J.* (2012). doi:10.1016/j.bpj.2012.06.019
156. Zhu, C., Jiang, N., Huang, J., Zarnitsyna, V. I. & Evavold, B. D. Insights from in situ analysis of TCR-pMHC recognition: Response of an interaction network. *Immunol. Rev.* (2013). doi:10.1111/imr.12016
157. Mege, J. L. *et al.* Quantification of cell surface roughness; a method for studying cell mechanical and adhesive properties. *J. Theor. Biol.* (1986). doi:10.1016/S0022-

5193(86)80070-4

158. Broughton, S. E. *et al.* Biased T Cell Receptor Usage Directed against Human Leukocyte Antigen DQ8-Restricted Gliadin Peptides Is Associated with Celiac Disease. *Immunity* (2012). doi:10.1016/j.immuni.2012.07.013
159. Anton van der Merwe, P., McNamee, P. N., Davies, E. A., Barclay, A. N. & Davis, S. J. Topology of the CD2-CD48 cell-adhesion molecule complex: implications for antigen recognition by T cells. *Curr. Biol.* (1995). doi:10.1016/S0960-9822(95)00019-4
160. Evans, E. J. *et al.* Crystal structure and binding properties of the CD2 and CD244 (2B4)-binding protein, CD48. *J. Biol. Chem.* (2006). doi:10.1074/jbc.M601314200
161. Demetriou, P. *et al.* CD2 expression acts as a quantitative checkpoint for immunological synapse structure and T-cell activation. *bioRxiv* (2019). doi:10.1101/589440
162. El Hentati, F. Z., Gruy, F., Iobagiu, C. & Lambert, C. Variability of CD3 membrane expression and T cell activation capacity. *Cytom. Part B - Clin. Cytom.* (2010). doi:10.1002/cyto.b.20496
163. Anton van der Merwe, P. & Neil Barclay, A. Transient intercellular adhesion: the importance of weak protein-protein interactions. *Trends Biochem. Sci.* (1994). doi:10.1016/0968-0004(94)90109-0
164. van der Merwe, P. A. *et al.* Human Cell-Adhesion Molecule CD2 Binds CD58 (LFA-3) with a Very Low Affinity and an Extremely Fast Dissociation Rate but Does Not Bind CD48 or CD59. *Biochemistry* (1994). doi:10.1021/bi00199a043
165. Davis, M. M. *et al.* LIGAND RECOGNITION BY  $\alpha\beta$  T CELL RECEPTORS. *Annu. Rev. Immunol.* (1998). doi:10.1146/annurev.immunol.16.1.523
166. Places, L., Calle, O. De, Romero, M. & Yagüe, J. Stimulation through the TCR / CD3 complex up-regulates the CD2 surface expression on human T lymphocytes . Information about subscribing to The Journal of Immunology is online at : (2016).
167. Zhu, D. M., Dustin, M. L., Cairo, C. W., Thatte, H. S. & Golan, D. E. Mechanisms of Cellular Avidity Regulation in CD2-CD58-Mediated T Cell Adhesion. *ACS Chem. Biol.* (2006). doi:10.1021/cb6002515
168. Thatte, H. S., Bridges, K. R. & Golan, D. E. Microtubule inhibitors differentially affect translational movement, cell surface expression, and endocytosis of transferrin receptors in K562 cells. *J. Cell. Physiol.* (1994). doi:10.1002/jcp.1041600216
169. Juang, J. *et al.* Peptide-MHC heterodimers show that thymic positive selection requires a more restricted set of self-peptides than negative selection. *J. Exp. Med.* (2010). doi:10.1084/jem.20092170
170. Bethune, M. T. *et al.* Isolation and characterization of NY-ESO-1-specific T cell receptors restricted on various MHC molecules. *Proc. Natl. Acad. Sci. U. S. A.* (2018). doi:10.1073/pnas.1810653115
171. Chen, Y.-T. *et al.* A testicular antigen aberrantly expressed in human cancers detected by autologous antibody screening. *Proc. Natl. Acad. Sci.* **94**, 1914–1918

- (1997).
172. Robbins, P. F. *et al.* Single and Dual Amino Acid Substitutions in TCR CDRs Can Enhance Antigen-Specific T Cell Functions. *J. Immunol.* **180**, 6116–6131 (2008).
  173. Chen, J.-L. *et al.* Structural and kinetic basis for heightened immunogenicity of T cell vaccines. *J. Exp. Med.* **201**, 1243–1255 (2005).

# Acknowledgements

*The more things change the more they stay the same.*

-Jean-Baptiste Alphonse Karr-



## Acknowledgements

A lot of people have been involved in my journey over the last four years and I would like to thank them for making this thesis possible.

First and foremost I would like to thank my supervisor **Peter Jönsson** for persuading me to do a PhD in physical chemistry. I was super hesitant to do so but thanks to you I learned a lot about numbers and equations, and I appreciated all the hours you sat down with me and explained whatever I did not understand. You motivated me to see why it is important to know a 'little bit' of physics too and so I started caring about intermolecular interactions which I would have never thought of when I started my PhD. This was only possible because of your patience, enthusiasm and optimism which I am so grateful for. It was very refreshing, especially on all those days where nothing seemed to work. I am very happy we could start this journey together and hope we will solve the conundrum about 'self' on our way to the finishing line.

My second big thanks goes to my co-supervisor **Simon J. Davis**. You managed to help me in so many ways that I am not even sure how to say thank you for it all other than thank you so much. I was very honoured I could work in your lab for a couple of months. You have a great ability to put things in a bigger context and convinced me that my research is important even though I might have doubted that at points. This kept me going with much more enthusiasm and energy. Thank you for that.

Third, but not last, I would like to thank my co-supervisor **Lena M. Svensson**. I think you connected Peter and I, and I am very happy about this. You also gave me the opportunity to work in your lab and use your incredible microscope which I appreciated so much since it made my life a lot easier taking all those pictures of thousands of cells without having to spend night shift after night shift. Thanks a lot for this opportunity.

My second round of thanks goes to all the people that supported me on my journey throughout the last four years inside and outside of work. I would like to start with my group companions Tommy D., Alexandra, Madeleine and Arif. **Tommy**, you have been an absolute blast. I don't think I have ever met such a sweet and funny person. You made us laugh almost daily with all your stories and questions about life. If squatting in the lab or guessing who will die in GOT for hours, it is obvious that without you our, and especially my life, would have much less laughter in it.

**Alex**, my big little sister in heart. How I will miss all our deep (and not so deep) discussions about life and the questionable Swedish-way of doing things. You have been an emotional support and I am so happy to have a strong and positive thinking woman sitting right behind me to whom I can simply turn around to for a nice and cheerful conversation. **Madeleine**?...you know what I mean 😊. Over the last weeks you have been my hero in shining armour. You were the first telling me how much you liked my thesis and that you could actually learn things from it. That made me incredibly happy. You have also put a lot of work into finishing up the last measurements for the paper for which I am so grateful for. I am looking forward to working more on this and am happy for any side stories you always seem to have! **Arif**, what would we do without you? You have the right story for every situation in your back pocket and you are always so happy to share it with us. Hours pass by once we all start talking and I have enjoyed and learned a lot from these life lessons. A huge thanks also goes to **Amélie** who has been with us for almost a year and has worked so hard on the hydrodynamic trapping experiments. I am very happy you wanted to work on this with me. You have been such a nice group member and I already miss all our complaining sessions in the office.

I would also like to thank all members of physical chemistry for creating such a nice environment to work in. My special thanks goes to **Luigi**, who has helped me with basically everything. You were open to my crazy ideas about measuring on my proteins and spent more than one night-shift on doing this, for which I thank you a thousand times. You have been my rock in a very bumpy sea, and I am happy to have you as my friend who loves science as much as I do (or maybe even a bit more). I would also like to thank **Jasper** for enriching my life with sing-alongs, non-sense stories, jokes and all this in every possible dialect you can image. Most importantly though, thanks for helping me through Colloidal Domain. What a pain!

**Tommy G.** thanks for all the lovely chats we had and for being my lab companion making the very boring glass-slide-cleaning-process much more exciting. **Maria V., Polina, Linda, Axel, Simon** and **Ilaria** thanks for all the chats and laughter's we had in the coffee room, in the offices as well as outside of work. It has been great to have you as my colleagues. **Solmaz**, thank you so much for making my entrance to the division as smooth as possible by showing me around, answering all my questions I have had and for all our little chats in the office. I couldn't have imagined a better office mate to start my journey with.

Nothing would have work as smoothly as it did without two very important people. **Helena** and **Maria S.** You have not only been super helpful in all administrative and chemical matters, but I also enjoyed every chat we had over lunch and coffee. And I am very happy that you two are part of physical chemistry and my journey ☺. Thank you for all your help and always being so kind and friendly. **Chris**, thank you so much for helping me with any Printer-Internet-Server-issue that came up and for rocking the 3D printing!

A special thanks goes to my colleagues in Oxford. Foremost **Mafalda** who has done so much to help me continue with my project. I don't know how you do it, but I am impressed by your patience and ability to manage helping everyone (and that is a lot!) and still be so positive and chilled. A true inspiration! Another big thanks goes to **Heather** who put all her effort into making a ton of proteins for us and for helping me in the lab whenever I had questions. I would also like to thank the rest of the group especially **Caitlin**, **Edward**, **Alex** and **Nicole** you helped me enjoy Oxford to the fullest and I loved every minute of it. You also taught me English in a way that I felt I am learning it all over again. I am so happy I understand you now (well most of the time!). Remember two plus two is four, minus one that's three, quick maths.!

**Kasia P.** and **Janne**, my co-workers in **Lena's** group. You have helped me so much to settle in to the lab and were always open to show me where things are or how to solve struggles I had with the microscope. Thank you for all the chats and fruitful discussions about imaging and image analysis.

During my PhD I have also been part of some extracurricular activities which added really nice moments to my time here for which I would like to thank the NDR student union working group **Andrea**, **Brian**, **Lana**, **Megan** and **Simona** as well as the ADMIRE members with a special thanks to **Maria M.** and **Lisa R.**

A huge thank you goes to **Madeleine**, **Alexandra**, **Tommy** and **Luigi** who have proof read my thesis and given me valuable input on what things to change. Thanks for spending so much time reading through these pages. Since I seem to have forgotten how to write in my mother tongue, I would also like to thank **Sebastian N.** for correcting my horrible German version and making it somewhat understandable (I hope!). My biggest thanks, however, goes to **Robert**. You have probably proof read this thesis more than I have and without you I would have had uncountable amounts of “however” and “furthermore” at the beginning of sentences. Thank you for your patience. I guess I can now stop asking: “Can you help me with *just* one more



sentence?“. And finally, thank you **Paula**, for turning my word document into a beautiful book.

Meine allerliebste **Laura**...was hätte ich in den letzten Jahren nur ohne dich getan? Du warst mir eine Freundin, eine Schwester und ja sogar in manchen Situationen eine tapfere Mutter, weil du meine Tränen mehr als einmal getrocknet hast. Ich danke dir für all die schönen Momente, die hitzigen Diskussionen, dass sich über alles aufregen, die vielen Stunden die wir zusammen auf der Couch verbracht und unsere Kindheit mit Gilmore Girls nochmal erlebt haben und endlich auch (nach 7 Jahren!!) GOT geschaut haben. Danke für die vielen Frühstücksmomente, die Abendessen und Lunches. Du bist mir ein Herzblatt und ich bin so froh das wir uns begegnet sind.

Ein großes Dankeschön geht auch an meine Familie und Freunde von daheim ☺. Ihr wart immer für mich da und habt mich in meiner Verrückten Idee ins Ausland zu gehen unterstützt. Danke für die vielen Besuche in meinem neuen Zuhause, die vielen Facetime anrufe und dafür das ihr immer an mich denkt. **Omi, Opi, Mutti** und **Peter**, vielen Dank dafür das ihr Heimat, Heimat macht, dass ihr mich die vielen, vielen Jahre unterstützt und begleitet habt. Nur so konnt ich den Weg gehen der mich jetzt zu einer kleinen Doktorin macht ☺. **Paps** und **Eileen**, die letzten Jahre waren manchmal ganz schön anstrengend aber ich hab mich immer wieder gefreut sobald ich meine Aioli fertig gekocht und an euch gedacht habe. Danke für die viele Unterstützung und Freuden die ihr mir habt zukommen lassen. Sie zaubern jeden Tag ein Lächeln auf meine Lippen. Und zu guter letzt, mein **Rob**. Danke für einfach alles... Danke das es dich gibt und du mir eine Hilfe in jeglicher Situation bist. Ohne dich wäre ich nur halb so stark.





Printed by Media-Tryck, Lund 2019. NORDIC SWAN ECOLABEL 3041 0903



ISBN: 978-91-7422-712-3

Physical Chemistry  
Department of Chemistry  
Faculty of Science  
Lund University

